University of Alberta

Sit-to-Stand Biomechanics and the Design of an Assistive Knee-Ankle- Foot-Orthosis

by

Jonathon Schofield

A thesis submitted to the Faculty of Graduate Studies and Research
in partial fulfillment of the requirements for the degree of

Master of Science

in

Structural Engineering

Department of Civil and Environmental Engineering

Abstract

Sit-to-stand (STS) transfer is a prerequisite for many daily tasks. Literature often assumes

symmetrical behavior across the body (bilateral symmetry) during healthy STS. However; little

research has been conducted to validate this assumption. Motion analysis was utilized to evaluate

STS in 10 healthy males. Asymmetry was found in the peak joint moments (JM) and ground

reaction forces. Asymmetry was also characterized over the whole STS movement. This analysis

suggested evaluating peak values alone may not fully represent asymmetry present during this

movement.

A knee-ankle-foot-orthosis (KAFO) augments weight bearing in populations with lower

extremity weakness by holding the knee extended and ankle neutral. However, this creates

complications for users performing STS. A novel KAFO attachment was designed to generate a

knee extension moment, thus alleviating these challenges. Testing on an able bodied participant

and a finite element analysis indicate the design has the potential to assist KAFO users.

Acknowledgements

I would like to take the opportunity to thanks those who have supported me throughout my Master's. Without your ideas, contributions and time I would not have been able to complete this research.

Thank-you very much:

Dr. Samer Adeeb, University of Alberta

Dr. Eric Parent, University of Alberta

Karen Benterud, Edmonton Glenrose Rehabilitation Hospital

Andreas Donauer, Edmonton Glenrose Rehabilitation Hospital

Nick Gilmour, University of Alberta

Justin Lewicke, Edmonton Glenrose Rehabilitation Hospital

Jason Sperry and Robert Rose, Bansbach North America

Dedications

To my brother Aaron, thank you for listening even though I know a lot of times you weren't interested. It is good to know two engineers can still hold a nerdy conversation.

To my mother and father, Judy and Collin, thanks for the support. I appreciate everything you have done to help me get to where I am.

Table of Contents

Appendicies

List of Abbreviations

FEA - Finite Element Analysis, in reference to the application of numerical approximations applied through software to characterize stress development in an object of interest

GRF- Ground Reaction Forces, the three dimensional force reaction developed between the ground and a participant's foot during sit to stand movements

JM- Joint Moment, the torque, or moment developed in a participant's lower extremity joints during sit to stand moments

JP- Joint Power, the power (a product of joint moment and joint velocity) developed in a participant's lower extremity joints during sit to stand moments

KAFO- Knee Ankle Foot Orthosis, an orthotic leg brace designed to assist in weight bearing during standing for populations with limited lower extremity weakness

LFD- Left Foot Dominant, in reference to the foot preferred to perform manipulative motor tasks

PAI- Percent Angular Impulse, a change in the angular moment of a lower extremity joint during sit to stand movements

PW- Percent Work, the angular work of a lower extremity joint during sit to stand movements

RFD- Right Foot Dominant, in reference to the foot preferred to perform manipulative motor tasks

SDIFF- Straight Difference, the subtraction of the right side joint moment or joint power curve from the left side

SI- Symmetry Index, a measure of percent or relative difference in kinetic and kinematic values developed across the body during sit to stand movements

STS- Sit to Stand, and abbreviation to describe the movements associated with rising from a chair

VGRF- Vertical Ground Reaction Forces, the vertical component of the three dimensional force reaction developed between the ground and a participant's foot during sit to stand movements

Thesis Outline

Sit-to-stand (STS) transfer is a common yet important daily movement. STS often precedes walking and therefore plays an important role for an independent lifestyle. This two chapter thesis will focus on two areas of STS related research. The first of the two chapters will concentrate on further understanding the biomechanics of STS movements in healthy populations, with a specific focus on the bilateral symmetry. The second chapter will highlight a novel knee-ankle-foot-orthotic prototype that has been developed to assist STS transfer in affected populations. The design, manufacturing and testing of this prototype will be discussed.

This mixed format thesis will therefore be divided into two chapters each comprised of a number of parts. Chapter one will focus on assessing bilateral symmetry during healthy STS movements. The first part will discuss the results of the peak joint moment development during this maneuver in 10 healthy males. The second part will expand the analysis to characterize asymmetry over the duration of the whole STS movement.

Chapter two will focus on the conception, design, manufacturing and testing of a novel knee-ankle-foot-orthosis (KAFO) attachment. The first part will be dedicated to the conception and design process. Part two will focus on testing the prototype with an able bodied participant. Finally part three will discuss a finite element model utilized to understand the stress distribution developed in the prototype components.

<center>**Chapter 1**</center>

<center>**Bilateral Symmetry during Healthy Sit-to-Stand Movements**</center>

Introduction

Rising from a chair or sit-to-stand (STS) is a critical prerequisite for many daily tasks. STS movements will often precede walking and as a result are a functional requirement for an independent lifestyle (1) (2). Therefore, an accurate understanding of the biomechanical requirements to successfully accomplish STS is necessary for rehabilitation and therapeutic programs focused on enhancing the independence of clients with limited lower extremity function.

In addition to its importance for an independent lifestyle, the kinetic and kinematic symmetry of STS can be used as a clinical assessment tool for lower extremity impairment. Boonstra *et al*. and Christiansen *et al*. have utilized STS symmetry to evaluate knee function following arthroplasty (3) (4) (5). Both researchers found vertical ground reaction forces (VGRF) to become more symmetrical with longer post-operative times. Furthermore, Christiansen *et al*. were able to quantify the degree of asymmetry present in two-dimensional VGRFs of a healthy control group (5). Outside of orthopaedics, STS symmetry has been used to assess movements in elderly populations, hemiparesis, and prosthetics among others (6) (2) (7) (8). Although asymmetry is often used as an indication of impairment, healthy populations do not necessarily exhibit perfect symmetry. Consequently, if the symmetry of STS is to be used as an assessment tool for affected populations, an accurate understanding of healthy STS motions is imperative.

Researchers often capture joint moment (JM) data two dimensionally, or in the sagittal plane only (9) (8) (10). Recording only sagittal JMs neglects contributions from the coronal and axial planes, potentially having a significant impact on estimates of STS biomechanics. Similarly, when evaluating ground reaction forces (GRF), few studies consider the shearing forces in the anteroposterior (AP) and medial-lateral (ML) directions and focus on vertical ground reaction forces (VGRF) (4) (1) (5). Ignoring shear forces potentially misrepresents STS biomechanics as all external forces are not accounted for. Furthermore; when quantifying STS movements, several studies assume bilateral symmetry in healthy populations; where the left and right sides

<center>1-2</center>

of the body are hypothesized to operate symmetrically. Consequently, (JMs) and GRFs are assumed contralaterally equivalent (11) (12) (13) (10).

However, asymmetry in the kinetics of lower limbs has been widely demonstrated in healthy populations performing lower extremity tasks such as gait. Seeley *et al*. found significant functional asymmetry in the ground reaction force impulses of healthy adults during fast walking (14). Furthermore, Seeley *et al*. determined asymmetry in able bodied JMs and power to be correlated with leg-length-inequality (15). Sadeghi *et al*. found gait asymmetry in healthy elderly subjects to be related to energy generated by the lower limbs for the propulsion function (16). Muscular strength asymmetry has also been demonstrated in healthy populations. Hadzic *et al*. showed significant hamstring asymmetry in international level-athletics relative to national-level (17). Finally, during isokinetic knee flexion and extension, it has been shown that healthy populations exhibit statistically stronger quadriceps and weaker hamstrings in their motor dominant side (18).

Lundin *et al*. evaluated the lower extremity peak JMs of 7 young and 7 elderly participants (9). Significant differences were found between left and right sagittal JMs at the hip in an elderly and young population with further asymmetry at the knees of the young group. However, this investigation was limited to sagittal plane movement. Moreover, Burnett *et al*. evaluated asymmetrical peak VGRFs in relation to leg dominance during STS. They found no significant difference between dominant and non-dominant sides VGRFs (1). These values were collected using a single force plate that was alternated between the participant feet for each trial. However, this protocol, inherently assumes a relationship between asymmetry and leg dominance by averaging and comparing the dominant to non-dominant side. If VGRFs during STS are asymmetrical but not related to leg dominance, peak values may be higher in the dominant side in one trial and the non-dominant in the next. This phenomenon would not be captured with one instrumented leg, and potentially skews results toward symmetricity.

It is also important to note that no study has addressed STS asymmetry across the whole STS cycle. Most studies found in the literature focus on a discrete value, or a single numerical indicator such as peak JMs or GRFs. A peak analysis allows for a comparison of the maximum

mechanical requirements during STS, and whether these requirements are bilaterally symmetric or not. Therefore it is important to realize that these studies are evaluating symmetry independent of when the body arrives at this condition and how it gets there.

This chapter will be divided into two parts. The first will investigate bilateral symmetry in peak JM and GRF values, and whether any asymmetry can be related to leg motor dominance. The second part will characterize asymmetry developed in JM and joint power JP values over the duration of the STS cycle.

Bilateral Symmetry in Peak Joint Moments and Ground Reaction Forces and their Relation to Leg Dominance

The objective of the first part is to quantify the peak ankle, knee and hip JMs as well as the peak GRFs during STS in 10 healthy participants by incorporating data in all three dimensions. Through the use of the Euclidian Norm , bilateral symmetry was quantified and whether asymmetrical results were associated with leg motor-dominance (footedness) was investigated.

Methods

Participants

Participants were recruited within the University of Alberta's Civil Engineering Department. Selected participants were males aged 21 to 35 years mean age (SD): 25yrs (4yrs), mean height (SD): 176.8cm (8.4cm) mean mass (SD): 70.5kg (8.3kg), mean body mass index (SD): 22.55kg/m^2 (2.44 kg/m^2). Males were selected to remove the possibility of biomechanical gender differences that have presented themselves in non-STS related motion analysis (19). Furthermore, all subjects reported no prior or current physical conditioning or injuries that may affect their STS movements. A convenience sample of 5 right and 5 left handed participants (self-reported) were selected to increase the chances of equal numbers of right and left leg motor-dominant participants. Ethics approval was obtained through the University of Alberta ethics review board (HERO ID#: Pro00021081). All participants gave informed consent prior to participating.

To determine leg motor-dominance, participants completed a questionnaire two weeks before testing and on the date of testing. The questionnaires followed the 11-item Chapman Inventory for foot preference (20). Participants indicated which foot they could most effectively execute each listed task. A score of 1, 0, or -1 was assigned to an indication of right foot, no preference, or left foot respectively. Participants were classified as right foot motor-dominant, ambidextrous, or left foot motor-dominant if total scores ranged from 4 thru 11, -3 through 3, and -4 through -11 respectively. Finally participants performed 4 tasks closely correlated with leg motor-

dominance these four tasks are seen in Table 1-1 (20). The foot the participant selected for each task was recorded and used to verify the questionnaire results. Although some participants test and retest scores were not identical, these changes did not affect their leg dominance categorisation.

Table 1-1 Participant's Footedness Scores and Leg Selection for Performed Tasks

|	Questionnaire		Performed Actions				
Participant Number	Self-Test Score	Re-Test Score	Trace Letters with Foot (L/R)	Pantomime Smoothing Sand (L/R)	Push Ball Around Circle (L/R)	High Kick (L/R)	Leg Dominance
1	9	9	R	R	R	R	Right
2	11	11	R	R	R	R	Right
3	10	11	R	R	R	R	Right
4	10	8	R	R	R	R	Right
5	7	9	R	R	R	R	Right
6	-8	-5	L	R	L	L	Left
7	-10	-9	L	L	L	L	Left
8	-11	-11	L	L	L	L	Left
9	-8	-6	L	L	L	L	Left
10	-7	-7	L	L	L	L	Left

Participant numbers and their corresponding score on the Chapman inventory questionnaire. The participants were classified as right foot motor-dominant, ambidextrous, or left foot motor-dominant if their total score fell in to the ranges of 4 thru 11, -3 thru 3, and -4 thru -11 respectively. The performed action category was utilized to confirm the category each participant was placed in. In the performed action category L signifies the left foot was chosen to perform the task, while R signifies a selection of the right foot.

Data Collection

Eighteen spherical reflective markers (1.5 cm diameter) were used on each participant to define 8 body segments (feet, shanks, thighs, pelvis and torso). Markers were adhered following a modified Helen Hayes protocol as follows (21): toe marker, (between the 2nd and 3rd metatarsal heads), heel marker (posterior calcaneus, leveled for height with the toe marker), lateral and medial malleolus markers (on the malleoli in line with the bimalleolar axis), shank wand (on the distal shank extended laterally to minimize motion artifact from muscle contraction), medial and lateral knee (placed on the epicondyles and adjusted to best represent knee flexion extension axis through the relevant range of motion), thigh wand (distal on the thigh extended laterally, again to reduce motion artifact and in the plane of the thigh), anterior superior iliac spine, sacrum (at the midpoint between the posterior superior iliac spines), iliac crest (for redundancy in case of

marker cover up), C7 and sternum (midpoint between the sternal-clavicular joints). Figure 1-1 illustrates the marker placement protocol.

Figure 1-1 Marker Placement Protocol
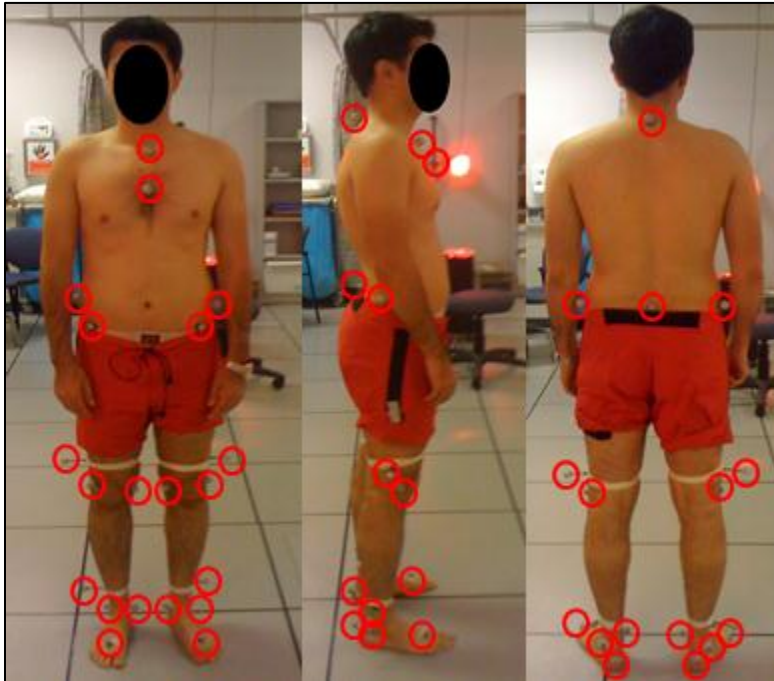
Marker placement, eighteen spherical reflective markers were utilized and are highlighted in the red circles

Markers' positions were captured using an 8 camera, Eagle Digital Motion Analysis system (Motion Analysis Corp., Santa Rosa, CA, USA) sampling at 120Hz. Two AMTI (Advanced Mechanical Technology Inc., Newton, MA, USA) force plates sampling at 2400Hz were utilized to capture GRFs.

A backless, armless, 48cm tall, chair was positioned such that the participant could place one foot approximately centered on each force place (9). Subjects folded their arms across their chest and rose at a self-selected pace when prompted. The use of upper extremities during the STS task was not permitted. The procedure was repeated 10 times (10 trials) for each participant. The STS cycle to commence at the onset of hip flexion and to finish once the participant reached upright posture and joint motion ceased. The peak JMs and GRFs were defined as the maximum value occurring in this time interval.

EVaRT 5 software (Motion Analysis Corp., Santa Rosa, CA, USA) was utilized to select the markers representative of each body segment and to define their corresponding local coordinate systems. This data was imported into Visual 3D software (C-Motion Inc., Germantown, MD, USA) where inverse dynamic calculations were performed. Body-segment properties were input according to 50th percentile anthropometric data (22) (23). A 4Hz, fourth-order, zero phase-shift Butterworth filter was utilized in Visual 3D to smooth raw data (22).

Numerical Procedures:

JMs were quantified in all 3 planes at the ankle knee and hip and normalized by each participant's body mass and body height (BMxBH); additionally, GRFs in three dimensions were recorded and normalized by body mass (BM) (19).

To account for JMs and GRFs in three dimensions, The Euclidian Norm was utilized at each sample point. The anteroposterior (ap), medial-lateral (ml) and superior-inferior (si) moments were summed using Equation 1-1. Similarly, GRFs in the x, y, and z directions were summed using Equation 1-2. The peak motor-dominant and non-dominant values for ankle, knee, and hip JMs as well as GRFs were identified as being the maximum value for each STS trial.

Equation 1-1 Euclidian Norm Vector Summation for Joint Moments

$$M_{total} = \sqrt{M_{ap}^2 + M_{ml}^2 + M_{si}^2}$$

The total resultant moment for each joint; defined as the Euclidian Norm (vector summation) of the anteroposterior (ap), medial-later (ml) and superior-inferior (si) direction moments

Equation 1-2 Euclidian Norm Vector Summation for Ground Reaction Forces

$$GRF_{total} = \sqrt{GRF_x^2 + GRF_y^2 + GRF_z^2}$$

The total resultant GRF; defined as the Euclidian Norm (vector summation) of the x, y and z, Positive z represents the vertical GRF, x and y represent the shearing components

Statistics

The side at which the larger peak JM or GRF occurred for each trial was identified as the favored side. It was recorded whether the motor-dominant or non-dominant side was favoured for the ankle, knee, hip and GRFs of each participant's 10 trials. Furthermore, the percentage of dominant or non-dominant favouring was calculated. The Symmetry Index (SI) of each

participant's JMs and GRFs was calculated based on the average between-side difference (24). SI values were obtained using Equation 1-3.

Equation 1-3 General symmetry index formula

$$SI = \left(\frac{|Left - Right|}{|(Left - Right)/2|} \right) \times 100\%$$

General SI formula where left and right represent the JM or GRF value of the left and right side respectively.

Asymmetry was defined as a difference in the normalized peak values of one side and the contralateral for each trial. The larger of these two values was grouped into one category and the smaller in another. If STS is a statistically symmetric movement, the means of these two categories should show no significant difference. A paired one-tailed t-test was conducted, and $P< 0.05$ was assumed to indicate a significant difference (i.e. asymmetry). This procedure was applied to the ankle, knee and hip JMs as well as the GRFs. Finally, SI calculations were performed on the means of the large and small groups.

To test if asymmetry was influenced by leg motor-dominance, the normalized left JMs, as well as GRFs, were subtracted from the right, and the average difference was calculated for each participant. Therefore, consistently producing a larger JM on the right side would yield a negative average value, inversely a positive value for a larger left side. An unpaired, two-tailed t-test was conducted on the average difference values of the right foot dominant (RFD) participants compared to the left foot dominant (LFD) participants. $P< 0.025$ was assumed to indicate a significant difference and therefore a relationship between leg motor-dominance and asymmetry.

Results

Typical curves highlighting the contributions of the JMs and GRFs in each body plane are illustrated in Figure 1-2. Although minor fluctuations between participants and trials were observed, the location of the peak JM or GRF remained fairly consistent between all 10 participants. Table 1-2 highlights the participant's mean peak JMs and GRFs according to leg motor dominance. These figures are meant to serve as a tool for visualization and further

interpretation of the results presented in this part. Further typical JM contributions curves can be seen in Appendix A for the first STS trial of participant 5 and 9.

Figure 1-2 Typical Component JM and GRF Curves Grouped According to Motor-Dominance
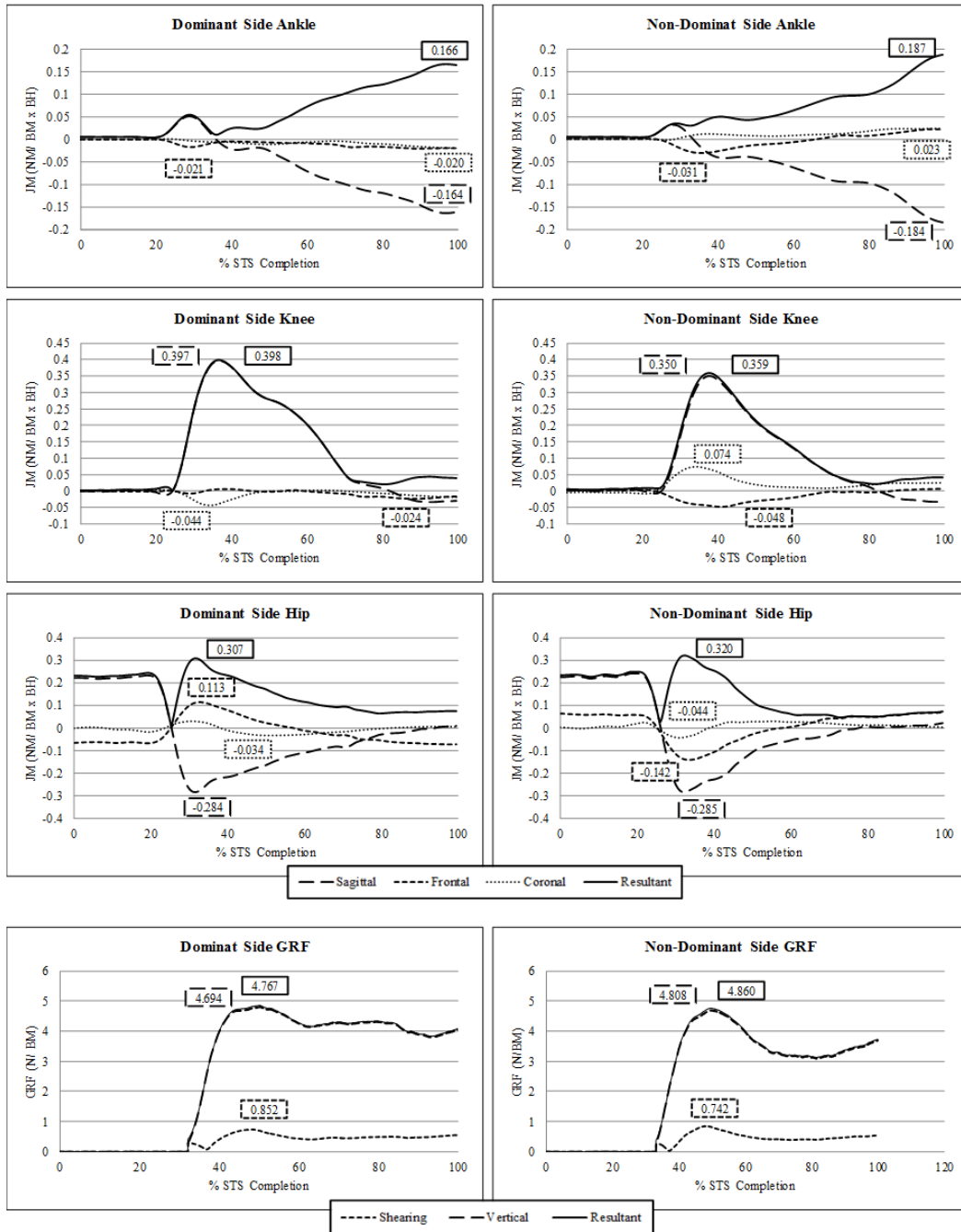
JMs normalized by body mass and body height reported in units of N.m./ (Kg.m). Sagittal, frontal, and coronal components are illustrated as well as the resultant vector summated curve. Normalized GRFs are reported in units of N/Kg. Vertical and shearing components are illustrated as well as the resultant vector summated curve.

Table 1-2 Participants' Mean Peak JMs and GRFs According to Leg Motor-Dominance

Participant	Ankle		Knee		Hip		GRF	
	D	ND	D	ND	D	ND	D	ND
1	0.55	0.65	1.25	1.14	0.89	1.05	4.73	4.78
SD	0.10	0.15	0.05	0.10	0.12	0.28	0.24	0.17
2	0.90	0.62	1.50	1.31	1.80	1.52	4.74	5.39
SD	0.16	0.11	0.17	0.07	0.25	0.19	0.23	0.31
3	0.55	0.61	0.86	1.02	1.34	1.37	5.07	5.19
SD	0.08	0.15	0.07	0.08	0.11	0.15	0.32	0.20
4	0.78	0.84	0.93	1.22	1.64	1.98	6.85	5.74
SD	0.16	0.10	0.10	0.07	0.10	0.13	0.32	0.26
5	0.83	0.61	1.49	1.58	1.46	1.56	5.24	4.79
SD	0.21	0.13	0.12	0.11	0.12	0.19	0.28	0.24
6	0.95	0.87	1.05	1.17	1.88	1.85	5.12	5.26
SD	0.11	0.11	0.14	0.13	0.20	0.22	0.24	0.17
7	0.66	0.80	1.59	1.80	1.34	1.00	5.23	5.17
SD	0.12	0.10	0.05	0.10	0.12	0.10	0.19	0.28
8	0.59	0.55	1.07	1.26	1.17	0.97	5.29	5.42
SD	0.11	0.09	0.09	0.10	0.12	0.12	0.17	0.11
9	0.76	0.79	1.06	1.21	1.72	1.18	5.34	5.76
SD	0.07	0.07	0.12	0.07	0.34	0.14	0.23	0.16
10	0.54	0.36	0.88	0.77	1.09	0.88	4.60	5.15
SD	0.11	0.10	0.10	0.07	0.10	0.10	0.18	0.21
Units	Nm/ BMxBH						N/BM	

Peak JM values and standard deviation (SD) are reported in units of N.m./(Kg.m.). Peak GRFs and standard deviations are reported in units of N/Kg. D signifies the motor-dominant leg and ND the non-dominant leg.

Side Favoritism and Association with Leg Motor-Dominance

As seen in Table 1-3, no discernible pattern was observed between a participant's favoured side and leg motor-dominance. Although many participants will show 100% favoritism toward one side, others will show little to no discrimination. For instance, participants 9 and 10 showed 100% favoritism on their non-dominant GRFs, whereas Participant 7 exhibited a 50% split; inversely participant 4 developed 100% dominant favoritism.

SI values, as well, show wide variations between participants. At the ankle, values ranged from as low as 7.59% to as high as 40.05%. The knee, hip and GRF also showed much fluctuation between participants, with again, no discernible pattern emerging between participants or leg dominance (Knee: 9.57-26.81%, Hip: 8.59-37.26%, GRF: 3.44-17.71%).

Table 1-3 Percent Favoritism and Symmetry Indexes Values

Participant	Ankle D (%)	Ankle ND (%)	Ankle SI (%)	Knee D (%)	Knee ND (%)	Knee SI (%)	Hip D (%)	Hip ND (%)	Hip SI (%)	GRF D (%)	GRF ND (%)	GRF SI (%)
1 RFD	0	100	16.56	90	10	9.57	20	80	17.56	40	60	3.85
2 RFD	100	0	37.19	100	0	13.73	100	0	16.90	0	100	12.83
3 RFD	40	60	13.63	0	100	16.80	30	70	8.59	40	60	7.42
4 RFD	40	60	9.38	0	100	26.81	0	100	18.84	100	0	17.71
5 RFD	90	10	31.18	20	80	10.38	30	70	15.75	90	10	9.22
6 LFD	80	20	9.79	0	100	10.61	60	40	8.96	20	80	4.00
7 LFD	0	100	19.38	0	100	11.91	100	0	29.22	50	50	5.37
8 LFD	70	30	10.46	0	100	16.33	80	20	21.93	20	80	3.44
9 LFD	30	70	7.59	20	80	15.59	100	0	37.26	0	100	7.57
10 LFD	100	0	40.05	10	90	13.65	100	0	21.56	0	100	11.33
Average	55	45	19.52	24	76	14.54	62	38	19.66	36	64	8.27

Favoritism is reported as the percent of the 10 trials either the motor-dominant (D) or non-dominant (ND) side produced a larger peak value. Symmetry Indexes (SI) are reported at each joint as well as GRFs. RFD signifies a right foot motor-dominant participant conversely, LFD a left foot motor-dominant participant.

JM and GRF Symmetry between lower extremities:

The paired one-tailed t-tests indicate that the ankle, knee and hip JMs as well as GRFs develop asymmetrical peak values during STS movements. Table 1-4 illustrates that with greater than 95% confidence, lower extremity JMs and GRFs are developed asymmetrically when accounting for movement in all three planes. The symmetry index values suggest that, the peak hip and ankle JMs can be expected to produce the largest discrepancy between sides (19.1% and 18.6% respectively). The knee joint moment shows a SI value of 3.8% and a SI value of 9.4% was found in the GRFs.

Table 1-4 Testing Bilateral Symmetry in the JMs and GRFs

	Units	Large Mean	Large SD	Small Mean	Small SD	P-value	Symmetry Index (%)
Ankle JM	Nm/BMxBH	0.24	0.05	0.20	0.05	< 0.01	18.6
Knee JM	Nm/BMxBH	0.43	0.07	0.41	0.07	< 0.01	3.8
Hip JM	Nm/BMxBH	0.48	0.11	0.40	0.10	< 0.01	19.1
GRF	N/BM	5.47	0.58	4.98	0.63	< 0.01	9.4

Means and standard deviations (SD), and P-values are reported. Normalized values are in units of Kilograms for body mass (BM) and meters for body height (BH). For each trial the larger peak value at each joint (and GRF) was grouped into the Large category, inversely the smaller values in the Small category. This procedure was repeated for each trial, and means for the large and small categories compared for each JM and GRF.

<u>Footedness and its Relation to Asymmetry:</u>

Results of the unpaired two-tailed t-tests suggest that differences between peak JMs and GRFs when comparing left foot motor-dominant to right foot motor-dominant participants do not reach statistical significance. The normalized left JMs and GRFs were subtracted from the right, and the average difference for each participant was recorded. These average difference values were statistically compared and at a 95% confidence interval. Resulting data suggests there are no significant differences between the motor-dominance subgroups in peak JMs or GRF asymmetry values.

Table 1-5 Comparing Asymmetry in Right Foot Motor-Dominant Participants to Left Foot Motor-Dominant Participants

	Units	Difference RFD		Difference LFD		P-value
		Mean	SD	Mean	SD	
Ankle JM	Nm/BMxBH	-0.01	0.05	0.01	0.04	0.42
Knee JM	Nm/BMxBH	0.02	0.06	-0.03	0.04	0.21
Hip JM	Nm/BMxBH	0.03	0.07	0.09	0.06	0.20
GRF	N/BM	-0.18	0.65	-0.24	0.25	0.80

The mean difference experienced in peak JMs and GRFs between RFD and LFD participants is reported,where SD is the standard deviation. Normalized values are in units of Kilograms for body mass (BM) and meters for body height (BH).

Discussion

This part addresses the extent of bilateral symmetry in peak JMs and GRFs during STS movements using the Euclidian Norm (vector summation) to account for data in all three dimensions. These resultant values were employed to investigate whether asymmetry can be associated with leg motor-dominance.

While our analysis shows significant asymmetry during STS, previous studies have failed to achieve such statistical significance (1). By dividing JM and GRF results into a large or small group for each trial we allowed asymmetry to be captured as an independent variable. This method removes statistical dependence on the leg at which a result occurred. It eliminates the effects of averaging seen by comparing the left and right leg, and addresses symmetry on a per-trial basis.

Lundin *et al.* found significant differences between the left and right sagittal JMs at the hip in an elderly and young population with further asymmetry at the knees of the young group (9). Similarly, our data shows that when all three dimensions are accounted for, JMs at the knee and hip, as well as ankle develop statistically significant asymmetry in their peak values. It is important to understand that in an accurate depiction of STS, JMs and GRFs must be accounted for in three dimensions. Those employing a sagittal-only- analysis, neglect contributions of naturally occurring movements in the axial and coronal planes, potentially misrepresenting the biomechanical requirements of the body.

Christiansen *et al.* quantified asymmetry in two dimensional VGRFs of healthy and post-operative knee-arthroplasty participants (5). Their work characterized asymmetry in VGRFs; however, it is important to recognize the contributions of the shearing GRFs (SGRFs). As an example, Figure 1-2 illustrates that VGRFs and resultant GRFs yield similar magnitudes; yet, broken into its components, SGRFs produce peak magnitudes approximately 15-18% that of peak VGRFs. Consequently research quantifying GRFs during STS must be aware of the effects of SGRFs. Newtonian physics dictates that a degree of the SGRFs will be translated into the ankle, knee and hip joints and therefore it is imperative to acknowledge that VGRFs may not be the only force variable affecting STS performance. This may be particularly relevant in the study of affected populations were compensatory and asymmetrical movements are more prevalent.

In the Burdett *et al.* study peak vertical ground reaction forces did not differ significantly with relation to leg dominances (1). Similarly, our data yielded no significant relationship between asymmetry and leg motor-dominance. Consequently, asymmetry is not predictable by evaluating footedness alone. From the favoritism analysis, participants did not consistently develop larger peak JMs or GRFs in one leg; favouring one side during one trial, and the contralateral in the next. No discernible patterns resulted from this analysis.

Further investigation is necessary to accurately predict the causes of asymmetry. As a result, when evaluating STS movements, it is important that both legs be evaluated at the same time, in addition to conducting several trials per participant. Due to the unpredictability of asymmetric peak JMs and GRFs, it is possible that one leg will develop higher JMs or GRFs in one trial and

the contralateral leg in the next trial. Therefore, if only one leg is instrumented per trial and no accurate prediction of asymmetry is available, the biomechanics of this movement may be misrepresented. From our data, the biomechanical requirements of the STS motion may be misrepresented by as much as 40% for peak JM at the ankle, 26% at the knee and 37% at the hip.

Limitations

The sample size of this study is the first limitation. Acquiring more data would potentially aid in emphasizing results observed during this study, or bring to light trends that may be in fact coincidental of the smaller sample.

This study, like most current literature, analyzes peak values developed during STS. Although this analysis will provide an indication of the maximum mechanical requirements of the body, investigation of how accurately peak values represent the entire STS cycle is warranted. Chapter 1 Part 2 further investigates this point.

Furthermore, our favoritism analysis potentially polarized results by selecting JMs or GRFs exclusively in one leg or the other as the favored without developing a category for very small or negligible differences. Further investigation is warranted to develop clinically meaningful values to dictate what degree of asymmetry will impact STS movements.

A further limitation lies in the choice of motion marker placement. No 'gold standard' exists for lower extremity placements and non-sagittal motion has been shown to vary with marker placement protocol in activities not related to STS (25). The effects of marker protocol on STS analysis should be addressed in future research.

Our investigation grouped participants through a series of tests addressing skill and ultimately leg motor-dominance. However, a potential relationship between leg strength asymmetry and JM or GRF asymmetry may exist. No measure of limb strength- dominance was collected and therefore warrants future investigation.

Part 2

Characterizing Asymmetry Across the Whole Sit-to-Stand Cycle

STS is a dynamic and time dependent movement in which the muscular force output and corresponding joint moments on each side follow a certain loading cycle. The peak JM is achieved at a single instant during that cycle and thus may not be a comprehensive measure of the asymmetry during STS movements. The aim of this part is to characterize asymmetry over the whole duration of the STS movement. This is achieved by introducing novel measures that are able to characterize various forms of asymmetry in the STS cycle.

As discussed in Chapter 1, Part 1, current literature commonly relies on peak JM and/or JP values as an indication of asymmetry however; the timing of this peak condition, and how the body arrives there has yet to be investigated. Therefore, the first objective of this part will be to investigate if a difference exists in the time at which each joint arrives at its peak condition relative to its contralateral joint. This measure will be defined as the peak offset.

The second objective will be to investigate JM and JP development in the left and right side of the body. Particular focus will be given to linear dependence; in other words, does the left side JM (or JP) increase (or decrease) while the right side is increasing (or decreasing)?

Symmetry index (SI) plots were created to address the objective of illustrating asymmetrical JM and joint (JP) development over the STS cycle, with the specific intent of identifying regions of maximal and minimal asymmetry.

Recognizing measures of linear dependence cannot fully describe differences between the left and right JM and JP development, and that SI characterizes the relative or percent difference between both sides, the fourth objective of this part was to describe the straight difference (one side subtracted from the other) across joints.

Finally, an analysis of angular impulse and work differences was conducted through integration of the straight difference plots. This analysis was performed to evaluate if a relationship existed

between the amount of time one side was dominating the cycle, and the total excess angular impulse (or work) performed by that side.

Methods

To characterize asymmetry across the whole STS cycle, the data set described in Chapter 1, Part 1 was utilized. Ten STS cycles of each of the 10 participants were evaluated in both legs. Whole cycle, lower extremity JMs, joint angles and joint velocities were extracted for this analysis. JM values were normalized according to participant body mass and height. Joint power (JP) development was determined through the multiplication of the JM value and joint velocity in each body plane at each discrete sample point (sample frequency= 120 Hz).

Data Preprocessing

The Euclidian Norm (vector summation) process discussed in Chapter 1, Part 1 was utilized to determine the resultant JM and JP development over the STS cycle. The STS cycle was defined as occurring during the time interval between mass transfer (anterior torso rotation characterized by hip flexion) and the point at which joint motion ceased (26). As a result of the data collection process, information was recorded prior to and after these points of interest. Consequently a numerical procedure was employed to crop the additional irrelevant data. The torso was assumed to initiate movement symmetrically, therefore either hip could be taken as a reference to identify the initiation of mass transfer, the left hip was selected as the reference joint. Static phase was termed as the areas of little to no hip angle change in the recoded data prior to and following the STS movement. STS initiation was defined as occurring when the hip joint angle fell outside +/- 3 standard deviations of the angle during static phase (as calculated by the first 20 data points). Again, data was sampled at 120 Hz, therefore, these 20 data points represented the first 0.17 seconds of data collection. In all cases, STS movement had not initiated during this time. Completion of the cycle was assumed when the hip joint angle value fell within 3 standard deviations of the final static phase (as determined through the final 10 data points). Similarly, these 10 data points represent the final 0.08 seconds of data collection. In all cases STS motion had ceased prior to this interval.

Since each STS trial now assumed a definite initiation and completion, average JM and JP curves for each participant were determined for each leg using the functional data analysis procedure described below (27). The goal was to average each participant's 10 trials across the whole STS cycle and report these values with reference to % STS completion. In other words the objective was to achieve an average JM (and JP) curve for each of the left and right side joints. These averaged JM and JP curves would be with reference to % completion of the STS cycle (0% indicating initiation of STS, and 100% indicating completion of STS).

Motion analysis ASCII files from Visual 3D software (C-Motion Inc., Germantown, MD, USA) were imported into Mathematica (Wolfram, Champaign, IL, USA). The percentage completion of each STS cycle was determined as a function of the number of data points (frames) recorded. Since the motion analysis data was as a collection of discrete data points (captured at 120Hz), traditional methods to average a participant's 10 trials were not possible since data points rarely lined up. In other words, each STS trial did not take precisely the same time and the resulting percent intervals in each of the 10 trials were not equivalent. As a result, a linear interpolation function was utilized in Mathematica. This function was able to 'bridge the gap' between discrete data points and allowed for the averaging of each participant's 10 trials. Average JM and JP values were calculated for each leg and reported with reference to % STS completion on 2% intervals (50 data points in total). Sample Mathematica code is provided in Appendix B.

Peak Offset Calculations

Peak offset was defined as the interval of time (in units of % STS completion) between the peak JM (or JP) value of a joint on one side and the contralateral joint. The peak value was defined as the maximum absolute value occurring during the STS interval. From the averaged JM and JP curves described above, the times at which peak values occurred (for each joint) were collected on the left and right leg independently. The time interval between the left and right side peak values determined the peak offset for each joint. Figure 1-3 graphically illustrates this procedure.

Figure 1-3 Graphical Representation of Peak Offset Procedure
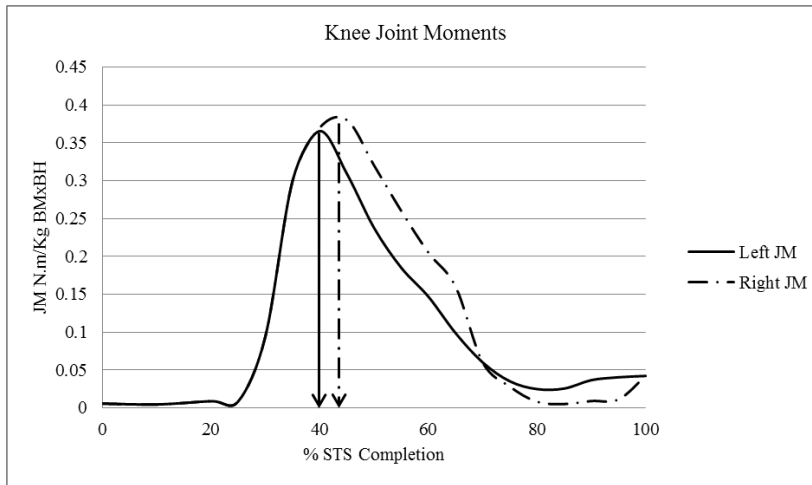
Typical procedure to identify the time at which each side's peak occurred. A typical knee JM curve is shown above, this procedure was conducted for both JM and JP curves at each joint for each participant.

The times at which each peak value occurred were also arranged into two groups, first side to peak and last side to peak. A paired, one-tailed t-test was conducted to investigate if a significant difference existed between the mean time at which the first peak occurs and the last peak occurs for each joint using data from all 10 participants. $P<0.05$ was assumed to indicate a significant difference between the means of any two groups. This procedure was repeated for both JM and JP at the ankle, knee and hip.

Pearson Correlation Calculations

Pearson Correlation was utilized to act as a single-numerical indicator to describe linear dependence of one joint to its contralateral. In other words, does the left side JM (or JP) increase (or decrease) while the right side is increasing (or decreasing)? Using the averaged JM and JP data, Pearson's Correlation Coefficients were determined between the left and right JM and JP curves of each joint.

Symmetry Index Calculations

As described in Chapter 1, Part 1, a commonly employed technique during peak JM or JP studies is to analyze the Symmetry Index (relative or percent difference of the left and right side). As a means of visualization of asymmetric JM and JP development, and identifying regions of maximal and minimal asymmetry, this technique was expanded upon. The symmetry index over

the whole STS cycle (at each 2% STS interval) was calculated between the averaged left and right sides. These JM and JP SI values were then plotted for each joint of each participant.

Straight Difference Calculations

To characterize the side dominance of JM and JP development over the STS cycle, straight difference (SDIF) plots were utilized. These plots allowed for a visualization of which side was producing the largest JM or JP values, and characterized the magnitude of these differences over the whole cycle. Using the left side as a reference, the difference (averaged right subtracted from averaged left) was calculated at each 2% STS interval. Since the left was assumed the reference side, a positive SDIF indicated an excess contribution from the left side relative to the right (inversely a negative SDIF for the right side excess). Straight difference values of each participant were calculated and plotted over the whole STS cycle for the JM and JP of all three joints. A graphical representation of this procedure is shown in Figure 1-4.

Figure 1-4 Graphical Representation of Straight Difference Procedure
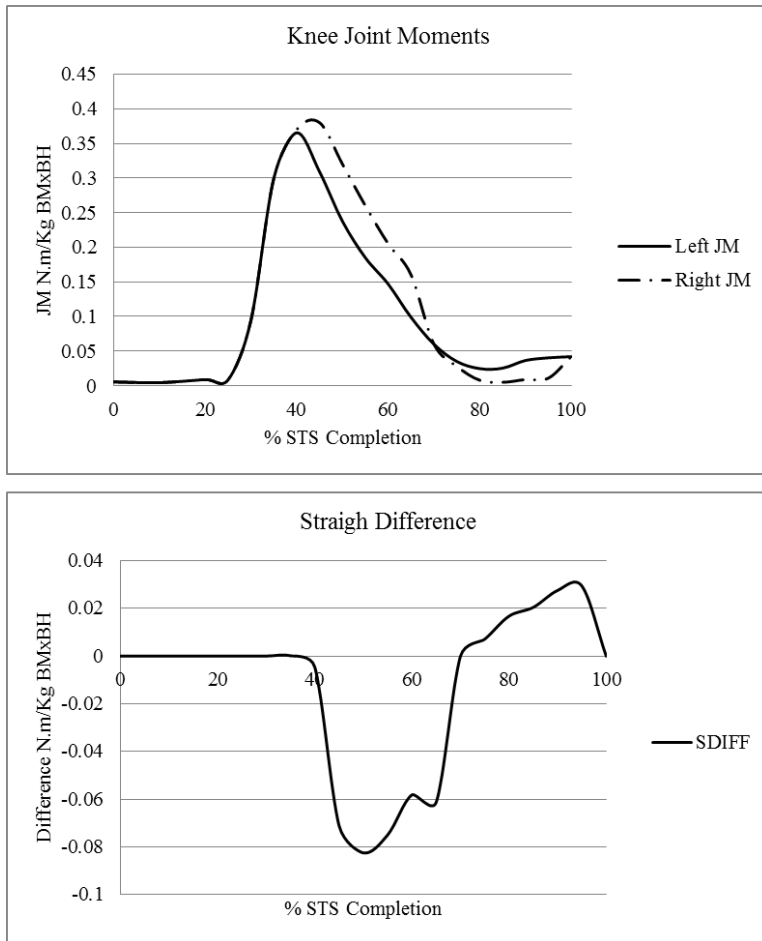
Top: a typical set of knee JM plots for the left and right side. Bottom: the resulting SDIFF plot (left JM – Right JM) from the typical knee JM data. This procedure was conducted for both JM and JP curves at each joint for each participant.

To understand the development of these excess contributions, the straight difference plots were categorized based on gross slope change. This procedure grouped each participant's SDIF plot based on slope reversals, a shift from positive to negative (or negative to positive) slope. A slope reversal was determined to occur if a shift from positive to negative (or negative to positive) slope took place and the amplitude of the SDIF to follow exceeded 25% the absolute peak value of the plot; in other words values in excess of 25% of the global maximum or minimum (whichever is largest). Therefore this procedure would neglect minor fluctuations in the SDIF and focus only on gross slope changes.

Corresponding to each joint, participants were categorized based on the number of slope reversal experienced. The number of categories participants fell in to for each joint was representative of the number of dominance strategies displayed in the participant group (n=10).

Angular Impulse, Work and Time Calculations

Percent angular impulse (PAI) and percent work (PW) were utilized as a measure to characterize the relationship between length of time a side produced an excess JM or JP (length of time a side dominated), and the total excess impulse (or work) that resulted from that side during this interval. Using the SDIF plots, the difference in the left and right side PAI was defined as the integral of the SDIF JM data across the whole STS cycle; similarly PW difference was defined as the integral of the SDIF JP data. Since JM and JP data sets were a series of discrete points at 2% STS completion intervals, a simple summation multiplied by the 2% interval was used to arrive at their integral values.

Since PAI and PW values were derived from the SDIF plots, the positive component of the total integral value would therefore be indicative of the excess impulse or work performed by the left joint, inversely a negative value would indicate right joint excess. Therefore, PAI and PW values were sub divided into two further categories representing positive and negative integral components. These categories were arrived at through exclusive integration of positive and negative JM (or JP) SDIF values respectively. The time (in units of % STS completion) a JM or JP SDIF plot remained positive in magnitude was recorded and defined as the positive %time, similarly, this was conducted for negative values and defined as negative %time. A graphical representation of this procedure is seen in Figure 1-5.

Figure 1-5 Graphical Representation of Percent Angular Impulse Procedure
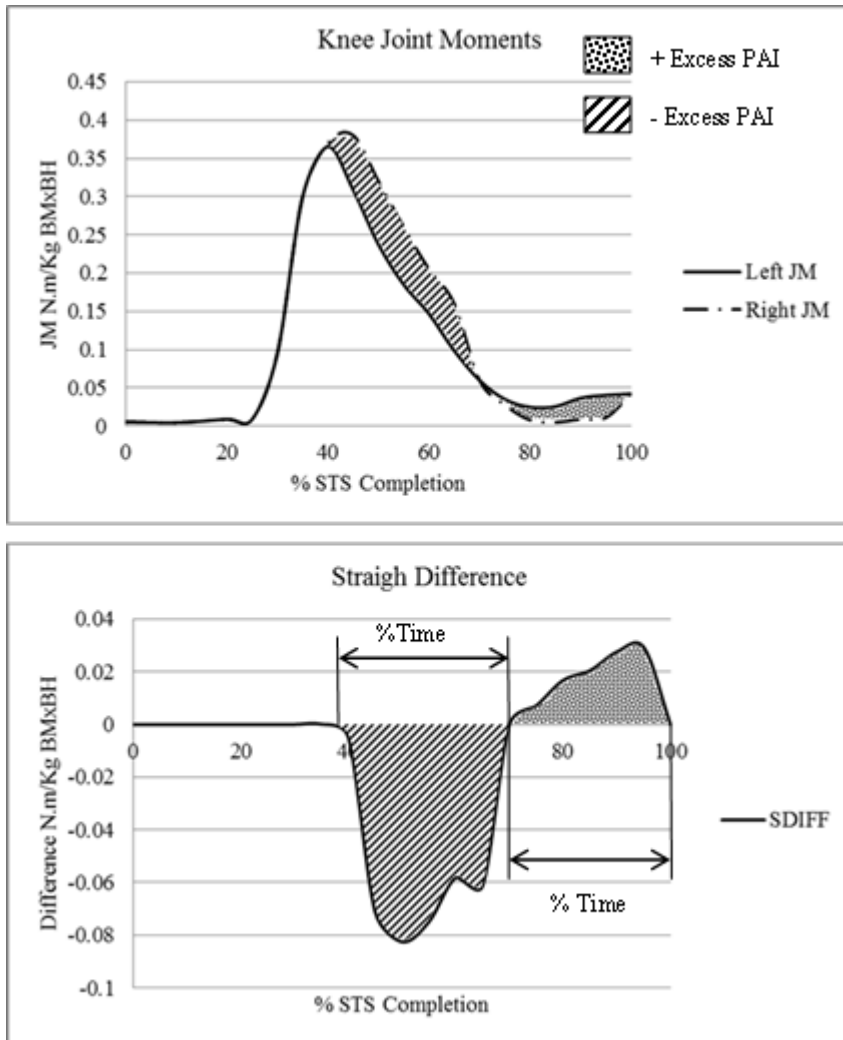
Top: identification of areas of excess JM contribution. Bottom: integration of the SDIFF curve to identify the excess PAI values. Negative PAI is representative of right side excess and positive values indicate areas of left side excess. The time period over which these areas of excess occur are highlighted in the figure.

In total the participant group produced 10 positive PAI and PW values (positive SDIF JM and JP integral components) and 10 corresponding positive %time values for each joint (similarly 10 negative PAI, PW and %time values). For each joint, each of the 10 participants' positive PAI values was plotted corresponding to their determined % time positive values. This procedure was repeated for % time negative and negative integral values as well as PW values.

The above plots were utilized to characterize the relationship between length of time (in unit of % STS completion) a side dominated, and the total excess impulse (or excess work) that resulted from that side during this interval. By assuming an intercept at the origin, polynomial regression

curves were applied to these plots in an attempt to mathematically interpret the relationships. Pearson Correlation Coefficients were utilized to describe the fit of the polynomial curves to their corresponding data.

Results

<u>Peak Offset</u>

Peak offset values ranged from 0 through 40% completion of STS. As seen in Table 1-6 offset values at each joint were found to be larger when evaluating JP when compared to JM. On average the ankle produced the largest JM and JP offset values of the three joints (3.6% STS completion, SD: 5.15 and 12.0% STS completion, SD: 14.30 respectively). The smallest average peak offset was determined at the knee, again this pattern was found in both JM and JP values (0.80% STS completion, SD: 1.03 and 1.00% STS completion, SD: 1.05 respectively). A table of offset results for each participant is included in Appendix C.

JM and JP peak time values were divided into two groups (first to peak and last to peaks) for each joint, and a series of t-tests were performed. These tests were utilized as a statistical interpretation of the significance of the differences in the mean values of these two groups for each joint. As seen in Table 1-6 a significant difference was found in the peak times of both JM and JP values in the ankles and knees of the participant group ($P<0.05$). Further significant differences were found in the JP peak timing of the hips. However the JM peak times at the hip displayed no significant difference.

Table 1-6 Average JM and JP Peak Offest Values and Corresponding P-values

Joint	JM (%)	SD	p-value	JP (%)	SD	p-value
Ankle	3.60	5.15	0.027	12.00	14.30	0.017
Knee	0.80	1.03	0.018	1.00	1.05	0.047
Hip	2.00	4.99	0.118	4.40	7.99	0.049

JM and JP are the average joint moment and joint power offset values in %time of the STS cycle. SD is the standard deviation of these values. P-value shows the results from the t-test of first to peak compared to last to peak. P<0.05 was assumed to show a significant difference in these mean times

Pearson Correlation

Pearson correlations across the left and right leg JM and JP values were determined. At all three joints in both JM and JP values were determined to be very close to a value of 1.00. This indicates a strong linear dependence between left and right JM and JP development across the STS cycle. R values as well as maximum, minimum, and mean values are reported in Table 1-7 and 8.

Table 1-7 Pearson Correlation Coefficients of the Left and Right Side

		Participant									
	Joint	1	2	3	4	5	6	7	8	9	10
JM	Ankle	0.976	0.988	0.995	0.972	0.957	0.978	0.976	0.957	0.973	0.959
	Knee	0.998	0.989	0.995	0.994	0.994	0.980	0.992	0.979	0.931	0.984
	Hip	0.970	0.973	0.989	0.989	0.891	0.987	0.924	0.853	0.968	0.984
Power	Ankle	0.952	0.973	0.912	0.705	0.944	0.948	0.988	0.804	0.771	0.821
	Knee	0.995	0.993	0.991	0.989	0.983	0.985	0.997	0.948	0.964	0.990
	Hip	0.936	0.970	0.989	0.969	0.828	0.993	0.953	0.783	0.984	0.994

The top half of the table represents joint moment Pearson correlation coefficients of each participant according to the joint of interest. Similarly the bottom half represents the correlation in joint power values.

Table 1-8 Minimum, Maximum and Mean Correlation Values

	Joint	Max	Min	Mean	SD
		Correlation Values			
JM	Ankle	0.995	0.957	0.973	0.013
	Knee	0.998	0.931	0.984	0.020
	Hip	0.989	0.853	0.953	0.048
Power	Ankle	0.988	0.705	0.882	0.098
	Knee	0.997	0.948	0.983	0.016
	Hip	0.994	0.783	0.940	0.074

The top half of the table represents joint moment R^2 correlation coefficients with the bottom representing joint power. SD signifies the standard deviation among participants.

Symmetry Index

Symmetry index values of the left side JM (and JP) values relative to the right were calculated at 2% STS completion intervals. This procedure allowed the plotting of SI values across the STS cycle for each joint's JM and JP values. Large fluctuations in SI values were found at each joint in both JM and JP. When visually comparing plots, little to no consistency was found between participants. Figure 1-6 illustrates the Symmetry index plots of participant 1. The remaining SI plots can be found in Appendix D.

Figure 1-6 Typical Symmetry Index Plots
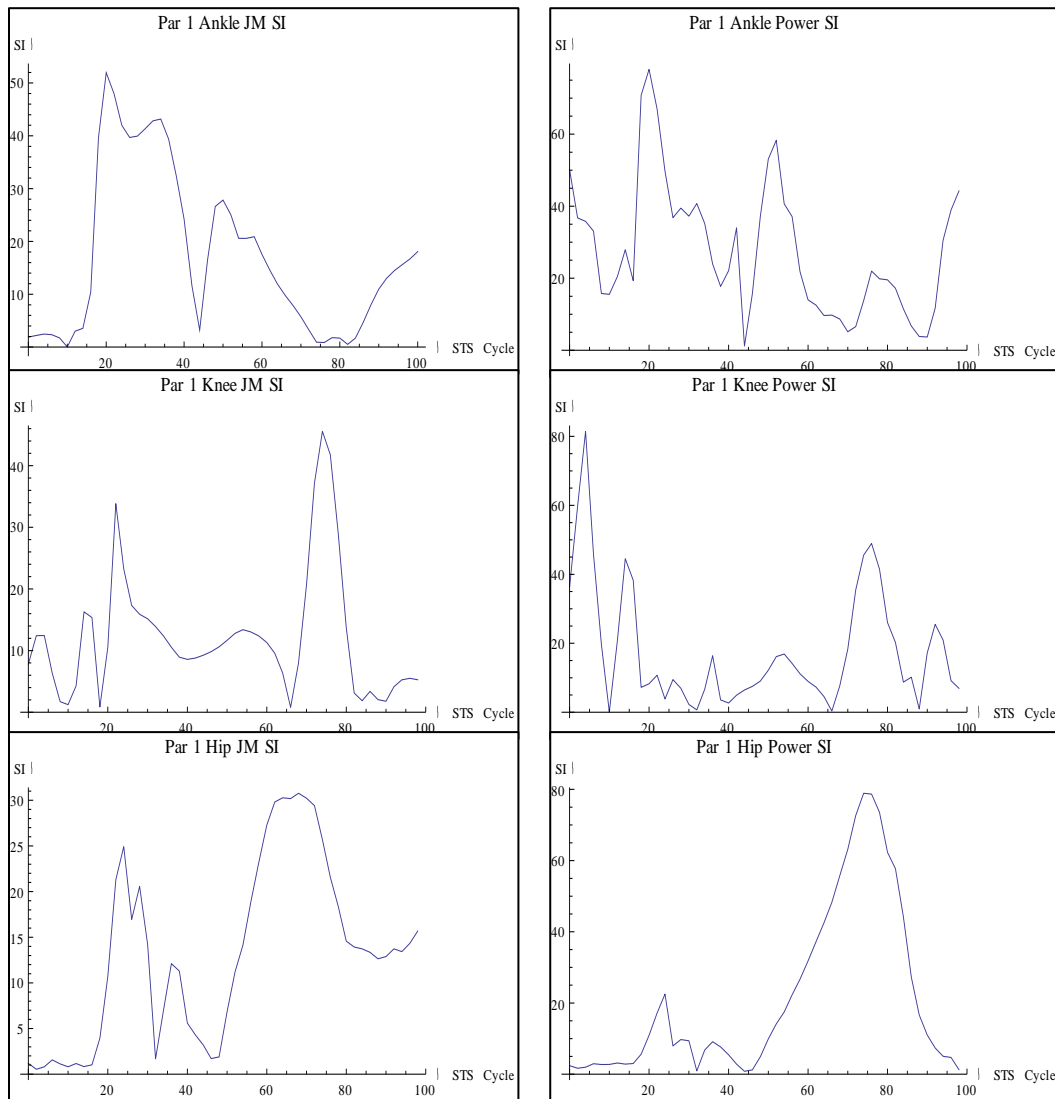
Typical plots were taken from Participant 1. The left column illustrates symmetry Index (SI) curves for the joint moment (JM) data, and the right column for the joint power (JP) data. The plots from top to bottom represent data found at the ankle, knee and hip respectively.

Straight Difference

The number of slope reversals in the JM and JP SDIF plots were recorded for each participant's three joints. Based on the number of slope reversals, participants were categorized into groups. In the JM data at the ankle, participants demonstrated 0 to 3 slope reversal. As a result participants can be divided into 4 groups, and correspondingly 5 groups for JP data. The ankle shows the largest number of slope reversal categories of all the three joints. The JM data at the knee and hip both show 3 groupings representative of 1, 2 or 3 and 1, 2 or 4 reversals

respectively. Finally the JP at the knee can be divided into 3 groups and 4 groups are found in the hip data. Table 1-9 highlights the number of slope reversals demonstrated by each participant and the corresponding number of groups determined at each joint.

Table 1-9 Gross Slope Changes in Joint Moment and Joint Power Data

		Number of Slope Reversals										Groups	Average	SD
	Participant	1	2	3	4	5	6	7	8	9	10			
Ankle	JM	3	0	2	1	3	3	3	2	2	1	4	2.00	1.05
	JP	6	6	4	2	3	6	5	2	6	6	5	4.60	1.71
Knee	JM	2	1	2	3	3	1	1	2	2	2	3	1.90	0.74
	JP	2	1	2	2	3	1	1	2	2	2	3	1.80	0.63
Hip	JM	4	1	2	2	2	4	2	2	2	1	3	2.20	1.03
	JP	4	1	3	2	2	4	2	2	2	1	4	2.30	1.06

The number of slope changes is organized by participant and joint. JM represents joint moment data and JP, joint power. Groups indicate the number of slope reversal categories seen in the participant. Average and SD show the mean number of slope reversals at each joint and the corresponding standard deviation.

Angular Impulse, Work and Time

To characterize the relationship between length of time (in unit of % STS completion) a side dominated, and the total excess impulse (or work) that resulted from that side during this interval, plots representing each participant positive PAI (or PW) difference and the corresponding %time positive value were created for each joint. Again, these positive plots were representative of left side dominance. This procedure was repeated for negative PAI (and PW) with respect to %time negative, and represented right side dominance. These plotted values can be seen in Figure 1-7.

To mathematically characterize the %time dominance and PAI (or PW) relationships from these plots, a second order polynomial curve of the form, $y=ax^2+bx$, was utilized (assuming an intercept at the origin). The coefficients of determination were calculated to evaluate the ability of the resulting polynomial expression to fit the experimental data. PAI results and their corresponding R^2 correlation values are reported in Table 1-10. The polynomial expression overlaid on the experiments PAI (or PW) values can be seen in Figure 1-7.

Table 1-10 Percent Angular Impulse (PAI) Polynomial Coefficients

		PAI		
		a	b	R^2
Ankle	Positive	3.0×10^{-4}	2.3×10^{-3}	0.55
	Negative	-5.0×10^{-4}	9.9×10^{-3}	0.93
Knee	Positive	-5.0×10^{-5}	2.3×10^{-2}	0.76
	Negative	-3.0×10^{-4}	4.5×10^{-3}	0.85
Hip	Positive	1.1×10^{-3}	-2.7×10^{-2}	0.58
	Negative	-9.0×10^{-4}	2.1×10^{-2}	0.85

Polynomial coefficient of the form $y=ax^2+bx$. R^2 represents the coefficient of determination of the polynomial formula to the experimental data. Each joint is subdivided into coefficients for positive PAI with its relation to %time positive, and negative PAI and its relation to %time negative.

Similar to the PAI results, PW results are reported in Table 1-11. Again a second order polynomial was used to describe the relationship between positive PW and % STS time. These percent work plots produced substantially lower correlation values than the PAI curves described above. In an attempt to find a stronger mathematical relation, a third order and fourth order polynomial were also fitted to the data and their corresponding correlation values are reported.

Table 1-11 Percent Work (PW) Polynomial Coefficients

		PW			3rd Order	4th Order
		A	B	R^2	R^2	R^2
Ankle	Positive	1.0×10^{-4}	-2.2×10^{-3}	0.69	0.70	0.70
	Negative	-1.0×10^{-4}	2.6×10^{-3}	0.75	0.82	0.83
Knee	Positive	-1.0×10^{-4}	1.7×10^{-2}	0.23	0.29	0.30
	Negative	-2.0×10^{-4}	-7.8×10^{-3}	0.69	0.69	0.69
Hip	Positive	-1.0×10^{-4}	3.1×10^{-2}	0.08	0.08	0.24
	Negative	-4.0×10^{-4}	4.1×10^{-3}	0.33	0.34	0.34

Polynomial coefficient of the form $y=ax^2+bx$. R^2 represents the coefficient of determination of the polynomial formula to the experimental data. Each joint is subdivided into coefficients for positive PAI with its relation to %time positive, and negative PAI and its relation to %time negative. Third and fourth order polynomial curves were also fit to the experimental data and the corresponding R^2 correlation coefficients are shown.

Figure 1-7 Positive PAI and PW Plotted Against %Time Positive or Negative
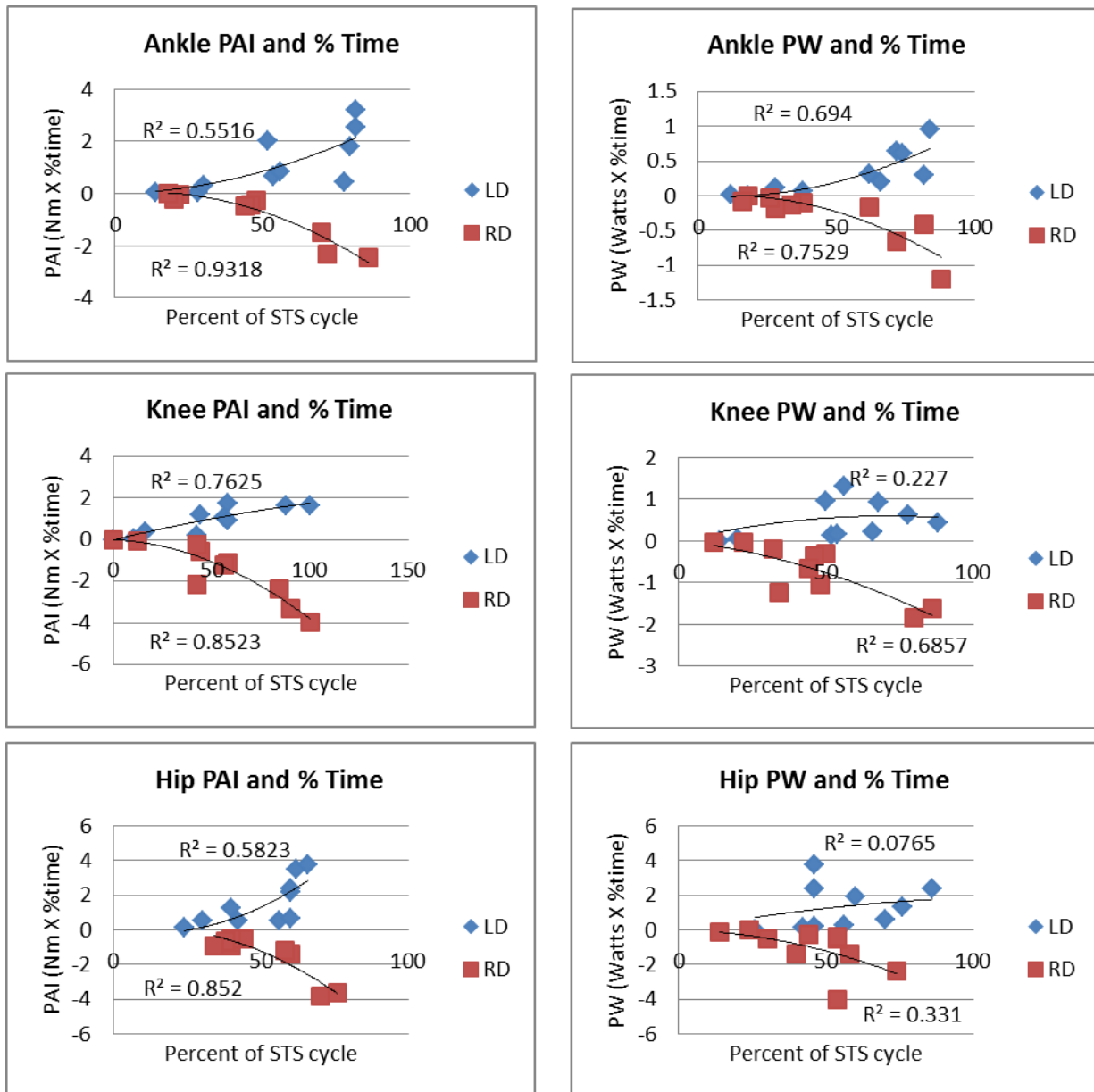
The blue diamonds represent the positive PAI or PW plot against time the JM or JP remain positive respectively. Since these values are positive, LD is an abbreviation for left side dominant. Inversely the red squares represent the negative equivalents. Since these values are negative, RD is an abbreviation for right side dominant. The black line represents the second order polynomial curve fit to the experimental data.

Discussion

STS is a dynamic and correspondingly time-dependent movement. Consequently, the magnitude of the biomechanical forces and moments developed during this maneuver vary with respect to time. Current literature addresses asymmetry during STS through a single numerical indicator, in

most cases peak joint moments (1) (4) (5) (6) (9), and often utilizes the symmetry index to quantify bilateral differences (1) (5) (6). Although the evaluation of peak JMs provides an indication of the maximum mechanical requirements of the body, it neglects how the body arrives at this condition, and when during the STS cycle this value occurs.

Peak Offset

The peak offset values allowed for the illustration of the differences in time of when one side's joint peaks compared to the contralateral joint. The ankle was found to produce the largest average peak offset of all three joints in both JM and JP data (5.15% and 12.00% respectively). Whereas the knee was found to produce the smallest average offset in both JM and JP data with values of 0.80% and 1.05% respectively. Statistically, these peak offset values were determined to be significant in peak JP values for all three joints, and in the JM values at the ankle and knee ($p<0.05$). No statistical difference was determined in the peak JM offset of the hip ($p>0.05$).

As a result, comparing peak values is not necessarily comparing values from the same point in time. It is merely a comparison of the maximum mechanical requirement during STS. This evaluation is not an indication of actual SI at the time point where an individual peak occurs; rather it is a comparison of two values that may occur at different time points during STS. Therefore, the evaluation of peak values alone may highlight one characteristic of asymmetry, but may not be sufficient to characterize asymmetry as a whole during STS.

Furthermore, the results suggest that, especially at the ankle level, symmetry should be evaluated using a time dependent measure since peak values may be occurring at significantly different time points. However, in the case of the knee, very little peak offset was found. Therefore, this presents an avenue for further research. The determination of clinically relevant offset values would help further understand the degree of validity a simple peak analysis holds at each joint.

Pearson Correlation

When comparing JM and JP development curves across the left and right side of each participant, the resulting Pearson Coefficients suggested very strong correlation. This is a result that one may intuitively predict. On average the weakest correlations were found at the hip for

the JM curves and the ankle for the JP curves (R= 0.95 and 0.88 respectively). However, even these values suggest a very strong linear dependence between the left and right side. In other words as the left side JM or JP is increasing positively, the right side can be expected to increase at a linearly comparable rate (similar for decreasing values). Ultimately Pearson correlation was not able to sufficiently characterize difference across the STS cycle, but it was able to show a strong overall relationship in how the left and right side accomplish the STS task.

Symmetry Index

When plotting the SI values over the STS cycle, little consistency across participants was found. Large fluctuations were displayed at all three joints in both JM and JP data. An explanation for this phenomenon can be offered through the nature of the SI calculation being a measure of relative (percent) difference. For example, at the early stages of STS, the knee JM values are relatively small when compared to its peak values. During this stage differences between the left and right side may be irrelevant since both values are already close to zero. Mathematically, a small (or irrelevant) difference between the left and right side would be divided by a very small denominator. This SI calculation would then result in a very large SI being calculated. This artificial inflation issue has been identified in motion analysis studies focusing on gait (28) (29). It would appear from the large fluctuations and inconsistencies found in this study's SI plots, that it is a relevant issue in STS motions as well. Therefore, SI may not produce reliable results when analysing JM and JP development over the whole STS cycle.

Straight Difference

The straight difference plot shows which side produces a larger JM or JP, with the magnitude of the difference being plotted against % STS completion. A positive difference would indicate an excess JM or JP contribution from the left side (left side dominance), conversely negative values indicates right side dominance. Furthermore, these straight difference plots allowed for the characterization of STS strategies based on slope reversals. A slope reversal characterizes changes in the rate of excess contribution of one joint relative to the contralateral. At these time points, either one joint is reducing its excess contribution to the STS movement, or the contralateral side is increasing its excess contribution. In either case a slope reversal is an indication of asymmetry in the rate of JM (or JP) development. These reversals can therefore be

viewed as different strategies for which the body develops JM and JP. In other words the different ways the body may share JM or JP requirements between the left and right side.

The ankle was determined to have the largest number of groups, or strategies, for both JM and JP (4 and 5 respectively). An explanation of this can be offered due to the high mobility of the ankle joint. Basic ankle function, flexibility and strength can be tied to balance and posture during functional tasks such as STS (30) (31). It can be argued that the ankle shows the largest number of STS strategies purely due to its integral role in balance and stability.

Furthermore, no apparent relationship presented itself between participants across joints. For instance participants 1 and 5 both demonstrated a 3 reversal ankle strategy; however this was the only similarity across joints that was shared. Participant 1 showed a 2 and 4 reversal strategy at their knee and hip respectively; whereas participant 5 illustrated a 3 and 2 reversal strategy for these joints. The lack of commonality suggests that reversal strategy of one joint may not be predictable by viewing the other two. This further suggests asymmetry is a result of less obvious causes. A possible explanation is to attribute asymmetry to the body dynamically balancing itself during STS transfer. This is again supported through the known role of the ankle in balance and stability, and the larger number of ankle strategies found during STS. However, further variables such as limb proportions, initial foot placement and strength dominance may also have an effect. Further investigation is warranted to determine appropriate predictors of asymmetry over the whole STS cycle.

Angular Impulse, Work and Time

Percent angular impulse difference (PAI) and percent work difference (PW) allow for a single numerical dominance-related value representative of the whole STS cycle. By further dividing these PAI and PW values into the positive and negative components, it was possible to see the total excess impulse or excess power developed by the left and right sider respectively. Since PAI and PW were arrived at through integration of SDIF JM and JP curves, it was also possible to calculate the time interval each side spent dominating during JM or JP development. By plotting the time a side spent dominating with respect to its resulting angular impulse and work, it was possible to illustrate a relationship between these two variables.

As one may intuitively predict, the amount of excess angular impulse or work of one side increased with the time that side spent dominating the JM or JP development. When evaluating the PAI data in Figure 1-7, the relationship between %time dominating and PAI difference are described with a concave descriptive function. This shows that the longer (in %time) a side spends dominating an exponentially larger PAI on that side will correspond.

Through visual inspection a similar relationship can be seen in the PW data of Figure 1-7. Again, the longer a side spends dominating, the larger the corresponding PW value that will be developed. However, the nature of this relationship was not able to be described in the same manner as the PAI data. PW values did not appear to fit a polynomial curve as well as the PAI curves, with R^2 values ranging from 0.75 through 0.08. Varying the order of polynomial may have provided better fits for individual joint data but not for all the data as a whole. The data set was unable to be adequately described by a polynomial relationship, and as a result it is recommended a larger sample size to be used. This would allow either for the development of a stronger %time to PAI/PW relationship, or further confirmation of a lack thereof.

Chapter 1 Conclusions

Healthy STS movements are often assumed bilaterally symmetric in current literature. However, little research has been conducted to validate this assumption. Of the current studies on healthy STS bilateral symmetry, all utilize a discrete value as a numerical indication of the degree of symmetry (most often peak JMs or GRFs) (9) (1). Furthermore these studies often evaluate STS movements two dimensionally by viewing only sagittal plane movements and vertical ground reaction force (9) (1).

This thesis utilized a Euclidian Norm vector summation process to account for joint moment, ground reaction forces and joint power development three dimensionally in 10 healthy male participants. A peak analysis study was conducted to analyze bilateral symmetry in peak JM and GRF forces. Statistically significant differences were found in all three lower extremity peak JMs as well as GRFs. A second test was conducted to evaluate if a relationship could be drawn between these asymmetric values and a participant's motor dominant limb. No statistical relationship was found, suggesting asymmetry may not be predictable through motor dominance alone.

Using the same data set, a second study was performed to characterize asymmetry over the whole STS cycle using a series of mathematical tests. The time at which the peak JM or JP value occurred on each side of the participants was recorded. Significant differences were found in all joints with exception of the hip JM. This suggests simply analyzing peak values may be one characteristic of STS asymmetry, but not representative of bilateral symmetry as a whole. Pearson correlation coefficients were determined between the left and right side of each participant. High correlation between both sides was found in all participants and joints suggesting a strong linear relationship between JM and JP development across the body. The symmetry index of the left and right side was plotted for each joint across the whole STS cycle. Little consistency was found in these plots across participants. This result can be explained due to an artificial inflation of the SI that is mathematically inherent to its calculation. The straight difference of the left and right side were plotted for JM and JP results. The number of slope reversals in these SDIF plots was indicative of shifting degrees of leg dominance during the

1-35

cycle. Participants were categorized by the number of slope reversals present at each of their joints. The number of categories formed from the participant group at the ankle, knee and hip represented the number of different strategies to achieve the STS task. In other words the number of different ways JM or JP requirements was shared between the left and right side. The ankle was found to have the largest variation in the number of reversal (or strategies) across participants. Finally integrating the JM and JP curves over the %completion of the STS cycle produced values for percent angular impulse and percent work. A polynomial relationship was found between the time the JM curve remains positive, and the positive component of the PAI (similarity for the negative values). The percent work values did not lend themselves to form as strong polynomial relationships with % time. A larger sample size would help alleviate this issue. However, in all cases the longer one side dominated JM or JP development, could be related to a larger excess angular impulse or work contribution.

Overall STS is a movement that displays a degree of asymmetry in healthy movements. It is important to realize that this movement is dynamic and time dependent. Therefore a simple peak analysis may not be able to capture the entirety of the asymmetry. From the whole cycle analysis it is possible to see a highly related nature of the left and right side JM and JP development. It is theorized that asymmetry developed during STS does not present itself predictably through the analysis lower extremity JM and JP values alone. It may therefore be a result of a combination of less predictable variable such as balance, joint proportions, and initial foot placement among others.

Bibliography

1. *Symmetry of ground reaction forces and muscle activity in asymptomatic subjects during walking, sit-to-stand, and stand-to-sit tasks.* **Burnett, D., et al., et al.** s.l. : Journal of Electromyography and Kinesiology, 2011, pp. 610-615.

2. *Kinematics of rising from a chair: Image-based anaysis of the sagittal hip-spine movement pattern in elderly people who are healthy.* **Fotoohabadi, M R., Tully, E A. and Galea, M P.** 4, s.l. : Journal of the American Physical Therapy Association, 2012, Vol. 90, pp. 561-571.

3. *How to quantify knee function after total knee arthroplasty?* **Boonstra, M., De Waal Malefijt, M. and Verdonschot, N.** s.l. : The Knee, 2008, Vol. 15, pp. 390-395.

4. *Sit-to-Stand Movement as a Performance-Based Measure for Patients With Total Knee Arthroplasty.* **Boonstra, M., et al., et al.** 2, s.l. : Physical Therapy, 2010, Vol. 90, pp. 149-156.

5. *Weight-Bearing Asymmetry During Sit-Stand Transitions Related to Impairment and Functional Mobility After Total Knee Arthroplasty.* **Christiansen, C., et al., et al.** 10, s.l. : Archives of Physical Medicine and Rehabilitation, 2011, Vol. 92, pp. 1624-1629.

6. *Weight distribution symmetry during the sit-to-stand movement of unilateral transtibial amputees.* **Agrawal, V., et al., et al.** 7, s.l. : Ergonomics, 2011, Vol. 54, pp. 656-664.

7. *Differences Between Grab Rail Position and Orientation During the Assisted Sit-to-Stand for Able-Bodied Older Adults.* **O'Meara, D. and Smith, R.** s.l. : Journal of Applied Biomechanics, 2005, Vol. 21, pp. 57-71.

8. *Side difference in the hip and knee joint moments during sit-to-stand and stand-to-sit tasks in individuals with hemiparesis.* **Roy, G., et al., et al.** s.l. : Clinical Biomechanics, 2007, Vol. 22, pp. 795-804.

9. *On the Assumption of Bilateral Lower Extremity Join Moment.* **Lundin, T M., Grabiner, M D. and Jahnigen, D W.** 1, s.l. : Journal of Biomechanics, 1995, Vol. 28, pp. 109-112.

10. *Biomechanical analysis of relationship between movement time and joint moment development during sit-to-stand task.* **Yoshioka, S., et al., et al.** 27, s.l. : Biomedical Engineering Online, 2009, Vol. 8, pp. 1-9.

11. *Kinemantics of Sagittal Spine and Lower Limb Movements in Healthy Older Adults During Sit-to-Stand from Two Seat Heights.* **Kuo, Y., Tully, E. and Galea, M.** 1, s.l. : SPINE, 2009, Vol. 35.

12. *Dynamics of sit-to-stand movement.* **Roberts, P D. and McCollum, G.** s.l. : Biological Cybernetics, 1996, Vol. 74, pp. 147-157.

13. *Biomechanical Analysis of Sit-to-Stand Movement in Normal and Obese.* **Sibella, F., et al., et al.** 5, s.l. : Clinical Biomechanics, 2003, Vol. 18, pp. 745-750.

14. *A test of the functional asymmetry hypothesis in walking.* **Seeley, M., Umberger, B. and R., Shapiro.** s.l. : Gait and Posture, 2008, Vol. 28, pp. 24–28.

15. *The relation between mild leg-length inequality and able-bodied gait asymmetry.* **Seeley, M., et al., et al.** s.l. : Journal of Sports Science and Medicine, 2010, Vol. 9, pp. 572-579.

16. *Simultaneous, bilateral, and three-dimensional gait analysis of elderly people without impairments.* **Sadeghi, H., et al., et al.** 2, s.l. : American Journal of Physical Medicine and Rehabilitation, 2004, Vol. 83, pp. 112-123.

17. *The isokinetic strength profile of quadriceps and hamstrings in elite volleyball players.* **Hadzic, V., et al., et al.** 1, s.l. : IOS Press, 2010, Vol. 18, pp. 31-37.

18. *Differences in muscle strength in dominant and non-dominant leg in females aged 20e39 years a population-based study.* **Lanshammar, K. and Ribom, E.** 2, s.l. : Physical Therapy in Sport, 2011, Vol. 12, pp. 76-79.

19. *Normalization of joint moments during gait: a comparison of two techniques.* **Moisio, K., et al., et al.** s.l. : Journal of Biomechanics, 2003, Vol. 36, pp. 599-603.

20. *The Measurement of Foot Preference.* **Chapman, J., Chapman, L. and Allen, J.** 3, s.l. : Neuropsychologia, 1987, Vol. 25, pp. 579-584.

21. *Measurement of lower extremity kinematics during level walking.* **Kadaba, M., Ramakrishnan, H. and Wooten, M.** 3, s.l. : Journal of Orthopaedic Research, 1990, Vol. 8, pp. 383-392.

22. **Winter, David A.** *Biomechanics and Motor Control of Human Movement.* [ed.] Second. s.l. : John Wiley & Sons, Inc., 1990. 0-471-50908-6.

23. **Zatsiorsky, V.** *Kinetics of Human Motion.* 1. s.l. : Human Kinetics, 2002.

24. *Use of force platform variables to quantify the effects of chiropractic manipulation on gait symmetry.* **Robinson, R., Herzog, W. and B., Nigg.** 4, s.l. : Journal of Manipulative and Physiological Therapeutics, 1987, Vol. 10, pp. 172-176.

25. *Can hip and knee kinematics be improved by eliminating thigh markers?* **Schulz, B. and Kimmelb, W.** 7, s.l. : Clinical Biomechanics, 2010, Vol. 25, pp. 687-692.

26. *Effects of Ageing on Quadriceps Muscle Strength and on the Foward Shift of the Center of Pressure During Sit-to-Stand Movement from a Chair.* **Miyoshi, K. and al., et.** s.l. : Journal of Physical Therapy Sciences, 2005, Vol. 17, pp. 23-28.

27. **Crane, E., et al., et al.** Functional Data Analysis for Biomechanics. *Theoretical Biomechanics.* s.l. : InTech, 2011.

28. *The symmetry angle: A novel, robust method of quantifying asymmetry.* **Zifchock, R., et al., et al.** s.l. : Gait & Posture, 2008, Vol. 27, pp. 622-627.

29. *Asymmetries in ground reaction force patterns in normal human gait.* **Herzog, W., et al., et al.** 1, 1989, Medicine and Science in Sport and Exercise, Vol. 21, pp. 110-114.

30. *Foot and Ankle Characteristics Associated With Impaired Balance and Functional Ability in Older People.* **Hylton, M., Morris, M. and Lord, S.** 12, s.l. : Journal of Gerontology: MEDICAL SCIENCES, 2005, Vol. 60A, pp. 1546–1552.

31. *Dorsiflexion and dynamic postural control deficits are present in those with chronic ankle instability.* **Hoch, M., et al., et al.** 6, s.l. : Journal of Science and Medicine in Sport, 2012, Vol. 15, pp. 574-579.

Chapter 2

Design, Manufacturing and Testing of an Assistive Sit-to-Stand Knee-Ankle-Foot-Orthosis

Introduction

Knee-Ankle-Foot-Orthoses (KAFOs) are leg braces designed to assist in standing for patients with limited lower extremity function. The brace encompasses the thigh to the foot holding the knee extended and the ankle in a neutral position; thereby controlling balance and joint alignment (1). The intent of the brace is to provide stability and rigidity to the knee and ankle joints as a means of augmenting weight bearing capabilities (2). KAFOs have a variety of applications including: broken bones, arthritic joints, bowleg, knock-knee, knee hyperextension as well as muscular weakness and paralysis (1). A typical KAFO can be seen in Figure 2-1.

Figure 2-1 A Typical KAFO and its Main Components
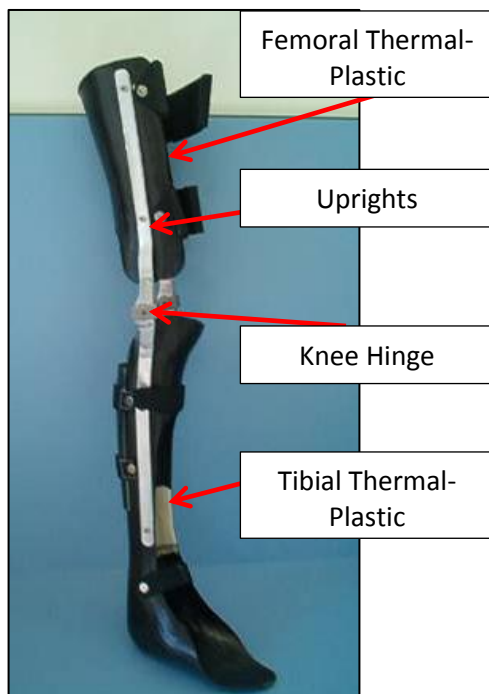
Patients requiring KAFOs are often dependent on a wheelchair. Therefore, standing becomes an important physiological function with benefits including pressure relief, spasticity reduction, bowel and bladder management, among others (3). However, since a KAFO limits knee and ankle motion, rising from a chair becomes a significant challenge. Attempting to stand with straight knees, as compared to flexed knees, creates a larger standing force-moment lever arm

between the ground and the patient's center of mass. As a result of the combination of this altered geometry and the inability to flex the knees, patients must adopt a modified STS strategy. Typically STS while wearing a KAFO involves using fore arm crutches or a walker and substantial upper body strength to hoist oneself from seated position. Due to the users' inability to create a knee extensor moment, the patients will rely on their upper body strength to compensate and provide the anti-gravity moments to stand (Figure 2-2 illustrates these adapted movements). Consequently, substantial demand is placed on the upper body and many KAFO users are unable to achieve STS independently.

Although electronic active-knee-KAFOs do exist, such as the Becker Orthopedic E-Knee, these products are designed to aid users during ambulation and do not develop sufficient forces to assist STS movement. Furthermore, technologically advanced options exist such as Exoskeleton's ReWalk system. However, these systems are not typically used by individual clients due to the significantly higher price when compared to a traditional KAFO. Presently no commercially available product exists to specifically address STS transfer in KAFO users.

Figure 2-2 An Upper Body Dependant Adapted STS Strategy

Due to the extended knees, a large standing force-moment lever arm is created. Consequently, the user must dependent on their upper body to create a moment at the shoulder for compensation. The arrow indicates the sequence of events (left to right).

The University of Alberta's technology transfer office (TEC Edmonton), conducted a series of interviews with five Alberta based physical therapy and orthotic clinicians on behalf of our research team. The first interviewee was Karen Benterude, a physical therapist at the Glenrose Rehabilitation Hospital. Her work includes the rehabilitation of clients with lower extremity

disabilities as well as teaching and training clients for KAFO use. Andreas Donnauer a certified orthotist at the Glenrose rehabilitation hospital was interviewed next. Much of his work includes the fitting manufacturing and maintenance of lower extremity prosthetics and orthotics such as KAFOs. A second orthotist was interviewed. Jim Toller is a practicing orthotist at an independent, Edmonton based orthotic firm, Orthotic Solutions. The fourth interviewee was Louise Miller, a spinal cord injury patient, and the president and founder of the Spinal Cord Injury Treatment Center (SCITCS). Finally Nicola Birchall, the Client Services Coordinator and Hospital Liason at the Canadian Paraplegic Association, was interviewed. The intent of these interviews was to further understand how clients interact with their KAFOs, as well as to seek clinical input on the importance of designing and manufacturing an Assistive STS attachment for existing KAFO braces.

The consensus among the interviewees was, that standing is an important daily function with physiological and physcological benefits associated. The typical KAFO user is generally an individual quick to adopt assistive technology as independence is often a motivator. However, a large deterrent for KAFO use is the lack of STS functionality. KAFO rejection occurs in a very high portion of early users. Literature reports this rejection rate to be as high as 58%-78% (5) (6) (7). This number is consistent with the rejection rates experienced by Karen Benterud. She also reported that of the clients seeking rehabilitative assistance to achieve STS independently, as few as 20% may be able to execute this maneuver independently. However; KAFOs, being a mobility aid, still remain an important part of therapy in clients with lower limb impairment. This is a direct result of the sense of accomplishment and progress the devices may impart.

Part 1

The Design of an Assistive Sit-to-Stand Knee-Ankle-Foot-Orthotic Attachment

The objective of this first part was to design an assistive device to aid KAFO users during STS transfer. Using the data set from Chapter 1, Part 1, the average peak knee extensor moment in healthy STS movements was determined. This value was to serve as a target design value to develop an assistive STS KAFO prototype. It is hypothesized that introducing a mechanically generated knee extension moment in the KAFO, will help alleviate the upper body demand placed on the user.

Methods

Prototype Design

The objective of the prototype is to generate a knee extensor moment in the user's existing KAFO. This additional external knee moment applied by the device, will remove the need for maintaining extended knees in the KAFO during STS; thereby, reducing the upper extremity moment required. To understand the mechanical forces required of the KAFO prototype, the STS motion capture data set described in Chapter 1, Part 1 was utilized. From this data, the average peak knee extensor moment value provided a target design value for the peak torque required of the prototype. According to the data set, average peak knee moments were found between 0.50 and 0.93 N.m./Kg-body mass (mean: 0.71N.m./Kg-BM, SD: 0.14). Therefore, the mean value of 0.71N.m./kg was used to guide the design of the KAFO prototype.

Presently no commercially available product exists to specifically address STS in KAFO users. To begin the prototype design process, device specifications had to be outlined. Discussions were held with engineers, clinicians, and orthotists, at the Edmonton Glenrose Hospital and University of Alberta. These discussions focused on the factors each professional felt were important to a successful design. Of primary importance was recognition that a successful design must perform its function (assist with knee extension), as well as have a high potential for end-user acceptance. Each clinician and engineer was asked to identify factors they felt are pertinent to achieve functionality and user acceptance. A master list of eleven criteria was created; this list

is seen in Table 2-1 of the results section. Based on the professional experience of the clinicians and engineers, these criteria were weighted according to importance. A weighting scale utilized values ranging from 1, indicating very little importance, to 3, indicating very high importance, respectively.

Through further collaboration with physical therapists and orthotists at the Glenrose Rehabilitation Hospital, four conceptual designs for an assistive KAFO were proposed. Each conceptual design would utilize a different method to mechanically generating a knee extension moment in the KAFO. The average peak knee moment value from the motion capture analysis dictated the peak torque each design must develop at the knee joint is 0.71 N.m/Kg. These four designs can be seen in Figure 2-3 and included: placing a motor and torque transmission device concentric with the knee, the use of a torsional spring concentric with the knee, positioning a linear actuator posterior to the knee, and a tensioned cable and pulley system to mimic quadricep force vectors.

Figure 2-3 The Proposed Four Conceptual Assistive Devices
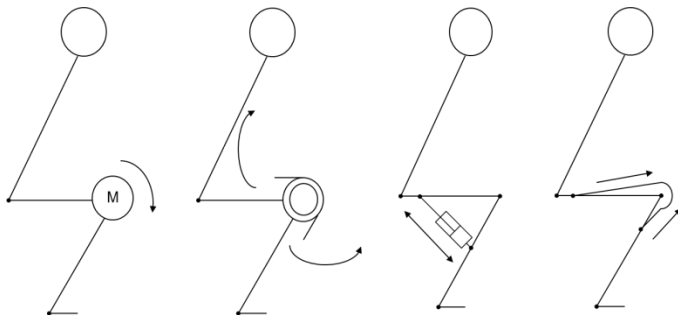
Initial Proposed Designs from left to right: a motor and torque transmission device concentric with the knee, a torsional spring concentric with the knee, a linear actuator posterior to the knee, a tensioned cable and pulley system

Each of the four conceptual designs was then rated on its ability to meet the 11 design criteria highlighted in Table 2-1. Again, a weighting system was used. This system used conformance values between 0 indicating an inability to meet the criteria and 1, a very strong ability to meet the criteria. It is important to note that the weight of the criteria and the scoring of each conceptual design's ability to meet these criteria were arrived at through consensus of the clinicians and engineers. A Pugh Matrix was used to sum the weighted criteria and ultimately determine the most appropriate design (8). A total summed score of 29 would be an ideal

candidate and a score of zero would have no ability to meet the design criteria. Results can be seen in Table 2-1, with the design with the highest potential for success being the pulley and cable tensioning system. Further descriptions of each conceptual design and discussed benefits and draw backs can be seen Appendix E.

Once the ideal candidate was selected, a three dimensional model of the prototype was created using SolidWorks (Dassault Systemes, Waltham, MA USA). It was first necessary to model a typical KAFO to which the additional prototype components could then be designed around. This was achieved by modelling the geometry of a demonstration KAFO that was provided from the Glenrose Hospital. The additional prototype components were then modelled in SolidWorks, and were designed to fit on the existing KAFO.

Through three-dimensional modelling, the design that was arrived at utilizes a gas compression spring to drive a guide block along a slider. This sliding action will create tension in the cable that is affixed to the guide block. Since the cable is wrapped over a pulley positioned at the knee, this action will introduce a knee extension moment. Figure 2-4 illustrates the prototypes function. Furthermore, this design also allows for a convenient reversibility of the device. In other words, the user can use the device to assist STS motions; however the device will also aid in controlling the decent back into the chair (stand-to-sit motions). This motion will also reload the spring readying the system for the next STS movement.

From the model geometry, the effective moment arm in the system could be determined. Using the 0.71N.m./Kg mean torque value found in the motion analysis trials, it was possible to determine the force the gas compression spring must develop. A gas compression spring with decreasing force characteristics from (900N to 450N over 100mm) was selected. This force output should theoretically provide knee torque sufficient for approximately a 90 Kg individual. Further analysis of these values will be provided in the results section.

Knowing the prototype geometry and the spring force characteristics, an engineering analysis was performed on key functional components of the KAFO prototype. Maximum allowable loading conditions for each component were determined using material yield stress values and

component geometries. The maximum allowable loads were then compared to the maximum actual loads present in the device. The ratio of these to values determined the safety factor of each component. Each calculation and its results are further described in the Results section and copies of the hand calculations are provided in Appendix F.

Utilizing the SolidWorks model, part drawings were created and guided the manufacturing and assembly of the first prototype. The parts utilized in this prototype were manufactured using the donated demonstration KAFO brace, brackets manufactured from a local water jet cutting vendor as well as off-the-shelf parts. Materials and part selection was largely guided based on availability.

Results

Prototype Design

As highlighted in the methods section, four initial conceptual designs were purposed an evaluated using a Pugh matrix. Each design was capable of mechanically achieving sufficient torque to complete a STS movement in a patient suffering from significant muscular weakness. Each concept utilized a different mechanical means to achieve a torsional moment at the knee.

The results of the Pugh matrix indicated that the tensioned cable design was the most appropriate to meet the design criteria (Table 2-1). This design uses a remote triggered locking-gas-compression spring positioned longitudinally along the femoral portion of the KAFO brace. When the spring extends, it drives a guide-block along a track and creates tension in the attached cable. Since the cable is anchored to the tibial KAFO upright and passes over a pulley positioned concentric to the KAFO knee joint, this tension generates an extensor moment at the knee. Figure 2-4 illustrates the operation of the device.

Table 2-1 A Pugh Matrix to weight relevant design criteria and each conceptual design's ability to meet these criteria

	Importance (3-Very, 1-Low)	Linear Actuators		Torsion Springs		Electric Motors		Tension Cables	
		Conformance	Score	Conformance	Score	Conformance	Score	Conformance	Score
Quiet actuation	1	0.5	0.5	1	1	0.5	0.5	1	1
Small – medial lateral profile	3	0.75	2.25	0.25	0.75	0.25	0.75	1	3
Light weight	3	0.75	2.25	0.5	1.5	0.25	0.75	1	3
Affordable	2	0.75	1.5	1	2	0.5	1	1	2
Reliable- simplicity	3	0.75	2.25	1	3	0.75	2.25	0.5	1.5
Durability	3	0.75	2.25	0.5	1.5	0.75	2.25	0.75	2.25
Easy maintenance	2	0.5	1	1	2	0.5	1	0.75	1.5
Manufacturability	2	0.75	1.5	0.75	1.5	0.75	1.5	0.75	1.5
Mechanical control – velocity, forces, etc	3	0.5	1.5	0	0	1	3	0.5	1.5
No external power Source Required?	2	1	2	1	2	0	0	1	2
Low impact of system failure	2	1	2	0.75	1.5	0.5	1	0.75	1.5
Aesthetically pleasing	3	0.5	1.5	0.5	1.5	0.25	0.75	0.5	1.5
Total Compliance Score		**20.50**		**18.25**		**14.75**		**22.25**	

Importance values ranged from 1, indicating very little importance, to 3, indicating very high importance, respectively. Each conceptual design was rated on its ability to meet these importance criteria, with conformance values between 0 indicating an inability to meet the criteria and 1 a very strong ability to meet the criteria, respectively. Each design's final score is indicated in the last row.

Figure 2-4 Prototype Design and Function
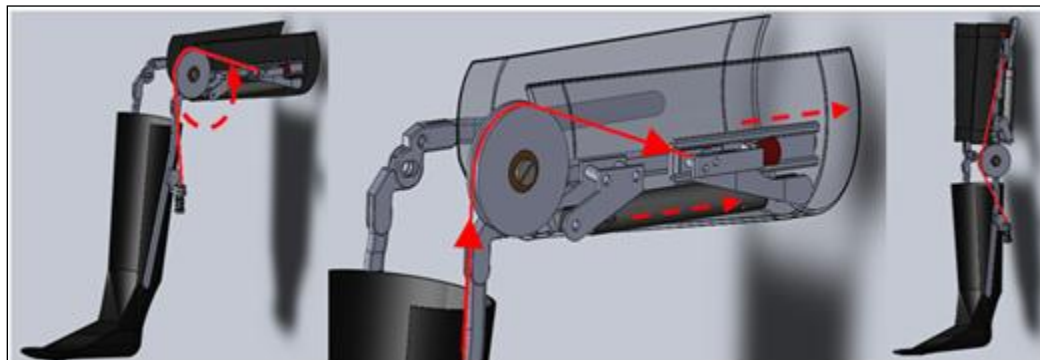
With extension of the remotely triggered gas compression spring, tension will be created in the cable (indicated in red). This tension will cause an extension moment at the knee hinge of the KAFO.

Based on geometry determined from the SolidWorks model, the effective moment arm of the prototype could be determined. Through this geometry, and using the peak 0.71 N.m./Kg knee torque value found in the motion analysis, it was determined that a compression spring with a peak force of 900N was required to drive knee extension in the prototype. Therefore, the first-prototype was designed to utilize a 900 N gas compression spring (Bansbach EasyLift model :

K0N0KK3-100-296/450N) to drive a cable tensioning system. The assistive system can be easily added and removed to most pre-existing KAFO designs with minor modifications. The prototype can be remote triggered by the user to drive knee extension. The additional components weigh approximately 1 Kg and are positioned as proximal to the body as possible to avoid a 'pendulum' effect on the user's leg due to the additional weight. Furthermore, the simplicity of the design allows for flexibility in performance characteristics. Torque of the prototype can be adjusted in two ways. Moderate torsional adjustment can be accomplished through altering the geometry of the pulley mounting bracket, while changing the model of gas compression spring can allow for dramatic changes in torque development of the prototype.

Knowing the force development characteristics of the gas compression spring, and using the prototype geometry from SolidWorks, five calculations were conducted to verify the safety of major components against failure. These calculations corresponded to the component of interest experiencing the maximum, or 'worst case' loading conditions. Further details of these calculations can be found in Appendix G. Figure 2-5 illustrates the first two loading conditions represented on the KAFO prototype. First, the #8 (4.2 mm diameter) 301 stainless steel screws were tested against shearing. These screws were utilized at any location where a prototype component was fixed to the KAFO uprights (aluminum frame). The 'worst case' loading scenario a single screw may experience is 900N, or the maximum force output of the compression spring. This loading may occur if the bracket mounting the gas spring to the uprights were to be supported by a single screw. From this force value and knowing the yield stress 301 stainless steel (276 MPa); a safety factor was determined and reported in Table 2-2. Inversely, the second calculation evaluated the imposed bearing stress of the screw on the aluminum upright (KAFO frame). Under the same loading conditions and knowing the upright thickness to be 6mm, a safety factor was calculated and is again reported in Table 2-2.

Figure 2-5 Assumed Loading of Screws Affixed to the KAFO uprights
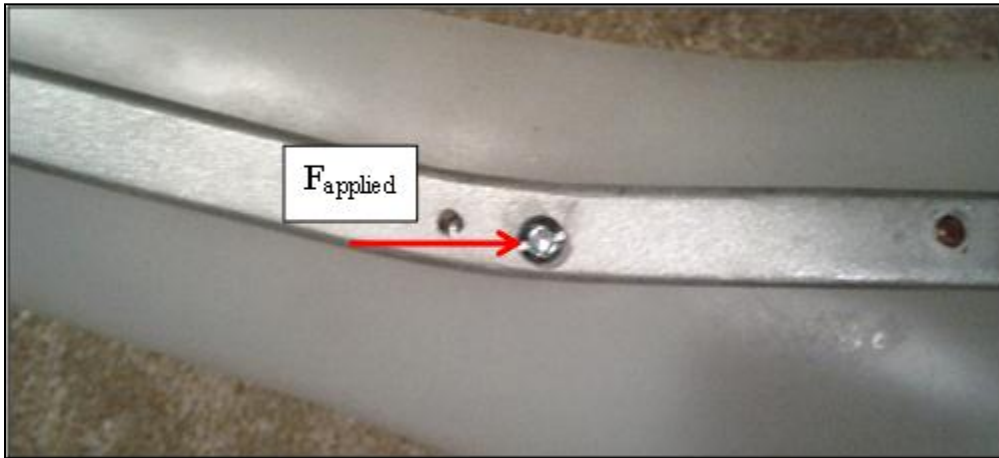
$F_{applied}$ was assumed to be 900N corresponding to the maximum force applied by the gas spring. The screw connecting the aluminum uprights to the stainless steel brackets was checked against shearing stress failure while the surrounding aluminum upright was checked against failure due to bearing stress.

A third calculation was performed to evaluate the bending stresses developed in the cable anchor bracket (pictured in Figure 2-6). This bracket was manufactured from 304 stainless steel. It was again assumed that the maximum load this component would experience was 900N (the maximum gas spring output) at 22mm from the point of fixation to the upright. Knowing the cross sectional dimensions of the bracket, bending stress calculations were performed.

Figure 2-6 Assumed Loading for Cable Anchor Bracket

$F_{applied}$ was assumed to be 900N corresponding to the maximum force applied by the gas spring. Calculations were performed to ensure the cable anchor bracket was safe under bending due to the applied cable tension force.

Bearing stresses in the spring mount bracket were also verified for safety (Figure 2-7). In this calculation the interaction between the pin fixing the gas compression spring and the mating stainless steel bracket were tested. Knowing the pin diameter to be 9.5mm and the bracket thickness to be 5mm, a simple bearing stress calculation was performed based on a maximum load of 900N.

Figure 2-7 Assumed Loading for the Spring Mount Bracket
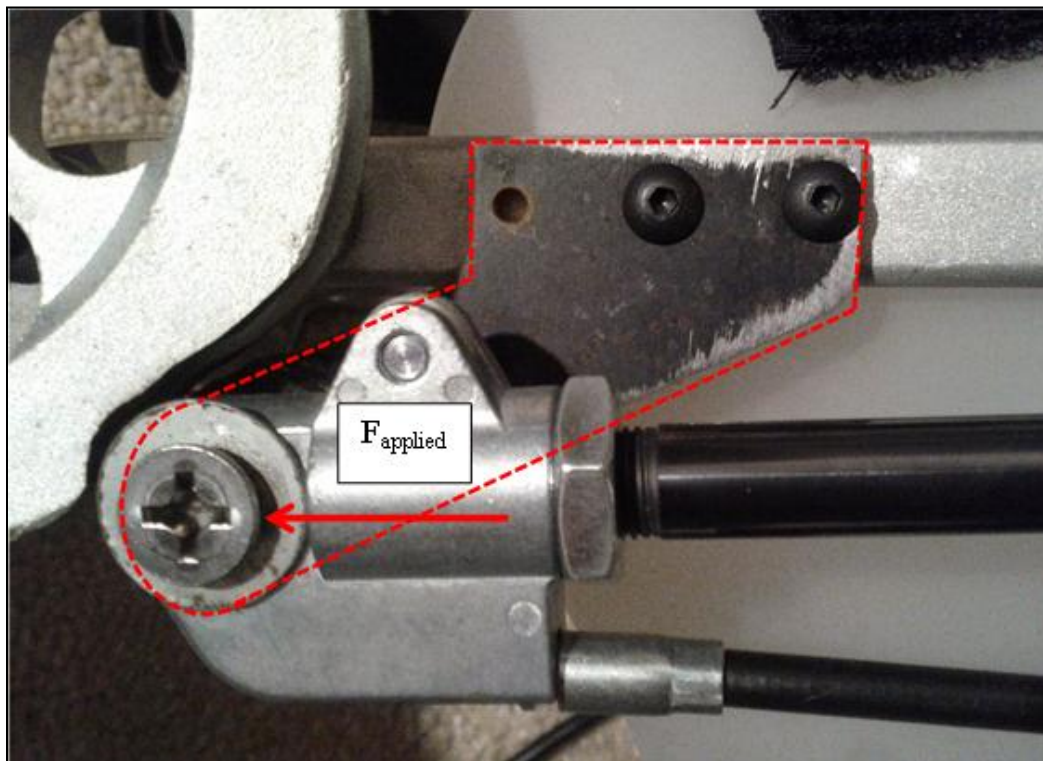
Spring mount bracket geometry can be seen by the red dashed line. $F_{applied}$ was assumed to be 900N corresponding to the maximum gas spring force. The safety of the spring mount bracket was checked against failure due to bearing stresses.

Finally a bearing stress calculation was conducted to ensure the safety of the guide track fixation. This calculation utilized the cable geometry to determine the component of the cable tension force acting perpendicular to the guide track (as seen in Figure 2-8). This value was determined to be 270N. For the maximum loading condition, a single screw was assumed to resist the whole load. Knowing the aluminum guide track had a 2.5mm bearing thickness and the diameter to be 4.27mm a bearing stress calculation was performed.

Figure 2-8 Assumed Loading for the Guide Track
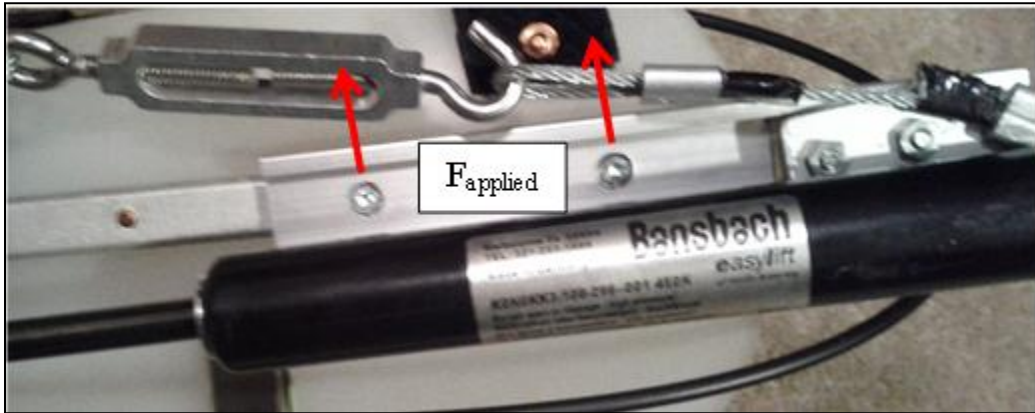
$F_{applied}$ was assumed to be 270N, the vertical component of the cable tension applied at one screw. Calculation 5 evaluated bearing stresses developed in the guide track as a result of slider loading.

Table 2-2 highlights the loaded force, maximum allowable force, and safety factor values of each component. Safety factors ranged from 1.2 to 15.3. The component most likely to fail was determined to be the Cable Anchor Bracket in bending.

Table 2-2 Stress Calculations in Critical KAFO Components

Stress	Location	Loaded Component	F_{max} (N)	F_{loaded} (N)	Safety Factor
Shearing	Screws to Uprights	Screw	3770	900	4.2
Bearing	Screws to Uprights	Upright	2752	900	3.1
Bearing	Screws to Guide Track	Guide Track	1147	270	4.2
Bending	Distal Cable Anchor	Cable Bracket	1044	854	1.2
Bearing	Spring Mount Bracket	Spring Mount Bracket	13811	900	15.3

The locations of the stresses are illustrated in Figures 2-5 through 2-8. F_{max} denotes the maximum load a component can resist prior to yielding. F_{loaded} represents the worst case scenario load a component may experience. Detailed calculations are highlighted in Appendix F

The components for the first prototype were manufactured using a series of stainless steel brackets, and off-the-shelf components purchased from local vendors. The components were assembled to the existing demonstration KAFO provided by the Glenrose Hospital. Figure 2-9 shows this first prototype.

Figure 2-9 General Assembly of the KAFO Prototype
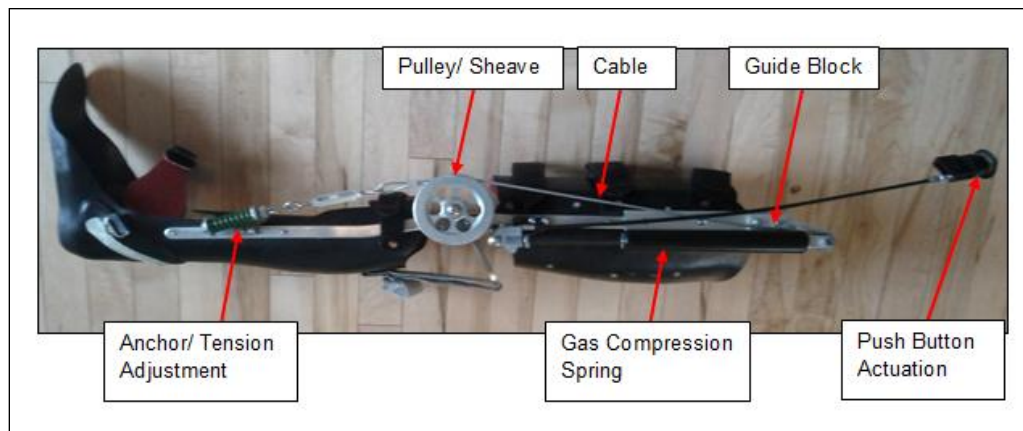
The assembled first prototype and it corresponding components

Calculations were performed to determine the moment (torque) output of the first prototype. Using the geometry of the prototype, the effective moment arm can be calculated at various positions of knee extension. Knowing the gas compression spring force decreases from 900N to 450N over 100mm of travel, a force curve was developed. The product of the geometry based moment arm curve (Figure 2-10), and the linear spring force curve (Figure 2-11) yields the theoretical torque development of the KAFO (Figure 2-12). The prototype develops a peak torque of approximately 65N.m. The average peak moment value from the STS trials described in Chapter 1 was 0.71N.m./Kg. implying that the device in its current configuration can approximately provide the peak torque required by a 90 Kg individual during STS.

As seen in Figure 2-12, the largest torque values developed in the prototype are at the greatest degree of knee flexion. In other words, the prototype provides the user with maximum assist at seat-off (when the user first loses contact with the seat) and gradually declines as the KAFO reaches full extension.

Figure 2-10 Moment Arm Development in the Prototype Based on Component Geometry

Moment Arm

A line chart with y-axis labeled "Moment Arm (mm)" ranging from 75.5 to 75.9, and x-axis labeled "Knee Flexion (Degrees)" ranging from 0 to 120. The curve decreases from about 75.87 at 0 degrees to about 75.54 at 115 degrees.
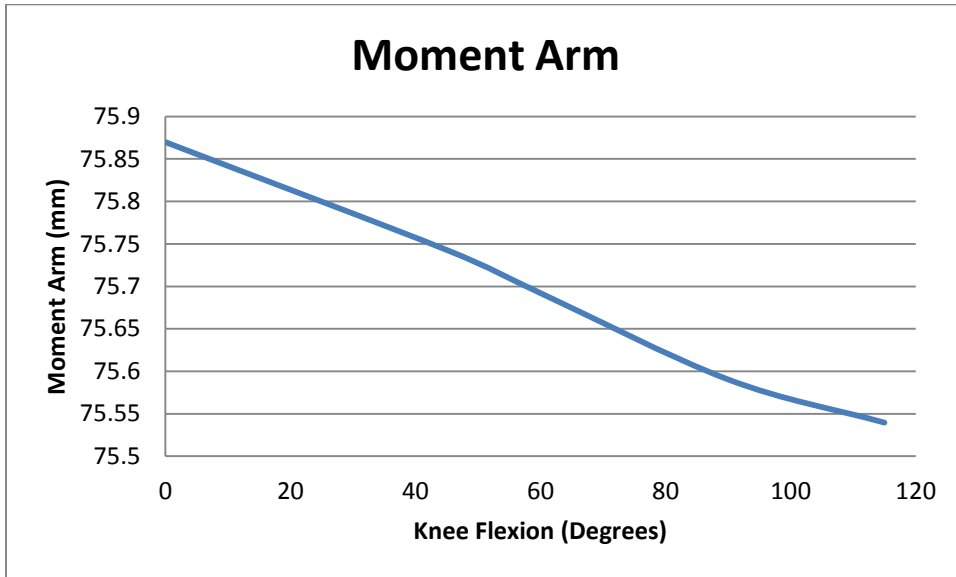
Figure 2-11 Manufacturer Specified Gas Compression Spring Force Development Across the Range of Extension

Spring Force

A line chart with y-axis labeled "Force (N)" ranging from 425 to 925, and x-axis labeled "Spring Extension (mm)" ranging from 0 to 100. The line decreases linearly from about 900 N at 0 mm to about 450 N at 100 mm.
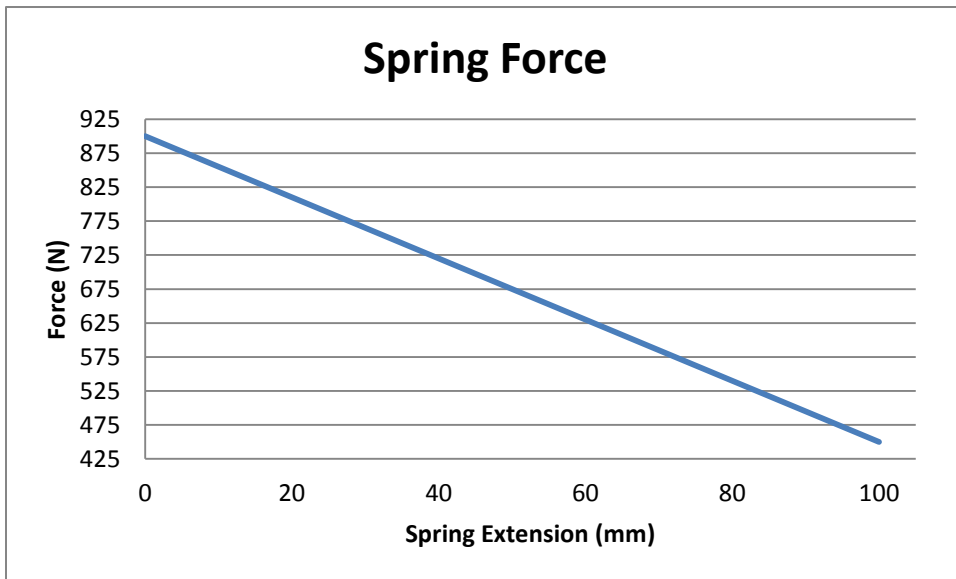
Figure 2-12 KAFO Torque With Respect to % STS Movement Completed

KAFO Torque vs. STS Torque
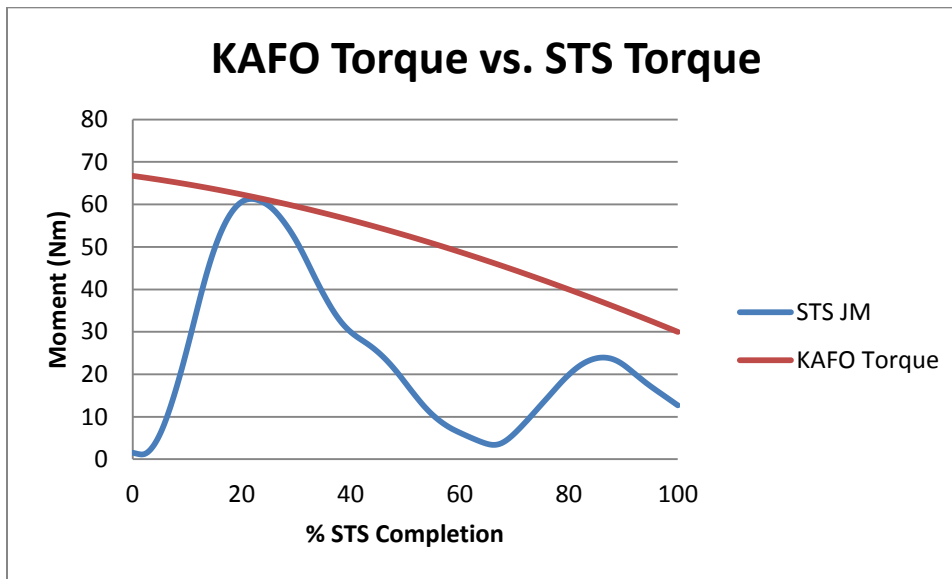
The red line represents the theoretical torque development of the KAFO porotype. The blue line illustrates a typical STS movement scaled to the demands of approximately a 90 Kg individual.

Discussion

For patients with disabilities in their lower extremities, the use of KAFO braces provides many physiological and social benefits. However, there are various challenges associated with the devices' use which often contribute to the high rejection seen among KAFO users. Interviews conducted by TEC Edmonton have identified STS as a movement that many KAFO users are unable to achieve independently. It is arguable that alleviating the difficulties experienced during this maneuver, may lead to higher acceptance rates and further long term use of KAFOs.

Attempting STS movements while wearing a traditional KAFO brace places a significant demand on the users' upper body. This is a direct result of compensatory movements due to the users' inability to develop knee extension moments. Through collaboration with clinician and engineers, a prototype was developed that can provide sufficient torque to assist in STS of KAFO dependent patients. The current gas compression spring and cable design provides a simplistic, reliable and affordable solution. Although other active knee orthotic devices do exist, their primary intent is stance control (ambulation assisting) and do not have the ability to develop the torque required in STS assist. Furthermore, technologically advanced options, such as exo-

skeletons are currently available on the market. What separates the current prototype from these technologies is simplicity. The current design has the advantage of providing knee extension torque using relatively few mechanical components that are readily available through local vendors. As a result, one may expect this design to provide a more affordable solution to assist STS than its technologically advanced counter parts.

The current prototype conforms to most of the 11 initial design criteria highlighted in the methods section. In particular the device actuates quietly, requires no external power sources and is relatively simple to install and maintain. The raw materials to manufacture the device cost approximately $250 ($CAD) with the total weight of the additional components reaching approximately 1Kg. However, criteria need to be given further attention in future prototypes. Specifically the size of the current prototype must be further reduced to satisfy the overall size criteria. Furthermore, industrial design is necessary to improve upon the prototype's aesthetics.

The prototype is designed such that the highest knee extension torque values are experienced at the greatest angles of knee flexion. As seen in Chapter 1, Part 2, biomechanically, the largest knee extension moment requirement would be expected in the early stages of the STS motion. The current prototype develops its peak torque value early in the STS cycle, and with user training, could closely coincide with seat off.

The engineering analysis suggested the prototype should be able to withstand the peak loading forces placed on its major components. A safety factor of 1.2 was found in the cable end bracket. In future prototypes the design of this component may have to be adjusted to provide a higher factor of safety. Similarly the bending stress calculation on the spring mount bracket yielded a safety factor greater than 15. To avoid over designing this component, further geometry refinement may be necessary in future prototypes. These hand calculations as well as the finite element analysis described in Chapter 2, Part 3 will allow for further refinement of material and geometry selection in future prototypes.

At present a prototype has been developed that can theoretically provide sufficient torque to assist in STS of KAFO dependent patients. However, further clinic-based testing must still be

conducted. A Custom-fit prototype was tested on an able-bodied subject and is described in Chapter 2, Part 2. This able bodied testing served two purposes: first to test the safety of the components against failure, and second, to address if STS was possible on a participant not requiring therapeutic training to operate the device.

Part 2

Able-bodied Testing of the KAFO Prototype

The intent of able bodied testing was to understand the prototype's behaviour under a live human load, as well as understand the interaction of the body and the prototype. Able-bodied testing was chosen to minimize the risk and potential training time associated with testing on a disabled subject. From Chapter 2 Part 1, the prototype can theoretically develop sufficient torque to assist a 90 Kg individual during STS. Furthermore, engineering calculations were performed to validate the safety of the prototype components against overloading and ultimately failure. This part will help bridge the gap between theory and clinical practicality. The two main objectives are to test for component safety while under a live human load, and to evaluate how the device is assisting STS.

Of particular concern was how the participant and device would adapt to the introduction of a mechanical knee extension moment. Specifically the interaction of the KAFO foot with the floor was of concern. If sufficient frictional forces were not developed in this area, the user's foot could slide anteriorly and the mechanical knee extension would create a kicking motion.

Two important aspects of device use needed to be investigated as well which are balance and system reloading. In terms of balance, the intent of the able-bodied testing was to investigate how a participant's balance may be affected while the device is actuating. In terms of system reloading, the device was designed to assist STS motion by applying an external moment to the KAFO knee joint. This moment must be slightly less that the full biomechanical requirement as the weight of the user sitting back down must reload the system. Therefore, it was important to address whether the weight of the user was enough to reload the system and the participant would not be 'stuck' in the standing position.

Methods

An able bodied participant was recruited within the University of Alberta's Civil Engineering Department. Ethics approval was obtained through the University of Alberta's ethics review board (HERO ID #: Pro00028100). The participant was a 70 Kg, 1.73 meter tall male, age 25. Informed consent was given prior to participation in this study.

To properly evaluate both prototype behavior and interaction with the body, custom fit prototypes had to be manufactured for the able bodied participant. The manufacturing of the KAFO brace followed the same fabrication procedures that a KAFO for a disabled client would undergo. Andreas Donauer (certified orthotist) and Nicholas Gilmour (orthotic assistant) at the Edmonton Glenrose Rehabilitation Hospital provided in-kind manufacturing services. This process began with the casting and plaster molding of the participant's legs. The orthotist then manipulated the geometry of these molds to relieve areas of high pressure contact between the leg and KAFO as well to maintain proper contact and fit with the leg. The molds were then draped with 5mm homopolymer polypropylene (thermal plastic). The thermal plastic was vacuum formed to the molds. As with any KAFO, specific attention was given to the location of the knee hinge center. Once the knee center was drilled through the molds, they would serve as a reference for the fixation of the aluminum uprights. The thermal plastic was trimmed such that only the areas to be in contact with the leg remained. The uprights were then hand bent to meet the specific contours of the participant's leg. Rivets were used to affix the hand bent uprights to the thermal plastic moldings. Finally, Velcro strapping was used to allow the KAFOs to be affixed to the participants' legs.

Following the orthotic manufacturing process, two custom KAFO braces were built and ready for the assembly of the prototype attachments. Similar to the prototype described in Chapter 2, Part 1 these components were affixed to the uprights through a series of screws and tapped holes. Again, water cut stainless steel bracket were utilized in combination with off the shelf components. Once the two KAFOs were assembled with their prototype components, they were ready to be tested with the able bodied participant. Figure 2-13 illustrate selected steps of the manufacturing process.

Figure 2-13 Able-bodied Prototype Manufacturing

Selected steps of prototype manufacturing, from left to right: casts taken of the participant's legs, locating and drilling the knee center, fixing prototype component to the manufactured KAFO, two manufactured and assembled prototypes

Testing was to be conducted under the assumption of bilateral KAFO assistance. A 48cm tall, armless chair was utilized and a spotter was present should the participant lose their balance and begin to fall. A successful STS trial was defined as no prototype component failure occurring, and the participant was able to achieve the movement without spotter intervention.

Once a successful trial was completed, specific instructions would be given to the participant. These instructions would change the way the participant was to achieve the STS movement and would modify the conditions under which the STS trial was performed. These conditions were intended to test the devices: performance under various frictional conditions (on two different floor surface), ability to reload the prototypes using stand-to-sit motions, and support the user mid STS movement should a failed STS attempt occur.

During, and at the completion of, each STS trial the participant was asked to provide feedback on how the KAFO was interacting with their body. Once a successful trial was achieved on carpet the participant was asked to repeat the STS motion on tile. Following the testing on two different surfaces, intermediate tests were performed to characterize the devices performance. Following the third successful STS movement, the participant would be asked to reload the device by

attempting to sit back down (stand-to-sit), this reloading procedure would then be conducted for all following trials. During the fifth STS trial the participant was asked to stop actuating the device mid-way through the STS cycle. They were then instructed to "sit back into the device" or have the device support their weight. This test was performed to ensure the components would support the user and to ensure component safety against failure under a high loading conditions. Finally the participant was instructed to continue the STS trial. In total 9 STS trials were conducted.

Results

As seen in Table 2-3 the first three STS attempts were unsuccessful due to component failure. Trial 1 resulted in a torsional deformation experience near the knee joint in the lateral upright. This twisting was a direct result of the complex geometry and contours of the participant's lateral leg. Following this unsuccessful trial, the distal cable anchor was modified such that it is mounted in closer proximity to the knee center. This reduced the torsional loading placed on the pulley and correspondingly the lateral upright. Figure 2-14 illustrates the failure mode.

Table 2-3 Results of Able-bodied STS Trials

Trial	Surface	Outcome	Comments
1	Carpet	Failed	Torsional plastic deformation in the right KAFO's distal-lateral upright
2	Carpet	Failed	Cable pull out at the proximal dead-end clamp
3	Carpet	Failed	Fastener shearing at the distal spring mount bracket
4	Carpet	Successful	Participant reported "minimal" use of quadriceps required
5	Tile	Successful	No report of friction issues (sliding) between the foot and tiled surface
6	Tile	Successful	STS achieved; as well as, stand to sit movements to reload the device
7	Tile	Successful	Minor loss, of balance spotter intervention was not required
8	Tile	Successful	No complications reported, participant was able to stop STS movement in the middle of the cycle then resume
9	Tile	Successful	No complications reported

Figure 2-14 Torsional Deformation Experienced in the Lateral
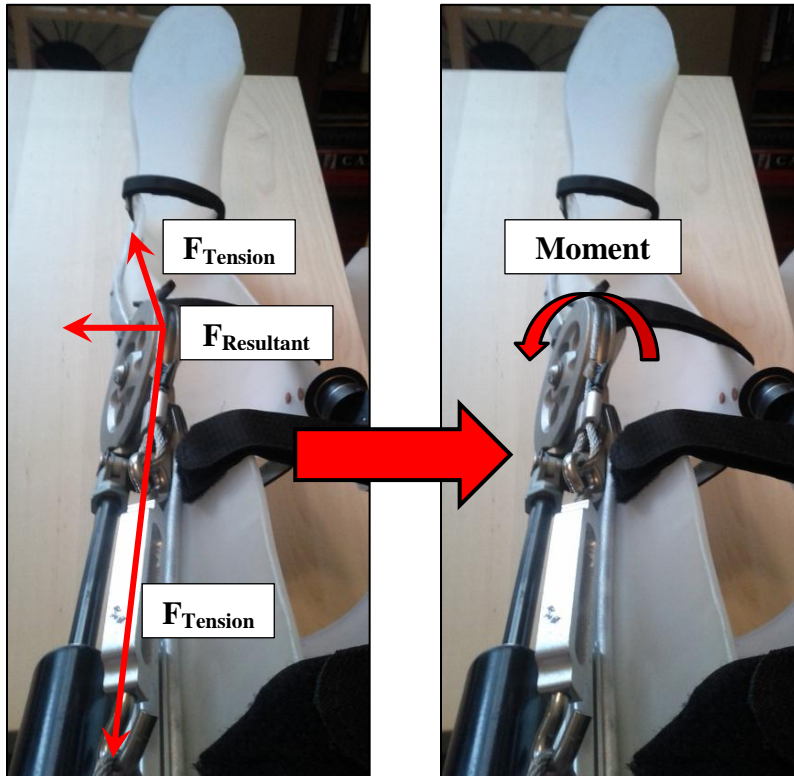
The resultant force from the cable tension created a lateral 'pulling' effect at the top of the pulley. This force created a moment around the knee joint that resulted in the lateral uprights experiencing plastic torsional deformation

Trial 2 resulted in a failure due to the cable pulling out of its dead-end clamp. The cable itself was not expected to fail since the manufacturer recommended safe working load of the 1/8" galvanized aircraft cable is approximately 1,500N and the maximum gas compression spring force was significantly less (900N) (9). The model of the dead end clamps was switched to a more robust design with more material and a larger area to 'grab' the cable, no further cable failure resulted. This failure is shown in Figure 2-15.

Figure 2-15 Cable Failure at the Dead-end Clamp

Failure in the dead end clamp allowed the cable to 'pull-out'

Finally Trial 3 was deemed a failure due to fracturing of the fasteners fixing the distal spring mount to the upright frame. Again this failure can be attributed to the complex geometry of the participant's lateral leg. Due to geometry, the compression spring was mounted to the bracket with a small, but unavoidable, eccentricity. This eccentricity created both a shearing and tensile load in the two mounting screws resulting in a failure through the cross section of the screw threads (Figure 2-18). To rectify this issue, the 'off-the-shelf' screws (with unknown tensile properties) were replaced with SAE Gr. 8 bolts (minimum tensile strength > 1000MPa) (10). No further failures were observed in this area. Following the initial 3 failed trials, 6 consecutive successful trials were conducted.

Figure 2-16 Screw Shear Failure
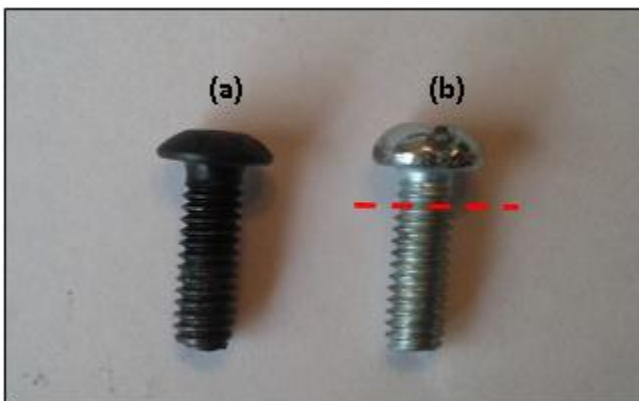
(a) shows the replacement SAE Gr. 8 bolt (b) illustrates the original 'off-the-shelf' bolts with the area of failure indicated by the dashed line

Participant Feedback

During the able-bodied testing, the participant was asked to report their experiences with the KAFO and how the KAFO was interacting with their body. In trial 4 the participant mentioned

they had to rely on their quadriceps to help the knee extension process. However, the degree of quadricep use was reported to be substantially less than without prototype intervention. They reported feeling a pushing force on the back of their thighs from the KAFO throughout the duration of the STS movement. They also noted that if they chose not to assist the device with their quadriceps, the prototype would simply hold the knees at the current position. Therefore the device was preventing a 'falling' motion back into the chair.

During trial 5 the STS movement was being performed on a tiled surface. Intuitively one would expect tile to have a lower friction coefficient than carpet. The participant was asked to comment if they felt 'sliding' between the KAFO foot and the floor surface. The participant reported no issues, and mentioned they were naturally shifting their torso center of gravity forward prior to actuating the device in order to prevent this issue.

In trial 6, the participant was instructed to actuate the device to assist their STS movement. Following completion, they were asked to try and return to the seated position (perform stand-to-sit). Once standing, the participant was able to press the actuation button and begin a decent back into their seat. They mentioned the device help resist a 'falling' back into the seat. Furthermore the stand-to-sit movement was able to reload the device. However, the participant did report having to use "a degree of hamstring force" to achieve the final degrees of knee flexion to reach sitting.

Trials 7 through 9 were performed successfully with little to no complications. In trial 7 a minor loss of balance was experienced; however, the participant was able to achieve a standing posture without the intervention of the spotter.

Discussion

The objective of Chapter 2 Part 2 was to bridge the gap between theoretical design and clinical relevance. Two KAFO prototypes were manufactured for an able-bodied participant and STS testing. The intent was to evaluate component safety against failure as well as further understand the KAFO interactions with the body.

The first three initial prototype trials experienced component failure, even though hand calculations performed in Chapter 2, Part 2 had predicted components safety. The torsional deformation seen in the lateral uprights was a direct consequence of the complex geometry of the KAFO uprights (as a result of the participant's leg geometry). Part 3 of this chapter will discuss a finite element analysis, and its predictions of stress development in the prototype components. Future prototypes will need to pay specific attention to this area to avoid future failures. The cable pullout failure was a result of applying and off-the-shelf part without the load bearing capacity to support the device's needs. No manufacturer information was provided on the cable dead end clamps with regard to maximum capacity. By switching manufactures to a larger 'grab area' on the cable, no further failures were observed. However, neither manufacturer supplied information on the maximum capacity of the cable dead end clamp. In future prototypes, these capacities must be known, and perhaps purchased from a manufacture with information more readily available. Finally the Screw failure was again, a direct result of the complex upright geometry. The hand calculations did not predict failure of the screws as only bearing and shearing stresses were investigated. Again, the unique geometry of the uprights created both a shearing and tensile loading in the screw. This combined stress ultimately failed the screw. In future prototypes the geometry of each user's will always be inherently different. Therefore it is necessary to pay specific attention to the screw selection, and the loads they experience.

While three minor design modifications were required due to under-sizing of mechanical components, 6 consecutive successful STS trials were conducted (Figure 2-17). At no point during these trials did the participant report a sliding motion between the KAFO foot and the floor. It would therefore appear; there is a minimal risk of the prototype kicking the lower leg out rather than driving knee extension during STS. The participant mentioned that during STS, their body naturally shifted the torso forward; they would then actuate the device. This forward movement of the torso is a characteristic phase of healthy STS movements known as mass transfer (11). If the prototype were to be used with a KAFO dependent subject, and similar to most mobility aids, proper training may be required to insure appropriate body positioning prior to actuation.

During the successful trials, the participant mentioned that a small degree of quadricep activity was still necessary to achieve STS. Therefore, the device appears to be assisting knee extension during STS, and not completely driving the participant up. This property of the device would translate to a degree of upper body input still being required to achieve STS. However, the device would still allow for a flexed-knee STS strategy, and ultimately a reduced upper body demand. The degree of reliance on the upper body would be directly related to the degree of assist being provided by the device. Again, it may be necessary to train KAFO users prior to using the device independently.

Figure 2-17 STS Movement While Wearing the KAFO

This figure depicts the use of a single KAFO prototype during STS movement

However; assisting the knee, as opposed driving knee extension, is an advantage of the design. The current design depends on the user's decent back into their chair (stand-to-sit) to reload the device. If the prototype were to provide greater than 100% the required knee extension moment, it may prove difficult for the user to properly achieve stand-to-sit and they would therefore be unable to return to a seated position as well as reload the prototype.

Another major advantage of the current design is the flexibility in adjusting the required torque provided by the gas spring. While the participant did report having to use a degree of hamstring force to help fully return the device to a seated position. The torque developed at the knee can be

further adjusted through sizing and fine tuning of the prototype. As highlighted in Chapter 2, Part 1 control of the torque development can be achieved by adjusting the pulley, and ultimately the effective moment arm, or through replacing the gas compression spring. Upon installation of the device, an orthotist may be required to properly tune the device to meet the appropriate torque demands of the user. Furthermore, torque tuning allows for the device to be utilized as a therapeutic aid. For recovering clients, the torque demands of the device may be continually adjusted during their therapeutic program. As a result a therapist may potentially reduce the amount of 'assist' the device is providing throughout a client's recovery process to promote independence during STS transfer.

Part 3

A Finite Element Model of the KAFO Prototype

Finite Element Analysis (FEA) is an approximate numerical technique often utilized in solid mechanics to solve the differential equations of equilibrium. This technique discretizes a body of interest into a number of finite elements. A force, or displacement condition can be introduced to the system, and each element would be assumed to displace according to a predetermined linear or nonlinear form as a weighted average of the displacements of the element nodes. The displacements across the interface of the elements are assumed to be continuous. Nodal displacements can be determined by minimizing an integral form of the differential equation of equilibrium (12).

FEA can provide useful information when analyzing stress development in complex systems.The goal of this part was to produce a Finite Element model that can be used to analyze the development of stresses in the KAFO prototype during its maximally loaded condition. The current prototype, although functional, lacks the design refinement required for end user acceptance. A FEA model can be utilized to guide design decisions in future prototypes. Specifically the analysis will enable the identification of low, or zero stress areas, and inversely, areas of potential failure. These results can be utilized to direct material and geometric choices as to reduce the overall size and weight of the future prototypes.

Methods

Creating a 3D Model Using SolidWorks

A three dimensional model was created using SolidWorks (Dassault Systemes, Waltham, MA, USA). This model had to geometrically represent the actual prototype as closely as possible without incorporating patient specific features. To achieve this requirement, two main geometric simplifications had to be made.

As described in Chapter 2, Part 2, the thermal plastic moulding in the KAFO was created using a mold of the patient's legs. Therefore, the geometry of these areas will be a direct result of the

patient's specific leg geometry. When modelling the thermal plastic components in SolidWorks, the unique curvatures present in the actual prototype were simplified into cylindrical shapes. To do this the geometry of thermal plastic portions was achieved by defining two arcs and extruding the three dimensional space in between with a linear geometric function (arc-loft function) Figure 2-18. The technique still maintains similar geometry to the original KAFO; however, they remove the specificity of the moulded thermal plastic.

Figure 2-18 Three Dimensional Model of the Thermal Plastic
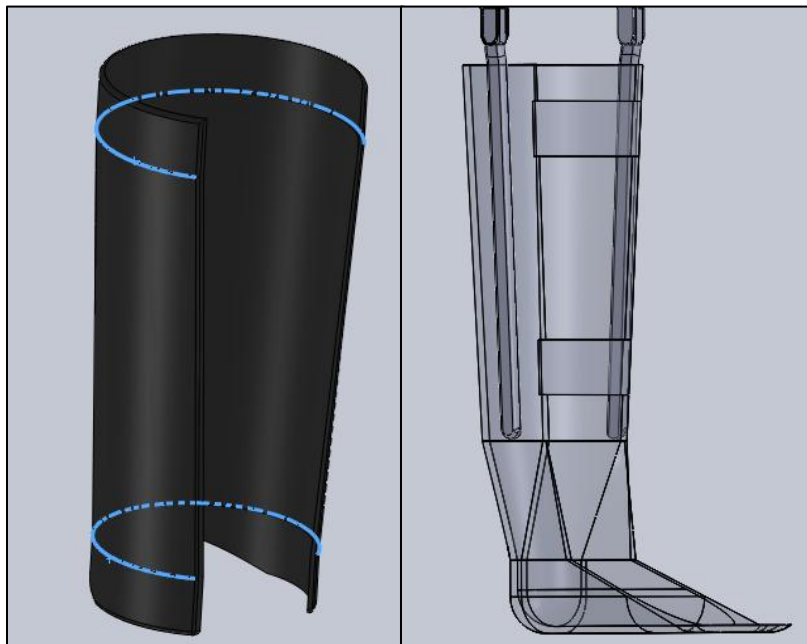
Creating the thermal plastic geometry, the blue arcs represent the geometry on which the thermal plastic was extruded. This procedure was used for both the tibial and femoral thermal plastic components.

Similarly, the aluminum upright on the KAFO prototype were created by bending and riveting the aluminum bar to the exterior of the thermal plastic. Therefore, similar to the prototype's plastic molding, the geometry of the aluminum uprights are derived from patient specific geometry. In SolidWorks this issue was addressed by having the aluminum frame follow the same loft angle as the thermal plastic in SolidWorks. The frame could then be made tangent to the curvature of the plastic. This method allowed the modelled uprights to geometrically mimic the prototype's frame; however, it removed any unique patient-specific curvatures. Although this procedure will limit the accuracy of stress predictions for an individual, specific KAFO, it will

allow for a better understanding of the stress expected to develop in a variety of KAFO models and designs.

Importing the Geometry into the FEA Software Abaqus

From SolidWorks, the modelled assembly could be exported as a STEP file. The STEP file was then imported into Abaqus (Dassault Systemes, Waltham, MA, USA) . However, Abaqus only has the functionality to import the SolidWorks STEP assembly as a single part, and then create multiple parts from this file. This limitation forced all the individual parts in the STEP file to be treated as a solid, shell, or wire exclusively.

Due to the large surface areas and the thin cross sections, shell elements are the optimum choice to model the two thermal plastic leg mouldings. However, the remaining parts in the assembly had geometry that lent themselves to a 3D solid part to be modelled with 3D solid elements. To accommodate these different shapes, two separate imports had to be performed, one for the thermal plastic components, and one for the remaining parts. Finally using geometric constraints, the thermal plastic components were positioned in their appropriate location in the final Abaqus assembly.

Discretizing, Section and Material Properties

Once the model was imported into Abaqus, it was discretized. The thermal plastic portions of the model were meshed using quad-dominated, reduced integration linear shell elements with a thickness of 5 mm (Abaqus defined, S4R, reduced integration, linear shell elements). The remaining parts were discretized using tetrahedral, linear, 3D stress (Abaqus defined, C3D4, 4-node linear tetrahedron elements) elements. Table 2-4 summarizes the individual parts, and the element properties used. It should be mentioned that during the import process, the SolidWorks file was brought into Abaqus as a solid file, rather than surface geometry file. Therefore when defining the linear shell mesh, the plastic components were discretized with two layers of shell elements (a hollow solid composed of two shell walls). This configuration would ultimately increase the stiffness behaviour of the plastic components. However, in reality, these components may be manufactured of various plastic materials, thickness, or even carbon fiber composites.

Therefore it does not necessarily introduce inaccuracies by modelling the thermal plastic components as a double-walled shell.

The KAFO prototype utilizes three primary materials. Therefore the Abaqus model is composed of three section properties, each corresponding to the material of the component. The sections were solid homogeneous for the majority of the parts, and shell continuum homogeneous for the thermal plastic portions. The three materials modelled were homopolymer polypropylene, 3003 aluminum, and 304 stainless steel. Table 2-5 summarizes the elastic moduli, Poisson's ratios, and yield stresses for each material.

Figure 2-19 KAFO Model Parts Identified
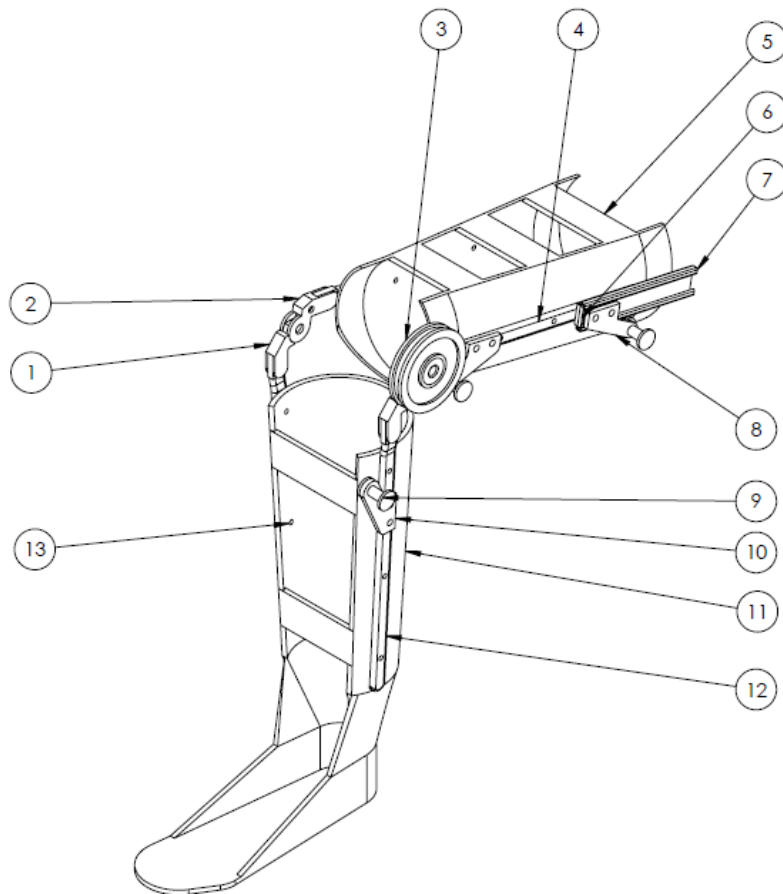
The main components of the FEA KAFO model

Table 2-4 KAFO Model Component Specifications

	Part Name	Element Type	Mesh Shape	Mesh Seed Size (mm)	Material
1	Distal Hinge	3D Solid	Linear Tetra	1.5	304 Stainless Steel
2	Proximal Hinge	3D Solid	Linear Tetra	1.5	3003 Aluminum
3	Pulley	3D Solid	Linear Tetra	7.0	304 Stainless Steel
4	Femoral Upright	3D Solid	Linear Tetra	10.0	3003 Aluminum
5	Femoral Thermal Plastic	Shell	Linear Quad	9.0	Homopolymer Polypropylene
6	Guide Block	3D Solid	Linear Tetra	3.0	3003 Aluminum
7	Guide Track	3D Solid	Linear Tetra	5.0	3003 Aluminum
8	Spring Mount Bracket	3D Solid	Linear Tetra	5.0	304 Stainless Steel
9	Cable/ Spring Pin	3D Solid	Linear Tetra	3.0	304 Stainless Steel
10	Cable Anchor	3D Solid	Linear Tetra	5.0	304 Stainless Steel
11	Tibial Thermal Plastic	Shell	Linear Quad	10.0	Homopolymer Polypropylene
12	Tibial Upright	3D Solid	Linear Tetra	6.0	3003 Aluminum
13	Rivet	3D Solid	Linear Tetra	1.3	3003 Aluminum
NS	Pulley Mount Bracket	3D Solid	Linear Tetra	4.0	304 Stainless Steel

Numbers in the left hand column correspond to the ballooned item numbers in Figure 2-19. NS signifies a component not shown in Figure 2-19.

Table 2-5 Material Properties of KAFO Components

Material	Elastic Modulus (Mpa)	Yield Stress (Mpa)	Poisson's Ratio
Homopolymer Polypropylene *	1300	33	0.45
3003 Aluminum **	69000	110	0.33
304 Stainless Steel **	200000	290	0.28

* Taken from INEOS Olefins and Polymers (13)
** Taken from Dassault Systemes material information (14)

Testing Model Behaviour

The created model consisted of multiple parts with a complex mechanical interactions between various components of the design. In order to ensure proper constrains and interactions between each the different components, a methodical 'ground-up' approach was followed. In the first step of this 'ground-up' approach each part in the assembled model was suppressed with the exception of one. A simplified model was then analyzed with this starting part. Subsequent parts were then added with proper constraints and analyzed one at a time to ensure that each part had appropriate deformation without any error messages

Testing the Thermal Plastic

For the model, 10 separate tests were completed. The tibial thermal plastic was introduced as the initial part. A boundary condition was specified for the bottom of the foot portion to fix its 6 degrees of freedom. A 5 MPa pressure was applied to the anterior medial face as shown in Figure 2-20. The analysis was then submitted. This simplistic analysis was able to confirm two requirements. First the mesh was appropriately defined, and second the 'fixed foot' boundary condition was appropriately defined.

Figure 2-20 Testing the Tibial Thermal Plastic
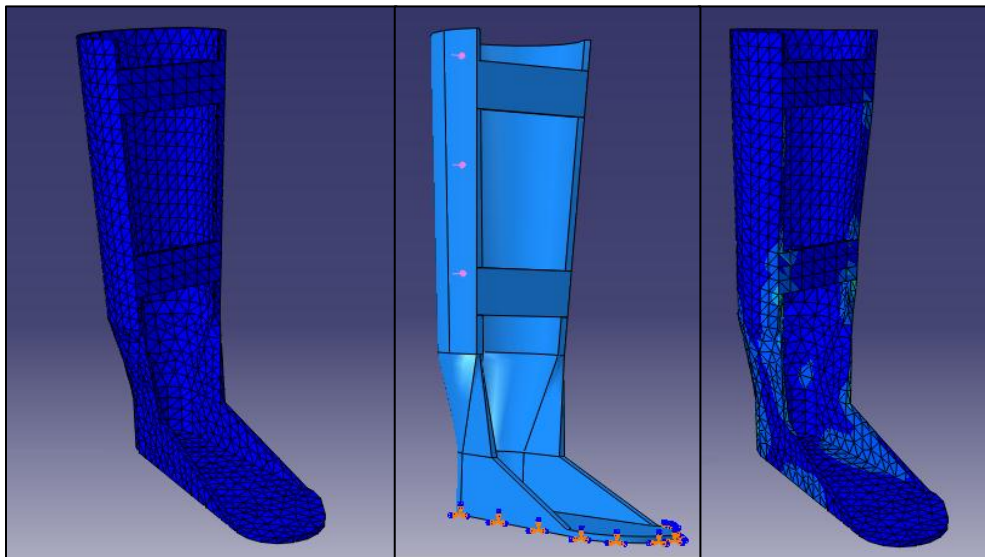
From left to right: the undeformed tibial thermal plastic, the introduction of boundary conditions and loading, the deformed tibial thermal plastic

Riveting the Uprights to the Thermal Plastic

Following the successful test on the distal thermal plastic model, the tibial uprights were added. A series of six pins were introduced to the model to represent the rivet present in the KAFO prototype. A rigid tie relationship was defined between the exterior of the pin and the interior of the corresponding holes in the thermal plastic and aluminum upright (Figure 2-21). Similar to the first step, a 5 MPa pressure was applied to the proximal interior faces of the uprights. The uprights and thermal plastic components developed reasonable deformations and stresses. This approach was continued for a total of 10 tests, which are summarized in Table 2-6. A selection of tests from the 10 are reported in Table 2-6 and are described below.

Figure 2-21 Rivet Definition
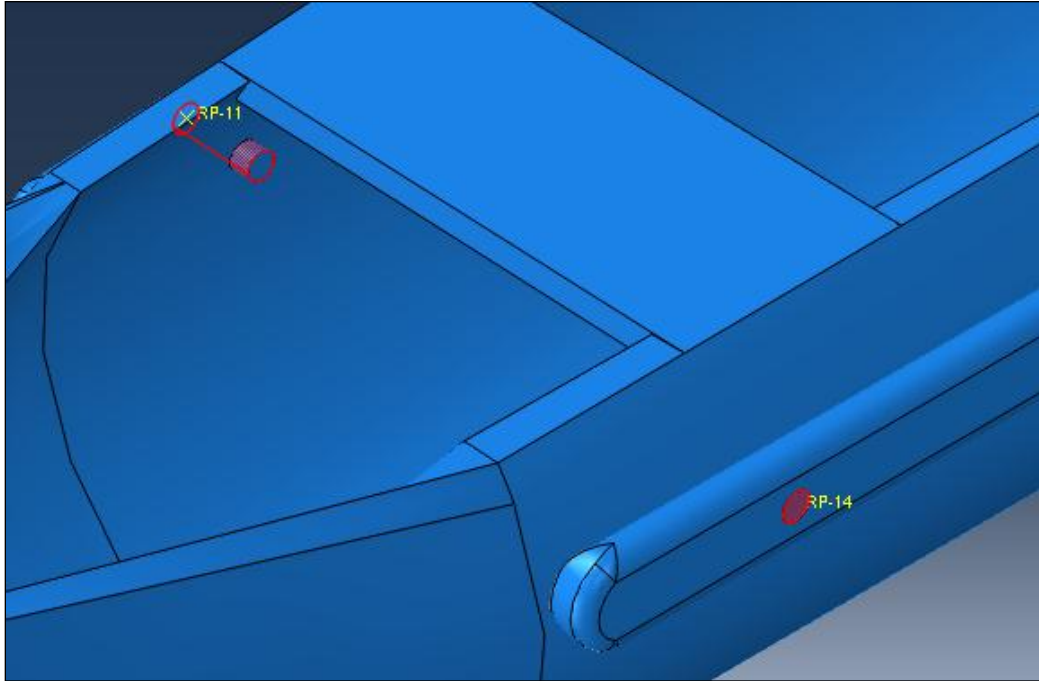
Rigid tie relationships were defined between the exterior of the pin and the interior of the corresponding holes in the thermal plastic and the aluminum uprights

Knee Hinge Testing

To define the knee hinge interactions, a pin had to be introduced and act as the center of rotation. Using this pin, it was assumed that the proximal portion of the hinge (hinge-half) would be fixed rigidly to the pin and the distal hinge-half would allow rotation of the pin face. Three tests were conducted to insure proper function of the hinges.

First a boundary condition was applied to fix the 6 degrees of freedom of the pin. An interaction was created between the distal hinge half (bottom half of the hinge) and the pin. A frictionless tangential sliding with a hard contact normal behavior was assumed. A boundary condition was implemented to define a displacement in the U2 and U3. By defining a linear displacement rather than a rotation, it was possible to see stresses being developed in both the pin and hinge due to the interaction, as well as a rotational displacement. (Figure 2-22)

Figure 2-22 First Knee Hinge Test
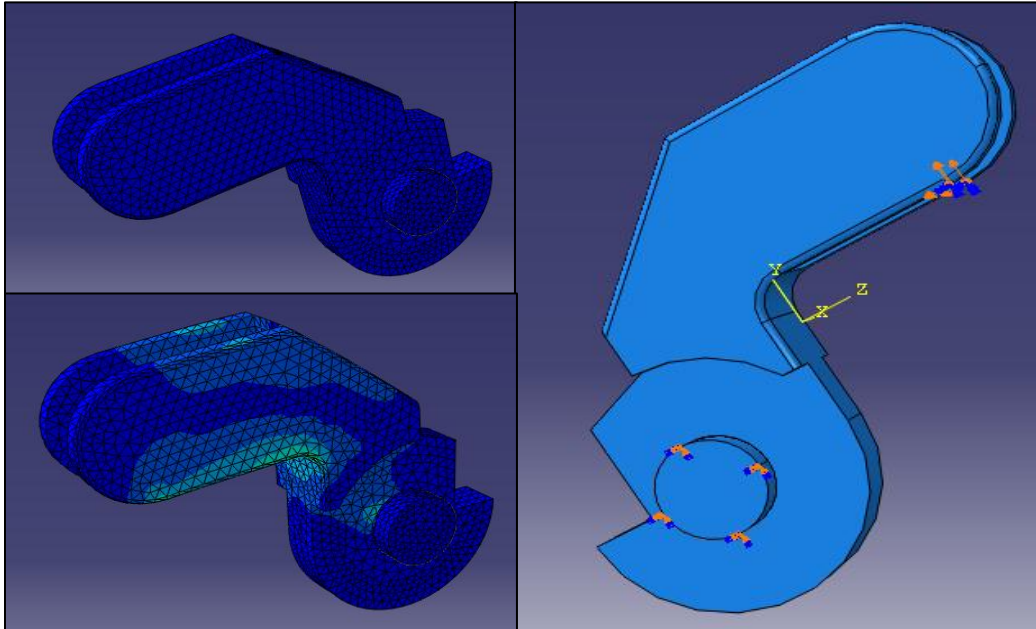
Top Left: the undeformed distal hinge half, Right: Boundary conditions applied to the pin, and displacement defined at the back of the pin, Bottom Left: The deformed hinge half

The second test involved tying the exterior pin surfaces to the interior surfaces of the proximal hinge-half (top half of the pin). Once these surfaces were tied, a 20 MPa pressure was applied to the posterior surface of the hinge. Since the pin was still fixed in its six degrees of freedom, the analysis was stable and a solution for the stresses and deformation was achieved.

The final test hinge test involved assembling the two halves of the hinge with the pin. Once all three components were assembled, the pin was again fixed, and the surface interactions and tie constraints introduced. This final analysis functioned to verify that the hinge components function together as a single unit. Again a displacement in the U2 and U3 directions was introduced. In this test it was expected that the distal hinge-half would rotate, with no movement of the pin or proximal hinge-half. The results of this third test confirmed that the hinge was functioning as predicted.

Figure 2-23 Second Knee Hinge Test
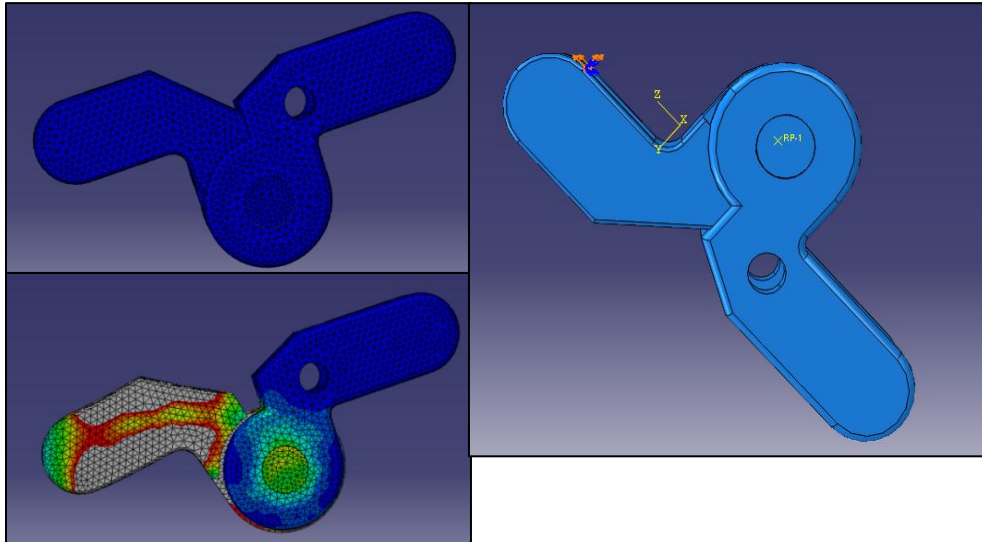
Top left: The undeformed full hinge, Right: Boundary conditions applied and displacements defines, Bottom left: The deformed full hinge

Testing the Assembled Model

The tenth test involved defining a small linear displacement in the proximal hinges in the U2 and U3 directions. Similar to the final hinge test, this procedure was designed to test the response of the entire Abaqus model. The small displacement boundary condition was translated throughout the model, and a small rotation at the knee hinges was experienced. Furthermore, all the parts remained constrained and appropriately mated to their corresponding surfaces.

Table 2-6 Model Behavior Test Summary

	Part	Load	Magnitude	Boundary Conditions	Constraints	Interactions	Success Criteria
Test 1	Distal Plastic	Pressure	5 Mpa	Fixed foot	N/A	N/A	No displacement
Test2	Tibial Frame	Pressure	5 Mpa	Fixed foot	Tie inner frame to tibial Plastic	N/A	Deformation of Frame and Tibial Plastic
Test 3	Distal Hinges	Pressure	5 Mpa	Fixed foot	Tie interior hinge to exterior frame	N/A	Deformationof frame, plastic and hinges
Test 4	Cable Anchor	Pressure	5 Mpa	Fixed foot	Tie anchor to lateral tibial frame	N/A	Deformation of anchor, small lateralframe and platic deformation
Test 5	Femoral Plastic Frame and Hinges	Pressure	5 Mpa	Fixed upper femoral plastic	Tie hinges to frame and frame to plastic	N/A	Deformation of hinges and frame, small deformation of plastic
Test 6	Frame and Brackets	Pressure	5 Mpa	Fixed upper femoral plastic	Tie brackets to frame	N/A	Deformation of brackets with small frame and plastic deformation
Test 7	Slider	Displacement	U1=5	Fixed back of tracks, displaced the guide block	N/A	Surface to Surface between slider and track	Displacement of slider only
Test 8	Proximal Half Hinge	Displacement	U2=1 U3=-1	Fixed pin face	N/A	Surface to Surface pin and interior hinge faces	Rotation of half hinge
Test 9	Fix Hinge to pin	Pressure	20 Mpa	Fixed pin face	Tie Interior hinge to exterior curvature of pin	N/A	Deformation of hinge
Test 10	Full Model	Displacement	U2=-1 U3=1	Fixed Foot	20 constraints necessary	Surface to Surface pin and interior hinge faces	Rotation of femoral portion of model

Model Loading

The non-linear geometry option within Abaqus was enabled to allow large displacements and large deformations. Boundary conditions and loading of the KAFO model were applied to mimic the maximum load conditions experienced during the STS movement. In the KAFO prototype,

the gas compression spring produces a maximum force of 900N when fully compressed. This compressed position corresponds to the user and prototype being in the seated, or knees fully flexed position. It is at the point of maximum spring force output that one may expect the maximum loading conditions in the KAFO system. The FEA model was design to be a static model that evaluates stress development at these maximum conditions.

A series of concentrated forces mimicking the seated position were applied on the KAFO model. These forces were representative of the reaction forces experienced in the model due to the spring force and cable tension. Figure 2-24 illustrates the individual forces placed on each component. Table 2-7 highlights the corresponding magnitude of each force. The force magnitudes were determined through basic free body diagrams and geometric calculations. Detailed free body diagrams can be seen in Appendix G.

Figure 2-24 KAFO Model Loading
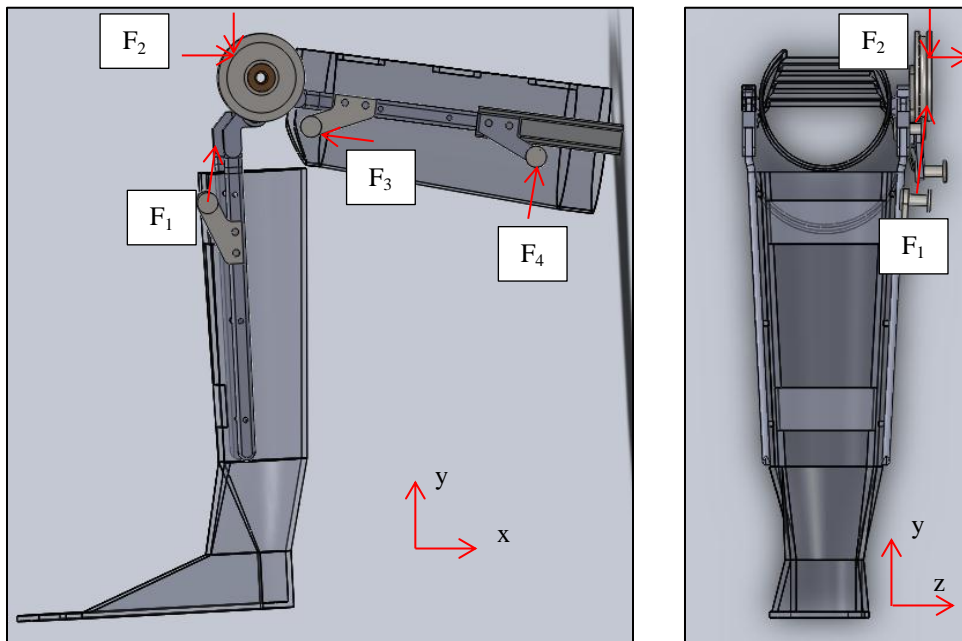
The red arrows represent the direction of the force applied at each component relative to the global coordinate system. The magnitude of these forces can be seen in Table 2-7.

Table 2-7 Force Placed on KAFO Model

Label	Force	
F_{1x}	185	N
F_{1y}	834	N
F_{2x}	958	N
F_{2y}	1194	N
F_{2z}	221	N
F_{3x}	900	N
F_{4y}	270	N

The left column represents the labelled forces in Figure 2-24, magnitude of each of these force are provided

Boundary Conditions

Two separate tests were conducted to help illustrate the interaction between the KAFO and user's leg. Test 1 applied boundary conditions to the femoral thermal plastic such as to model realistic KAFO loading as closely as possible. The second test implemented boundary conditions in the femoral thermal plastic to represent an idealized worst case scenario in which the KAFO is restrained at the bottom of the foot with minimal restraint in the femoral thermal plastic. In this second test, it was assumed that the subject leg would only provide a vertical restraint to the KAFO thermal plastic.

Test 1

Two Boundary conditions were utilized to appropriately fix the model in space. As seen in Figure 2-25 the bottom of the KAFO foot was fixed against displacement and rotation. The femoral thermal plastic was partitioned longitudinally down its centerline. The medial half of the thermal plastic was fixed against displacement and rotation. This boundary condition served to mimic the prototypes interaction with the user's leg at the point of maximum loading.

Figure 2-25 Boundary Conditions for Test 1
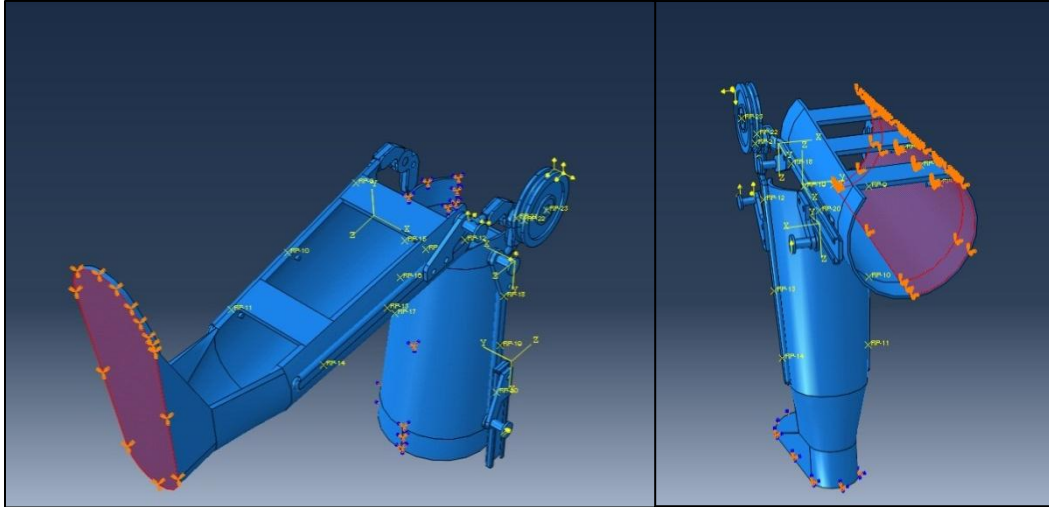
Left: the bottom of the KAFO foot fixed against movement and rotation, Right: The lateral half of the femoral thermal plastic fixed against movement and rotation

Test 2

Similar to Test 1, the bottom of the KAFO foot was fixed against displacement and rotation. However, the second boundary condition differed. As seen in Figure 2-26 a small line of nodes on the proximal, posterior, femoral thermal plastic had displacement boundary conditions applied. This node group was fixed against Z-direction movement only (I.E. only knee extension would be prohibited). Although this boundary condition may not occur in reality, it represents an idealized worst case scenario in which the KAFO can exhibit large deformations without restraints. This boundary condition configuration is representative of the prototypes performance in the absence of an interaction with the user's leg.

Figure 2-26 Boundary Conditions for Test 2
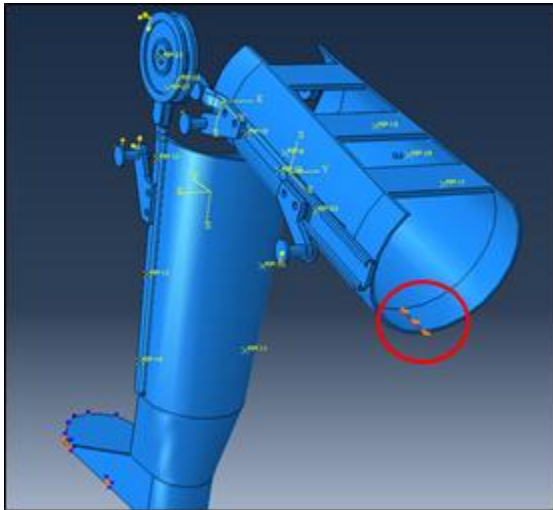
The red circle represents the region where the zero displacement boundary condition was applied

Results

Test 1

Figure 2-27 illustrates the thermal plastic component experiencing the largest von Mises stresses. The highest stress developed in the thermal plastic components was found to be 13.5 MPa, well below the 33 MPa yield stress of the plastic. The high stress region can be seen located in close proximity to the rivet location on the distal lateral side of the femoral thermal plastic.

Figure 2-27 Elements in Excess of 33 MPa
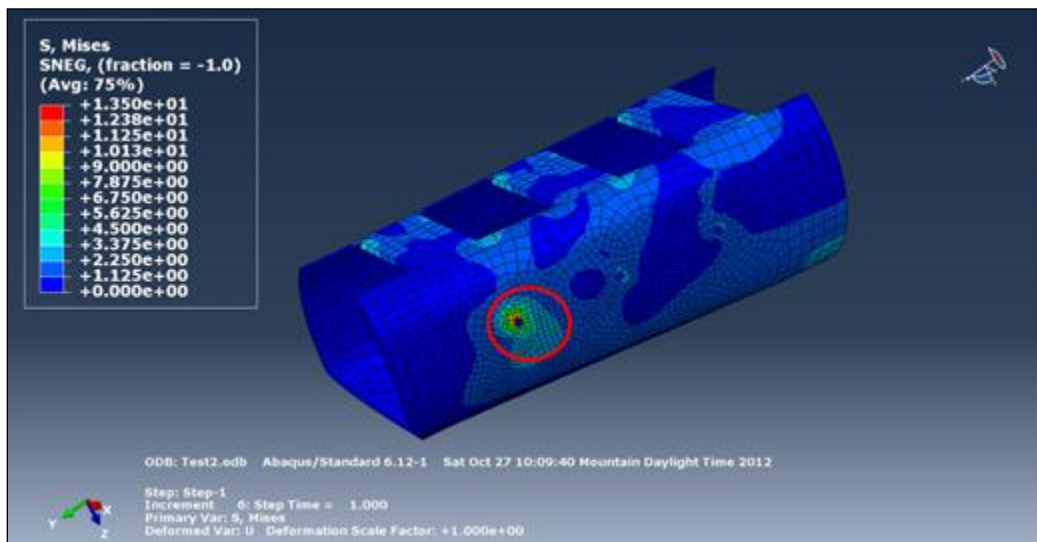
The red circles highlight the nodal region belonging to the highest stresses in the thermal plastic; this region does not exceed 33MPa

Figure 2-28 illustrates the components of the model that develop von Mises stresses in excess of 110 MPa (the yield strength of the aluminum). The aluminum upright components do appear to display regions in excess of this threshold. In other words, the prototype may be expected to experience yielding in these areas.

Figure 2-28 Nodal Areas in Excess of 110 MPa
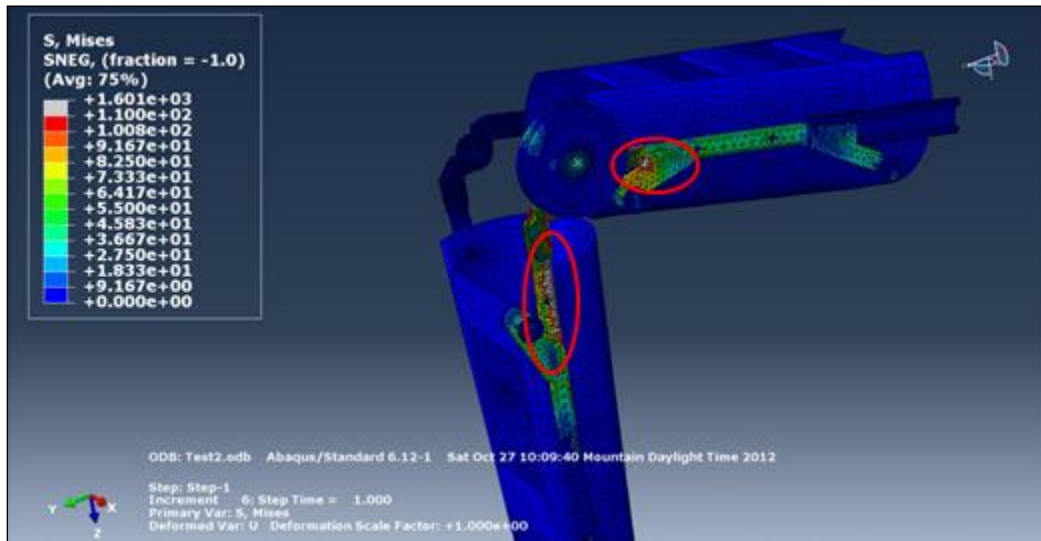
The red ovals highlight the area on the aluminum components in excess of their 110 MPa yield strength

Figure 2-29 and Figure 2-30 highlight the regions of the model that develop von Mises stresses in excess of 290 MPa. This stress threshold represents the yield stress of the 304 Stainless steel. One element was found to exceed this threshold producing a stress value in excess of 1600 MPa (highlighted in Figure 2-29). An explanation and implications of this singular high stress element are provided in the discussion section.

Figure 2-29 Nodal Areas Exceeding 290 MPa
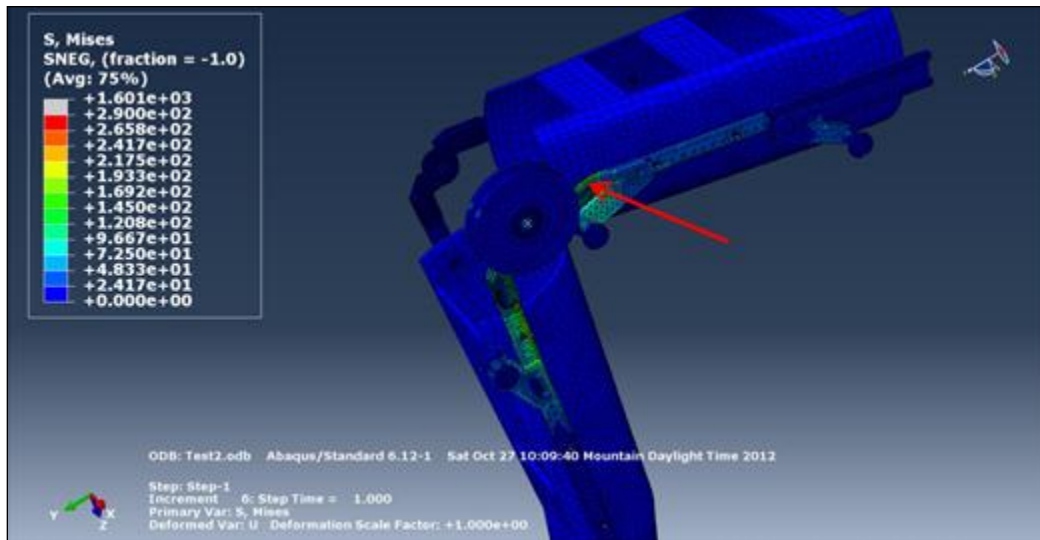
The red arrow signifies the relative location of the maximum stress element (approximatel 1600 MPa). This was a single element in the lateral femoral upright with a very small relative volume

Figure 2-30 Stress Development in KAFO Components
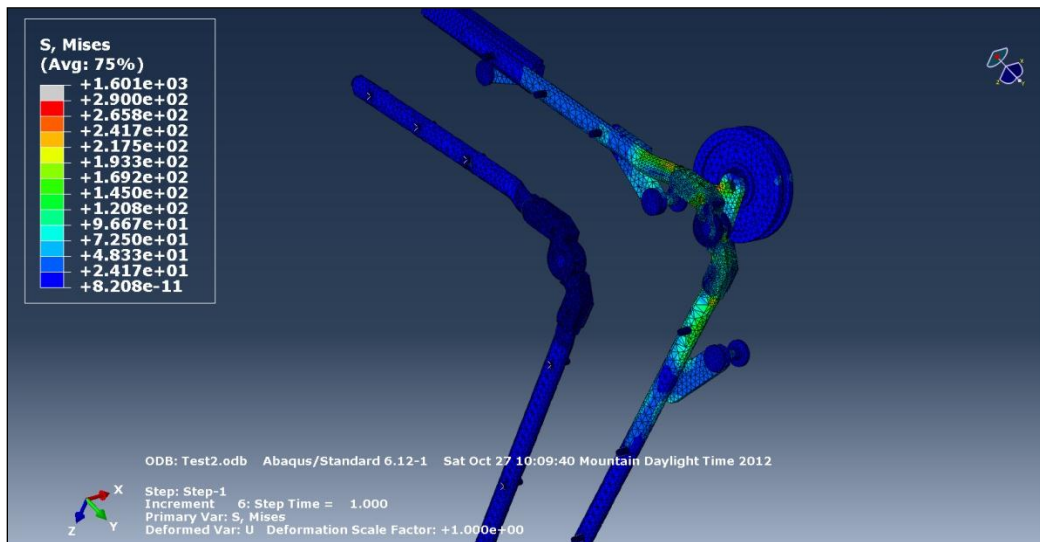
Stress development on the medial surface of the lateral uprights (thermal plastic removed from figure for clarity)

Test 2

Figure 2-31 shows the undeformed and deformed model. Substantially large deformations were experienced in the model. The maximum von Mises stress predicted in the model was 1790 MPa. Similar to test 1, this value occurred in the lateral uprights in close proximity to the knee hinges.

Figure 2-31 Test 2 Deformation Results
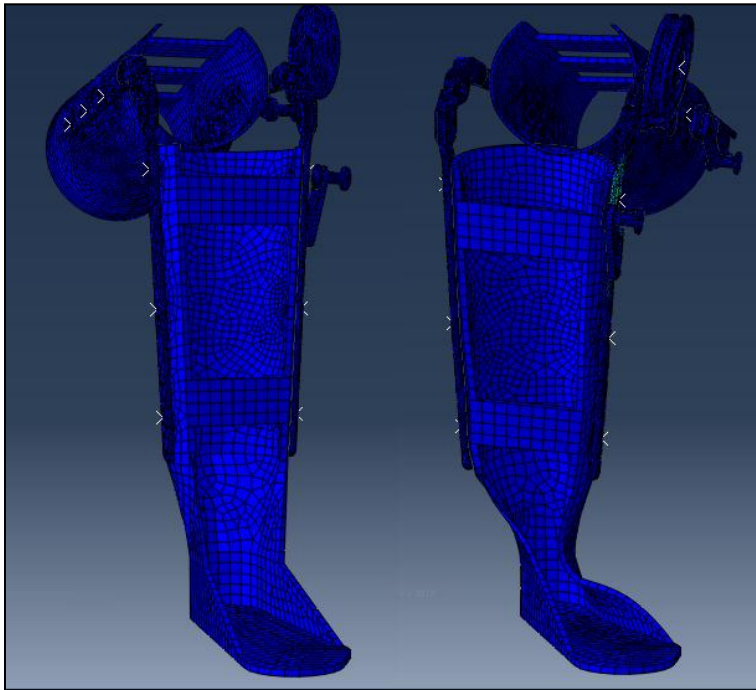
Left: The undeformed KAFO model, Right: The deformed KAFO model (deformation scaled 1:1)

Figure 2-32 shows the regions of the model exceeding 33 MPa and are highlighted in white. It is possible to see the areas of thermal plastic around the lateral side of the ankle would be expected to fail. Figure 2-33 illustrates the regions of the model exceeding 110 MPa. These stress vales were observed in the lateral aluminum uprights close to the knee hinge. Finally Figure 2-34 illustrates the areas in the metallic components of the KAFO brace with von Mises stresses in excess of 290 MPa.

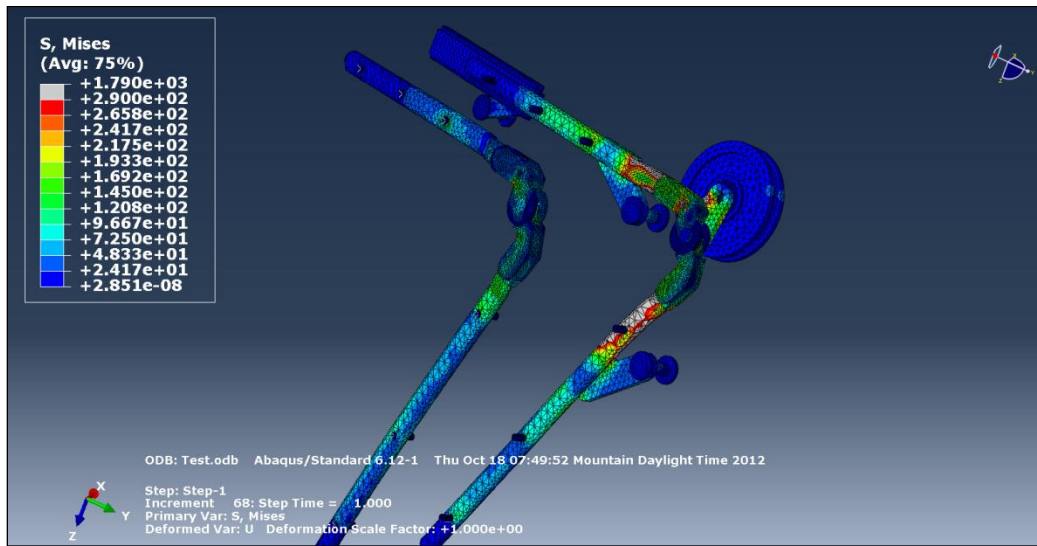Figure 2-32 Nodal Regions in Excess of 33MPa
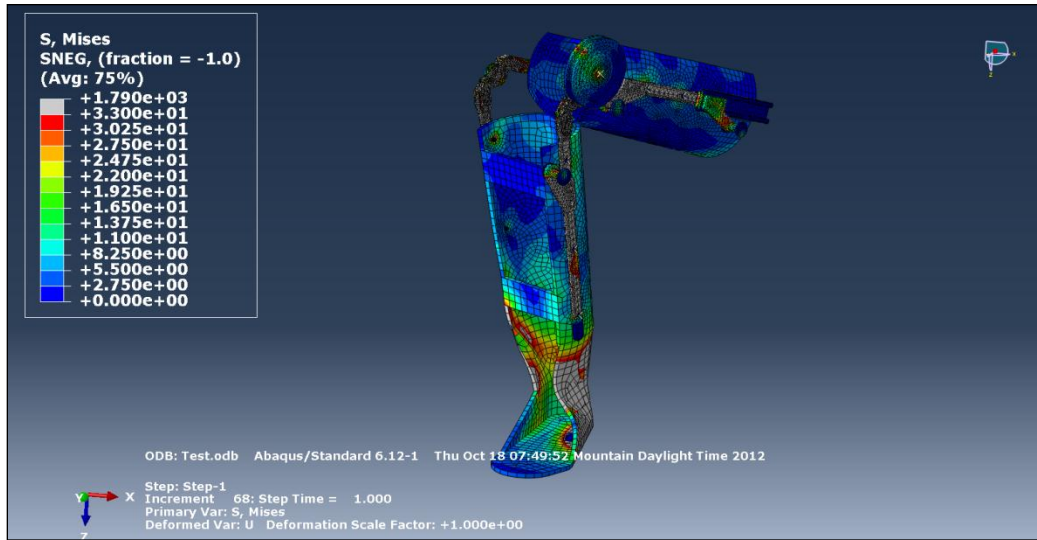
The areas highlighted in white represent nodal areas in excess of 33 MPa

Figure 2-33 Nodal Regions in Excess of 110 MPa
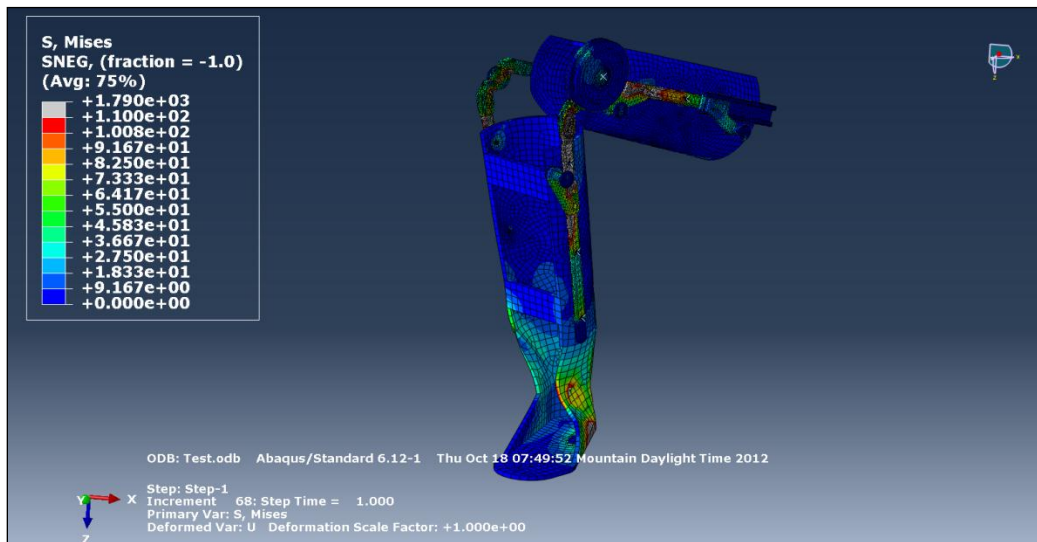
The areas highlighted in white represent nodal areas in excess of 110 MPa

Figure 2-34 Nodal Regions in Excess of 290 MPa

Stress development on the medial surface of the lateral uprights (thermal plastic removed from figure for clarity)
Areas highlighted in white represent nodal areas in excess of 290 MPa

Discussion

The objective of the finite element model was to characterize stress development in the prototype components. Two tests were conducted, each implementing a different set of boundary conditions. The first test applied boundary conditions to the femoral thermal plastic to closely mimic the interaction of the KAFO and the user's leg. The second test represented an idealized worst case scenario. A small area of the femoral thermal plastic was fixed only to prevent vertical movement of the plastic, in other words, preventing knee flexion and causing lateral movement and twist in the KAFO. This second test can be viewed as the device behaving without the effects of the user's leg.

Test 1

The highest von Mises stresses predicted in the thermal plastic components were found to be approximately 13.5 MPa. This stress value is significantly less than the 33 MPa yield stress of the homopolymer polypropylene plastic. Therefore it can be argued that the plastic components in the KAFO should be able to resist the loading forces. The areas of highest stress were found to be in close proximity to the most distal lateral rivet. This result can be expected as, in this area; the rivet would fix the thermal plastic to the uprights. Therefore, any load being transferred from

2-46

the uprights to the thermal plastic (or inversely the thermal plastic to the uprights) would be supported by one of the twelve rivets.

When evaluating the areas of the model exceeding 110 MPa, it can be seen that the lateral aluminum uprights around the knee joint exceed this value. This was confirmed during the able bodied testing. As highlighted in Chapter 2, Part 2 this area in the KAFO prototype experienced torsional deformation when placed under a human load. Therefore, the FEA model was able to highlight this area of the uprights as a region of high potential for failure. Further design and material considerations should be given to this area when further developing the prototype. Furthermore, a single element in the lateral femoral uprights exceeded the 110 MPa yielding stress of the aluminum producing von Mises stresses in excess of 1600 MPa. However, this element does not represent the realistic stress conditions of the KAFO but was rather a mesh artefact. This single element had a very small volume relative to the adjacent elements and was almost flat. Due to the corresponding small volume, very little displacement resulted in very high stress values. This element is not a cause for concern, but rather a limitation of the component geometry and element mesh in the area. Further mesh refinement would be required to alleviate this limitation.

When highlighting the components developing von Mises stresses in excess of the 304 Stainless steel yield strength (290 MPa), it was observed that none of the components manufactured from stainless steel exceeded the 290 MPa threshold. As a result, the FEA model is predicting the design of these components to be sufficient to with stand the maximum loading conditions of the prototype.

Test 2
Test two showed significantly higher deformations and stress development in its components. Many of the elements significantly exceed the yield stress limits of their corresponding material. Since this model is not considering the effect of plasticity, it is difficult to predict the behaviour of the model when large numbers of elements exceed their yield stress limits. However this model does allow for a realization of the role of the human prototype interface. Test 2 models the prototypes ability to resist loading forces without a user; as a result it is apparent to see the

crucial role the user's leg plays in prototype's performance. Failure would have occurred, if not in the thermal plastic, then in the lateral uprights. It can therefore be argued that for the prototype to perform in an optimal and predictable manner, a well fit KAFO is necessary.

Although redesigning the KAFO that the prototype components are mounted to falls outside the scope of this thesis, it is possible to comment on its design from a strictly solid-mechanics view point. Under the maximum loading condition, relatively low stresses were developed in the thermal plastic portions of the KAFO. Intuitively one may suggest that due to the low stresses, areas of the thermal plastic may be removed as they appears to provided little mechanical effect. This approach could be applied to each component, building up areas of high stresses, and removing material in areas of low stresses. Ultimately FEA modeling could be utilized as a tool to fine tune the prototype geometry, material selection, and overall design.

However, this model does come with some limitations. This model is a static model representative of the maximum mechanical requirements of the prototype. The foot and femoral plastic of the model had static displacement boundary conditions defined and forces representative of the loading each component would experience were introduced. However, this model does not account for the dynamic forces developed during STS. Future modelling should incorporate analysing stresses while the model is loaded across the whole STS cycle. This would provide a more accurate picture of the models behavior and the stresses experienced during the duration of STS movements.

A second limitation must be acknowledged. This finite element model incorporates simplified geometry that is not representative of patient specific conditions. This model therefore provides insight of how the prototype can be expected to behave in most cases. It must be acknowledged that it does not necessarily represent the behaviour of all individual cases.

Chapter 2 Conclusions

KAFOs are designed to assist standing in patients with limited lower extremity function. These braces hold the knee extended and the ankle neutral, thereby controlling balance and joint alignment. KAFOs are prescribed for a wide range of patients from those with orthopedic complications through to muscular weakness and paralysis. Consequently, users are often dependant on a wheelchair, and standing becomes physiologically important. Since a KAFO limits knee and ankle motion, rising from a chair creates a challenging task; requiring substantial upper body strength to hoist oneself from seated position. Many KAFO users are unable to achieve sit-to-stand (STS) independently. Currently few to no products exist on the market to aid users during these movements.

This chapter highlighted the design and testing of a novel assistive STS KAFO design. The mechanical requirements of this device were determined using the data set collected in Chapter 1 to serve as target design values. Collaborating with physical therapists and orthotists, a design to mechanically generate knee extension in a KAFO was proposed. A prototype was manufactured and assembled using basic machine shop equipment and off-the-shelf parts. The design utilizes a 900N gas-spring to drive a cable tensioning system. This device can be installed on most existing KAFOs with minor modifications. It can be remote triggered and calculations suggest it can develop knee extension torque sufficient for a 90 kg patient (63Nm based on 0.71Nm/Kg peak).

To bridge the gap between theory and clinical relevance, a pair of prototypes were built for testing on an able bodied subject. Part design and material selection were based on availability and manufacturability considerations. The participant donned the devices and operated the STS function on two floor surfaces, carpet and tile. Testing was aimed to confirm safety of the components and verify the devices' ability to aid knee extension in a low-risk environment. A trial was considered a success if the participant achieved STS without intervention from a spotter, and all components showed no visible damage at completion. In total, 9 trials were conducted (4 on carpet and 5 on tile). Able bodied testing verified that the device is able to assist knee extension. The participant reported a forward lean of their torso prior to initiation of knee extension assisted with balance during the STS task. The first three trials were unsuccessful and

are attributed to unforeseen component failures due to high mechanical stresses. Minor modifications were made to the prototype and included repositioning the distal cable anchor, replacing the cable dead end clamps, and replacing component mounting screws. 6 consecutive successful trials followed.

Finally a Finite Element Model was created to further understand stress development in the prototype components. A three dimensional model was created in SolidWorks and imported into Abaqus. Individual loads were applied to components in the software to simulate the maximally loaded conditions of the KAFO. Two sets of boundary conditions were applied. One to mimic the interaction between the user's leg and KAFO as closely as possible and another to illustrate the device ability to resist loading forces without. In the first test, areas of high stress were predicted in the lateral uprights close to the knee joint. A similar behavior was found during the able-bodied testing. Significantly higher stresses were found in Test 2. As a result it can be shown that KAFO fit plays a crucial role in the prototypes performance.

Currently an assistive KAFO prototype has been designed and tested with an able bodied subject. Numerically the device has the potential to assist KAFO users during STS. Furthermore able-bodied testing show the device can function practically, and the components can withstand the loading conditions. However, to further validate the design, testing on KAFO dependent subjects is necessary. An inherent gap exists in the biomechanics of healthy and disabled movements. How the KAFO interacts with disable subjects should be further analyzed in future work.

Bibliography

1. *KAFO (Knee Ankle Foot Orthosis).* **Sheck and Siress.** s.l. : Sheck & Siress Prosthetics Orthotics Pedorthotic , 2011.

2. *Ambulatory KAFOs: A Physiatry Perspective.* **Herbert, J.** 3S, s.l. : JPO, 2006, Vol. 18, p. 169.

3. *AAOS atlas of orthoses and assistive devices.* **Hsu, J., Michael, J. and Fisk, J.** 4, s.l. : American Academy of Orthopaedic Surgeons , 2008.

4. *Comparison of functional electrical stimulation to long leg braces for upright mobility for children with complete thoracic level spinal injuries.* **Bonaroti, D., et al., et al.** 9, s.l. : Archives of Physical Medicine and Rehabilitation, 1999, Vol. 80, pp. 1047-1053.

5. *Ambulatory KAFOs: A Physical Therapist's Perspective.* **Edelstein, J.** s.l. : American Academy of Orthotists & Prosthetists, 2006, Vol. 18, p. 183.

6. *Consumer Opinions of a Stance Control Knee Orthosis.* **Bernhardt, K., Irby, S. and K., Kaufman.** s.l. : Prosthetics and Orthotics International, 2006, Vol. 30, p. 246.

7. *Usage Follow-up After a Knee Ankle Foot Orthosis Selection and Training Program in Spinal Cord Injury Patients.* **Gatti, M. and al, et.** 3, s.l. : Journal of Pediatric Orthopedics, 2010, Vol. 22.

8. **Process Excellence.** The Pugh Matrix. *Process Managment and Analysis.* [Online] 2011.

9. 1/8" Aircraft Cable. *Princess Auto.* [Online] 2012. http://www.princessauto.com.

10. ASTM, SAE and ISO Grade MArkings and Mechanical Properties for Steel Fasteners. *American Fastener.* [Online] 2012. http://www.americanfastener.com.

11. *Effects of Ageing on Quadriceps Muscle Strength and on the Foward Shift of the Center of Pressure During Sit-to-Stand Movement from a Chair.* **Miyoshi, K. and al., et.** s.l. : Journal of Physical Therapy Sciences, 2005, Vol. 17, pp. 23-28.

12. **Adeeb, S.** Introduction to Finite Element Analysis. *Introduction to Solid Mechanics and Finite Element Analysis Using Mathematica.* Dubuque, IA : Kendall Hunt, 2011.

13. Typical Engineering Properties of Polypropylene. *INEOS Olefins and Polymers .* [Online] 2010. http://www.ineos-op.com.

14. Material Properties. s.l. : Dassault Systemes SolidWorks, 2010.

Appendix A

Typical Component JM and GRF Curves Grouped According to Motor-Dominance for Participant 5 STS trial 1.
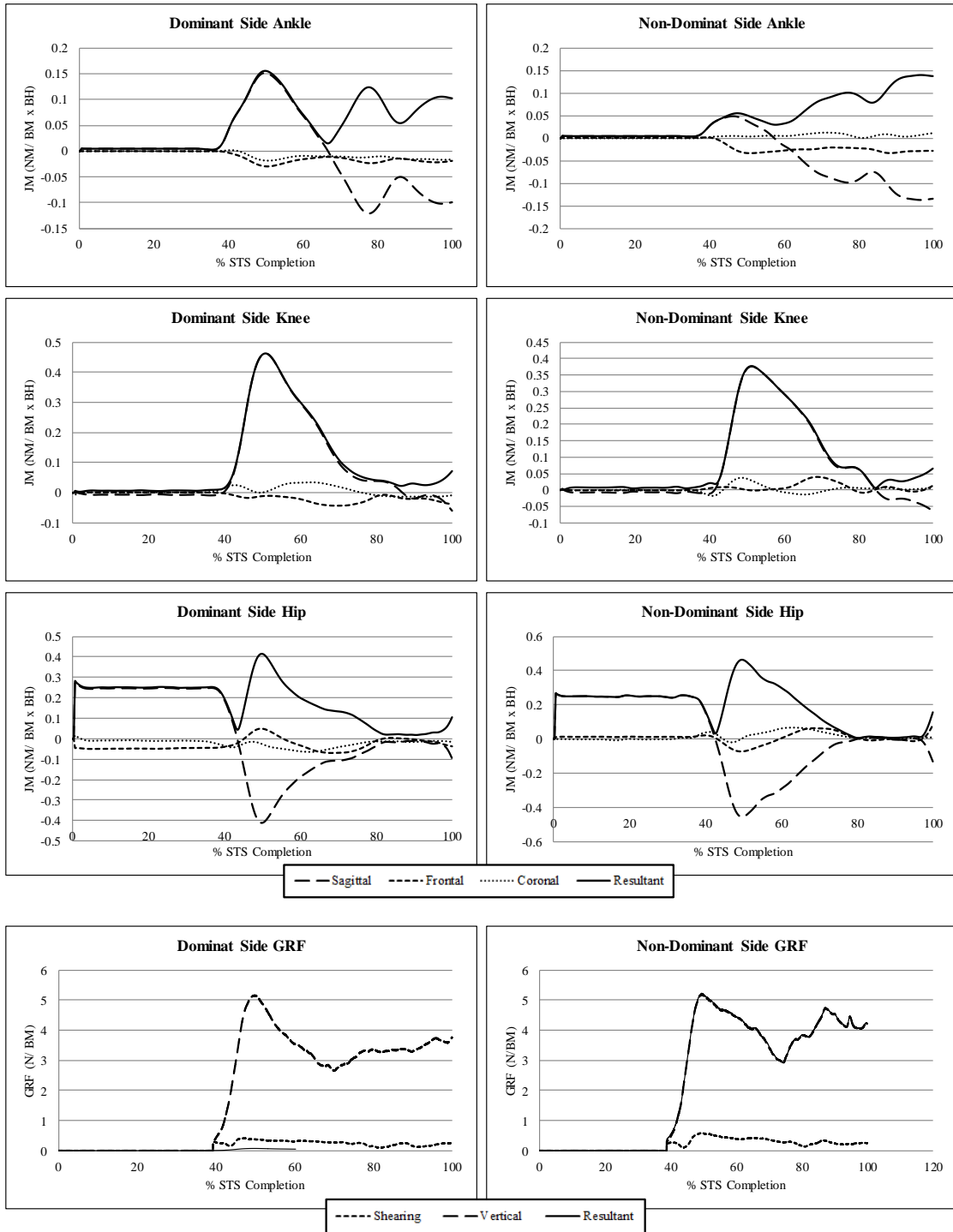
Normalized JMs are reported in units of N.m./ (Kg.m). Sagittal, frontal, and coronal components are illustrated as well as the resultant vector summated curve. Normalized GRFs are reported in units of N/Kg. Vertical and shearing components are illustrated as well as the resultant vector summated curve.

Typical Component JM and GRF Curves Grouped According to Motor-Dominance for Participant 9 STS trial 1.
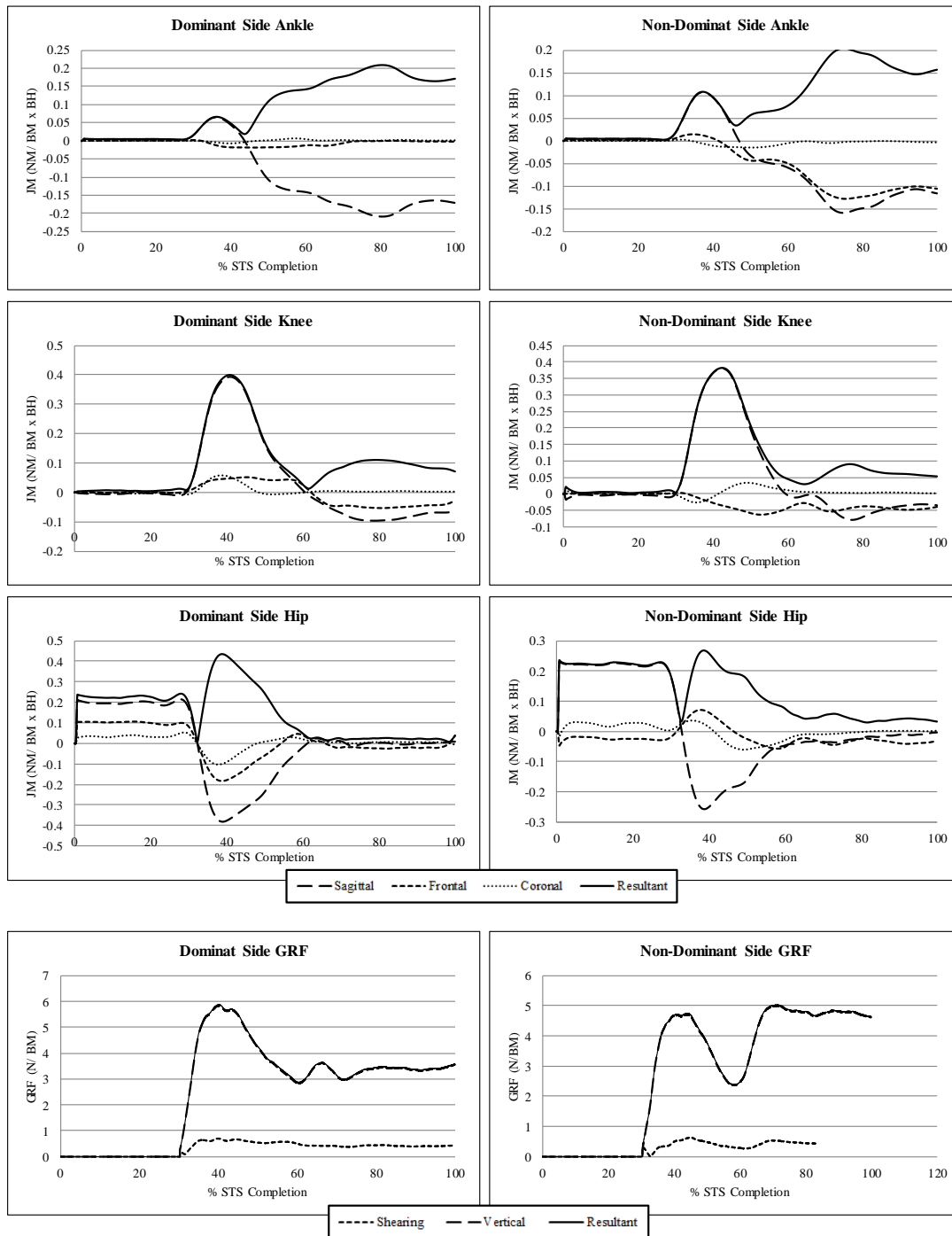
Normalized JMs are reported in units of N.m./ (Kg.m). Sagittal, frontal, and coronal components are illustrated as well as the resultant vector summated curve. Normalized GRFs are reported in units of N/Kg. Vertical and shearing components are illustrated as well as the resultant vector summated curve.

Appendix B

Sample Mathematica code used for averaging of STS trials in the left and right leg

```
(* Input participant's mass and height *)
Mass=70;
Height=1.77;

(* Import data from excel *)
sts1=Import["C:\\Users\\Jon Laptop\\Desktop\\School\\Bilateral Symmetry Study\\Glenrose Data\\Whole
Cycle\\Mathematica Import\\1-1.xls"];
sts2=Import["C:\\Users\\Jon Laptop\\Desktop\\School\\Bilateral Symmetry Study\\Glenrose Data\\Whole
Cycle\\Mathematica Import\\1-2.xls"];
sts3=Import["C:\\Users\\Jon Laptop\\Desktop\\School\\Bilateral Symmetry Study\\Glenrose Data\\Whole
Cycle\\Mathematica Import\\1-3.xls"];
sts4=Import["C:\\Users\\Jon Laptop\\Desktop\\School\\Bilateral Symmetry Study\\Glenrose Data\\Whole
Cycle\\Mathematica Import\\1-4.xls"];
sts5=Import["C:\\Users\\Jon Laptop\\Desktop\\School\\Bilateral Symmetry Study\\Glenrose Data\\Whole
Cycle\\Mathematica Import\\1-5.xls"];
sts6=Import["C:\\Users\\Jon Laptop\\Desktop\\School\\Bilateral Symmetry Study\\Glenrose Data\\Whole
Cycle\\Mathematica Import\\1-6.xls"];
sts7=Import["C:\\Users\\Jon Laptop\\Desktop\\School\\Bilateral Symmetry Study\\Glenrose Data\\Whole
Cycle\\Mathematica Import\\1-7.xls"];
sts8=Import["C:\\Users\\Jon Laptop\\Desktop\\School\\Bilateral Symmetry Study\\Glenrose Data\\Whole
Cycle\\Mathematica Import\\1-8.xls"];
sts9=Import["C:\\Users\\Jon Laptop\\Desktop\\School\\Bilateral Symmetry Study\\Glenrose Data\\Whole
Cycle\\Mathematica Import\\1-9.xls"];
sts10=Import["C:\\Users\\Jon Laptop\\Desktop\\School\\Bilateral Symmetry Study\\Glenrose Data\\Whole
Cycle\\Mathematica Import\\1-10.xls"];
STS1=sts1[[1]];
STS2=sts2[[1]];
STS3=sts3[[1]];
STS4=sts4[[1]];
STS5=sts5[[1]];
STS6=sts6[[1]];
STS7=sts7[[1]];
STS8=sts8[[1]];
STS9=sts9[[1]];
STS10=sts10[[1]];

(* Count terms in each excel sheet *)
k1=Length[STS1];
k2=Length[STS2];
k3=Length[STS3];
k4=Length[STS4];
k5=Length[STS5];
k6=Length[STS6];
k7=Length[STS7];
k8=Length[STS8];
k9=Length[STS9];
k10=Length[STS10];

(* Extracting individual variables *)
percent1=STS1[[1;;k1,2]];
percent2=STS2[[1;;k2,2]];
percent3=STS3[[1;;k3,2]];
```

```
percent4=STS4[[1;;k4,2]];
percent5=STS5[[1;;k5,2]];
percent6=STS6[[1;;k6,2]];
percent7=STS7[[1;;k7,2]];
percent8=STS8[[1;;k8,2]];
percent9=STS9[[1;;k9,2]];
percent10=STS10[[1;;k10,2]];

(* Extract and assemble ankle JMs *)
Lank1=STS1[[1;;k1,3]];
Rank1=STS1[[1;;k1,4]];
Lank2=STS2[[1;;k2,3]];
Rank2=STS2[[1;;k2,4]];
Lank3=STS3[[1;;k3,3]];
Rank3=STS3[[1;;k3,4]];
Lank4=STS4[[1;;k4,3]];
Rank4=STS4[[1;;k4,4]];
Lank5=STS5[[1;;k5,3]];
Rank5=STS5[[1;;k5,4]];
Lank6=STS6[[1;;k6,3]];
Rank6=STS6[[1;;k6,4]];
Lank7=STS7[[1;;k7,3]];
Rank7=STS7[[1;;k7,4]];
Lank8=STS8[[1;;k8,3]];
Rank8=STS8[[1;;k8,4]];
Lank9=STS9[[1;;k9,3]];
Rank9=STS9[[1;;k9,4]];
Lank10=STS10[[1;;k10,3]];
Rank10=STS10[[1;;k10,4]];
JMLank1=Table[{percent1[[i]],Lank1[[i]]},{i,1,k1}];
JMRank1=Table[{percent1[[i]],Rank1[[i]]},{i,1,k1}];
JMLank2=Table[{percent2[[i]],Lank2[[i]]},{i,1,k2}];
JMRank2=Table[{percent2[[i]],Rank2[[i]]},{i,1,k2}];
JMLank3=Table[{percent3[[i]],Lank3[[i]]},{i,1,k3}];
JMRank3=Table[{percent3[[i]],Rank3[[i]]},{i,1,k3}];
JMLank4=Table[{percent4[[i]],Lank4[[i]]},{i,1,k4}];
JMRank4=Table[{percent4[[i]],Rank4[[i]]},{i,1,k4}];
JMLank5=Table[{percent5[[i]],Lank5[[i]]},{i,1,k5}];
JMRank5=Table[{percent5[[i]],Rank5[[i]]},{i,1,k5}];
JMLank6=Table[{percent6[[i]],Lank6[[i]]},{i,1,k6}];
JMRank6=Table[{percent6[[i]],Rank6[[i]]},{i,1,k6}];
JMLank7=Table[{percent7[[i]],Lank7[[i]]},{i,1,k7}];
JMRank7=Table[{percent7[[i]],Rank7[[i]]},{i,1,k7}];
JMLank8=Table[{percent8[[i]],Lank8[[i]]},{i,1,k8}];
JMRank8=Table[{percent8[[i]],Rank8[[i]]},{i,1,k8}];
JMLank9=Table[{percent9[[i]],Lank9[[i]]},{i,1,k9}];
JMRank9=Table[{percent9[[i]],Rank9[[i]]},{i,1,k9}];
JMLank10=Table[{percent10[[i]],Lank10[[i]]},{i,1,k10}];
JMRank10=Table[{percent10[[i]],Rank10[[i]]},{i,1,k10}];

(* Extract and assemble knee JMs *)
Lkne1=STS1[[1;;k1,5]];
Rkne1=STS1[[1;;k1,6]];
Lkne2=STS2[[1;;k2,5]];
Rkne2=STS2[[1;;k2,6]];
Lkne3=STS3[[1;;k3,5]];
```

```
Rkne3=STS3[[1;;k3,6]];
Lkne4=STS4[[1;;k4,5]];
Rkne4=STS4[[1;;k4,6]];
Lkne5=STS5[[1;;k5,5]];
Rkne5=STS5[[1;;k5,6]];
Lkne6=STS6[[1;;k6,5]];
Rkne6=STS6[[1;;k6,6]];
Lkne7=STS7[[1;;k7,5]];
Rkne7=STS7[[1;;k7,6]];
Lkne8=STS8[[1;;k8,5]];
Rkne8=STS8[[1;;k8,6]];
Lkne9=STS9[[1;;k9,5]];
Rkne9=STS9[[1;;k9,6]];
Lkne10=STS10[[1;;k10,5]];
Rkne10=STS10[[1;;k10,6]];
JMLkne1=Table[{percent1[[i]],Lkne1[[i]]},{i,1,k1}];
JMRkne1=Table[{percent1[[i]],Rkne1[[i]]},{i,1,k1}];
JMLkne2=Table[{percent2[[i]],Lkne2[[i]]},{i,1,k2}];
JMRkne2=Table[{percent2[[i]],Rkne2[[i]]},{i,1,k2}];
JMLkne3=Table[{percent3[[i]],Lkne3[[i]]},{i,1,k3}];
JMRkne3=Table[{percent3[[i]],Rkne3[[i]]},{i,1,k3}];
JMLkne4=Table[{percent4[[i]],Lkne4[[i]]},{i,1,k4}];
JMRkne4=Table[{percent4[[i]],Rkne4[[i]]},{i,1,k4}];
JMLkne5=Table[{percent5[[i]],Lkne5[[i]]},{i,1,k5}];
JMRkne5=Table[{percent5[[i]],Rkne5[[i]]},{i,1,k5}];
JMLkne6=Table[{percent6[[i]],Lkne6[[i]]},{i,1,k6}];
JMRkne6=Table[{percent6[[i]],Rkne6[[i]]},{i,1,k6}];
JMLkne7=Table[{percent7[[i]],Lkne7[[i]]},{i,1,k7}];
JMRkne7=Table[{percent7[[i]],Rkne7[[i]]},{i,1,k7}];
JMLkne8=Table[{percent8[[i]],Lkne8[[i]]},{i,1,k8}];
JMRkne8=Table[{percent8[[i]],Rkne8[[i]]},{i,1,k8}];
JMLkne9=Table[{percent9[[i]],Lkne9[[i]]},{i,1,k9}];
JMRkne9=Table[{percent9[[i]],Rkne9[[i]]},{i,1,k9}];
JMLkne10=Table[{percent10[[i]],Lkne10[[i]]},{i,1,k10}];
JMRkne10=Table[{percent10[[i]],Rkne10[[i]]},{i,1,k10}];

(* Extract and assemble hip JMs *)
Lhip1=STS1[[1;;k1,7]];
Rhip1=STS1[[1;;k1,8]];
Lhip2=STS2[[1;;k2,7]];
Rhip2=STS2[[1;;k2,8]];
Lhip3=STS3[[1;;k3,7]];
Rhip3=STS3[[1;;k3,8]];
Lhip4=STS4[[1;;k4,7]];
Rhip4=STS4[[1;;k4,8]];
Lhip5=STS5[[1;;k5,7]];
Rhip5=STS5[[1;;k5,8]];
Lhip6=STS6[[1;;k6,7]];
Rhip6=STS6[[1;;k6,8]];
Lhip7=STS7[[1;;k7,7]];
Rhip7=STS7[[1;;k7,8]];
Lhip8=STS8[[1;;k8,7]];
Rhip8=STS8[[1;;k8,8]];
Lhip9=STS9[[1;;k9,7]];
Rhip9=STS9[[1;;k9,8]];
Lhip10=STS10[[1;;k10,7]];
```

```
Rhip10=STS10[[1;;k10,8]];
JMLhip1=Table[{percent1[[i]],Lhip1[[i]]},{i,1,k1}];
JMRhip1=Table[{percent1[[i]],Rhip1[[i]]},{i,1,k1}];
JMLhip2=Table[{percent2[[i]],Lhip2[[i]]},{i,1,k2}];
JMRhip2=Table[{percent2[[i]],Rhip2[[i]]},{i,1,k2}];
JMLhip3=Table[{percent3[[i]],Lhip3[[i]]},{i,1,k3}];
JMRhip3=Table[{percent3[[i]],Rhip3[[i]]},{i,1,k3}];
JMLhip4=Table[{percent4[[i]],Lhip4[[i]]},{i,1,k4}];
JMRhip4=Table[{percent4[[i]],Rhip4[[i]]},{i,1,k4}];
JMLhip5=Table[{percent5[[i]],Lhip5[[i]]},{i,1,k5}];
JMRhip5=Table[{percent5[[i]],Rhip5[[i]]},{i,1,k5}];
JMLhip6=Table[{percent6[[i]],Lhip6[[i]]},{i,1,k6}];
JMRhip6=Table[{percent6[[i]],Rhip6[[i]]},{i,1,k6}];
JMLhip7=Table[{percent7[[i]],Lhip7[[i]]},{i,1,k7}];
JMRhip7=Table[{percent7[[i]],Rhip7[[i]]},{i,1,k7}];
JMLhip8=Table[{percent8[[i]],Lhip8[[i]]},{i,1,k8}];
JMRhip8=Table[{percent8[[i]],Rhip8[[i]]},{i,1,k8}];
JMLhip9=Table[{percent9[[i]],Lhip9[[i]]},{i,1,k9}];
JMRhip9=Table[{percent9[[i]],Rhip9[[i]]},{i,1,k9}];
JMLhip10=Table[{percent10[[i]],Lhip10[[i]]},{i,1,k10}];
JMRhip10=Table[{percent10[[i]],Rhip10[[i]]},{i,1,k10}];

(* Extract and assemble anlkle power *)
Lankp1=STS1[[1;;k1,9]];
Rankp1=STS1[[1;;k1,10]];
Lankp2=STS2[[1;;k2,9]];
Rankp2=STS2[[1;;k2,10]];
Lankp3=STS3[[1;;k3,9]];
Rankp3=STS3[[1;;k3,10]];
Lankp4=STS4[[1;;k4,9]];
Rankp4=STS4[[1;;k4,10]];
Lankp5=STS5[[1;;k5,9]];
Rankp5=STS5[[1;;k5,10]];
Lankp6=STS6[[1;;k6,9]];
Rankp6=STS6[[1;;k6,10]];
Lankp7=STS7[[1;;k7,9]];
Rankp7=STS7[[1;;k7,10]];
Lankp8=STS8[[1;;k8,9]];
Rankp8=STS8[[1;;k8,10]];
Lankp9=STS9[[1;;k9,9]];
Rankp9=STS9[[1;;k9,10]];
Lankp10=STS10[[1;;k10,9]];
Rankp10=STS10[[1;;k10,10]];
PWLank1=Table[{percent1[[i]],Lankp1[[i]]},{i,1,k1}];
PWRank1=Table[{percent1[[i]],Rankp1[[i]]},{i,1,k1}];
PWLank2=Table[{percent2[[i]],Lankp2[[i]]},{i,1,k2}];
PWRank2=Table[{percent2[[i]],Rankp2[[i]]},{i,1,k2}];
PWLank3=Table[{percent3[[i]],Lankp3[[i]]},{i,1,k3}];
PWRank3=Table[{percent3[[i]],Rankp3[[i]]},{i,1,k3}];
PWLank4=Table[{percent4[[i]],Lankp4[[i]]},{i,1,k4}];
PWRank4=Table[{percent4[[i]],Rankp4[[i]]},{i,1,k4}];
PWLank5=Table[{percent5[[i]],Lankp5[[i]]},{i,1,k5}];
PWRank5=Table[{percent5[[i]],Rankp5[[i]]},{i,1,k5}];
PWLank6=Table[{percent6[[i]],Lankp6[[i]]},{i,1,k6}];
PWRank6=Table[{percent6[[i]],Rankp6[[i]]},{i,1,k6}];
PWLank7=Table[{percent7[[i]],Lankp7[[i]]},{i,1,k7}];
```

```
PWRank7=Table[{percent7[[i]],Rankp7[[i]]},{i,1,k7}];
PWLank8=Table[{percent8[[i]],Lankp8[[i]]},{i,1,k8}];
PWRank8=Table[{percent8[[i]],Rankp8[[i]]},{i,1,k8}];
PWLank9=Table[{percent9[[i]],Lankp9[[i]]},{i,1,k9}];
PWRank9=Table[{percent9[[i]],Rankp9[[i]]},{i,1,k9}];
PWLank10=Table[{percent10[[i]],Lankp10[[i]]},{i,1,k10}];
PWRank10=Table[{percent10[[i]],Rankp10[[i]]},{i,1,k10}];

(* Extract and assemble knee power *)
Lknep1=STS1[[1;;k1,11]];
Rknep1=STS1[[1;;k1,12]];
Lknep2=STS2[[1;;k2,11]];
Rknep2=STS2[[1;;k2,12]];
Lknep3=STS3[[1;;k3,11]];
Rknep3=STS3[[1;;k3,12]];
Lknep4=STS4[[1;;k4,11]];
Rknep4=STS4[[1;;k4,12]];
Lknep5=STS5[[1;;k5,11]];
Rknep5=STS5[[1;;k5,12]];
Lknep6=STS6[[1;;k6,11]];
Rknep6=STS6[[1;;k6,12]];
Lknep7=STS7[[1;;k7,11]];
Rknep7=STS7[[1;;k7,12]];
Lknep8=STS8[[1;;k8,11]];
Rknep8=STS8[[1;;k8,12]];
Lknep9=STS9[[1;;k9,11]];
Rknep9=STS9[[1;;k9,12]];
Lknep10=STS10[[1;;k10,11]];
Rknep10=STS10[[1;;k10,12]];
PWLkne1=Table[{percent1[[i]],Lknep1[[i]]},{i,1,k1}];
PWRkne1=Table[{percent1[[i]],Rknep1[[i]]},{i,1,k1}];
PWLkne2=Table[{percent2[[i]],Lknep2[[i]]},{i,1,k2}];
PWRkne2=Table[{percent2[[i]],Rknep2[[i]]},{i,1,k2}];
PWLkne3=Table[{percent3[[i]],Lknep3[[i]]},{i,1,k3}];
PWRkne3=Table[{percent3[[i]],Rknep3[[i]]},{i,1,k3}];
PWLkne4=Table[{percent4[[i]],Lknep4[[i]]},{i,1,k4}];
PWRkne4=Table[{percent4[[i]],Rknep4[[i]]},{i,1,k4}];
PWLkne5=Table[{percent5[[i]],Lknep5[[i]]},{i,1,k5}];
PWRkne5=Table[{percent5[[i]],Rknep5[[i]]},{i,1,k5}];
PWLkne6=Table[{percent6[[i]],Lknep6[[i]]},{i,1,k6}];
PWRkne6=Table[{percent6[[i]],Rknep6[[i]]},{i,1,k6}];
PWLkne7=Table[{percent7[[i]],Lknep7[[i]]},{i,1,k7}];
PWRkne7=Table[{percent7[[i]],Rknep7[[i]]},{i,1,k7}];
PWLkne8=Table[{percent8[[i]],Lknep8[[i]]},{i,1,k8}];
PWRkne8=Table[{percent8[[i]],Rknep8[[i]]},{i,1,k8}];
PWLkne9=Table[{percent9[[i]],Lknep9[[i]]},{i,1,k9}];
PWRkne9=Table[{percent9[[i]],Rknep9[[i]]},{i,1,k9}];
PWLkne10=Table[{percent10[[i]],Lknep10[[i]]},{i,1,k10}];
PWRkne10=Table[{percent10[[i]],Rknep10[[i]]},{i,1,k10}];

(* Extract and assemble hip power *)
Lhipp1=STS1[[1;;k1,13]];
Rhipp1=STS1[[1;;k1,14]];
Lhipp2=STS2[[1;;k2,13]];
Rhipp2=STS2[[1;;k2,14]];
Lhipp3=STS3[[1;;k3,13]];
```

```
Rhipp3=STS3[[1;;k3,14]];
Lhipp4=STS4[[1;;k4,13]];
Rhipp4=STS4[[1;;k4,14]];
Lhipp5=STS5[[1;;k5,13]];
Rhipp5=STS5[[1;;k5,14]];
Lhipp6=STS6[[1;;k6,13]];
Rhipp6=STS6[[1;;k6,14]];
Lhipp7=STS7[[1;;k7,13]];
Rhipp7=STS7[[1;;k7,14]];
Lhipp8=STS8[[1;;k8,13]];
Rhipp8=STS8[[1;;k8,14]];
Lhipp9=STS9[[1;;k9,13]];
Rhipp9=STS9[[1;;k9,14]];
Lhipp10=STS10[[1;;k10,13]];
Rhipp10=STS10[[1;;k10,14]];
PWLhip1=Table[{percent1[[i]],Lhipp1[[i]]},{i,1,k1}];
PWRhip1=Table[{percent1[[i]],Rhipp1[[i]]},{i,1,k1}];
PWLhip2=Table[{percent2[[i]],Lhipp2[[i]]},{i,1,k2}];
PWRhip2=Table[{percent2[[i]],Rhipp2[[i]]},{i,1,k2}];
PWLhip3=Table[{percent3[[i]],Lhipp3[[i]]},{i,1,k3}];
PWRhip3=Table[{percent3[[i]],Rhipp3[[i]]},{i,1,k3}];
PWLhip4=Table[{percent4[[i]],Lhipp4[[i]]},{i,1,k4}];
PWRhip4=Table[{percent4[[i]],Rhipp4[[i]]},{i,1,k4}];
PWLhip5=Table[{percent5[[i]],Lhipp5[[i]]},{i,1,k5}];
PWRhip5=Table[{percent5[[i]],Rhipp5[[i]]},{i,1,k5}];
PWLhip6=Table[{percent6[[i]],Lhipp6[[i]]},{i,1,k6}];
PWRhip6=Table[{percent6[[i]],Rhipp6[[i]]},{i,1,k6}];
PWLhip7=Table[{percent7[[i]],Lhipp7[[i]]},{i,1,k7}];
PWRhip7=Table[{percent7[[i]],Rhipp7[[i]]},{i,1,k7}];
PWLhip8=Table[{percent8[[i]],Lhipp8[[i]]},{i,1,k8}];
PWRhip8=Table[{percent8[[i]],Rhipp8[[i]]},{i,1,k8}];
PWLhip9=Table[{percent9[[i]],Lhipp9[[i]]},{i,1,k9}];
PWRhip9=Table[{percent9[[i]],Rhipp9[[i]]},{i,1,k9}];
PWLhip10=Table[{percent10[[i]],Lhipp10[[i]]},{i,1,k10}];
PWRhip10=Table[{percent10[[i]],Rhipp10[[i]]},{i,1,k10}];

(* Interpolate assembeled JMs and Powers *)
fLa1=Interpolation[JMLank1,InterpolationOrder□1];
fLa2=Interpolation[JMLank2,InterpolationOrder□1];
fLa3=Interpolation[JMLank3,InterpolationOrder□1];
fLa4=Interpolation[JMLank4,InterpolationOrder□1];
fLa5=Interpolation[JMLank5,InterpolationOrder□1];
fLa6=Interpolation[JMLank6,InterpolationOrder□1];
fLa7=Interpolation[JMLank7,InterpolationOrder□1];
fLa8=Interpolation[JMLank8,InterpolationOrder□1];
fLa9=Interpolation[JMLank9,InterpolationOrder□1];
fLa10=Interpolation[JMLank10,InterpolationOrder□1];
fRa1=Interpolation[JMRank1,InterpolationOrder□1];
fRa2=Interpolation[JMRank2,InterpolationOrder□1];
fRa3=Interpolation[JMRank3,InterpolationOrder□1];
fRa4=Interpolation[JMRank4,InterpolationOrder□1];
fRa5=Interpolation[JMRank5,InterpolationOrder□1];
fRa6=Interpolation[JMRank6,InterpolationOrder□1];
fRa7=Interpolation[JMRank7,InterpolationOrder□1];
fRa8=Interpolation[JMRank8,InterpolationOrder□1];
fRa9=Interpolation[JMRank9,InterpolationOrder□1];
```

fRa10=Interpolation[JMRank10,InterpolationOrder□1];

fLk1=Interpolation[JMLkne1,InterpolationOrder□1];
fLk2=Interpolation[JMLkne2,InterpolationOrder□1];
fLk3=Interpolation[JMLkne3,InterpolationOrder□1];
fLk4=Interpolation[JMLkne4,InterpolationOrder□1];
fLk5=Interpolation[JMLkne5,InterpolationOrder□1];
fLk6=Interpolation[JMLkne6,InterpolationOrder□1];
fLk7=Interpolation[JMLkne7,InterpolationOrder□1];
fLk8=Interpolation[JMLkne8,InterpolationOrder□1];
fLk9=Interpolation[JMLkne9,InterpolationOrder□1];
fLk10=Interpolation[JMLkne10,InterpolationOrder□1];
fRk1=Interpolation[JMRkne1,InterpolationOrder□1];
fRk2=Interpolation[JMRkne2,InterpolationOrder□1];
fRk3=Interpolation[JMRkne3,InterpolationOrder□1];
fRk4=Interpolation[JMRkne4,InterpolationOrder□1];
fRk5=Interpolation[JMRkne5,InterpolationOrder□1];
fRk6=Interpolation[JMRkne6,InterpolationOrder□1];
fRk7=Interpolation[JMRkne7,InterpolationOrder□1];
fRk8=Interpolation[JMRkne8,InterpolationOrder□1];
fRk9=Interpolation[JMRkne9,InterpolationOrder□1];
fRk10=Interpolation[JMRkne10,InterpolationOrder□1];

fLh1=Interpolation[JMLhip1,InterpolationOrder□1];
fLh2=Interpolation[JMLhip2,InterpolationOrder□1];
fLh3=Interpolation[JMLhip3,InterpolationOrder□1];
fLh4=Interpolation[JMLhip4,InterpolationOrder□1];
fLh5=Interpolation[JMLhip5,InterpolationOrder□1];
fLh6=Interpolation[JMLhip6,InterpolationOrder□1];
fLh7=Interpolation[JMLhip7,InterpolationOrder□1];
fLh8=Interpolation[JMLhip8,InterpolationOrder□1];
fLh9=Interpolation[JMLhip9,InterpolationOrder□1];
fLh10=Interpolation[JMLhip10,InterpolationOrder□1];
fRh1=Interpolation[JMRhip1,InterpolationOrder□1];
fRh2=Interpolation[JMRhip2,InterpolationOrder□1];
fRh3=Interpolation[JMRhip3,InterpolationOrder□1];
fRh4=Interpolation[JMRhip4,InterpolationOrder□1];
fRh5=Interpolation[JMRhip5,InterpolationOrder□1];
fRh6=Interpolation[JMRhip6,InterpolationOrder□1];
fRh7=Interpolation[JMRhip7,InterpolationOrder□1];
fRh8=Interpolation[JMRhip8,InterpolationOrder□1];
fRh9=Interpolation[JMRhip9,InterpolationOrder□1];
fRh10=Interpolation[JMRhip10,InterpolationOrder□1];

fLap1=Interpolation[PWLank1,InterpolationOrder□1];
fLap2=Interpolation[PWLank2,InterpolationOrder□1];
fLap3=Interpolation[PWLank3,InterpolationOrder□1];
fLap4=Interpolation[PWLank4,InterpolationOrder□1];
fLap5=Interpolation[PWLank5,InterpolationOrder□1];
fLap6=Interpolation[PWLank6,InterpolationOrder□1];
fLap7=Interpolation[PWLank7,InterpolationOrder□1];
fLap8=Interpolation[PWLank8,InterpolationOrder□1];
fLap9=Interpolation[PWLank9,InterpolationOrder□1];
fLap10=Interpolation[PWLank10,InterpolationOrder□1];
fRap1=Interpolation[PWRank1,InterpolationOrder□1];
fRap2=Interpolation[PWRank2,InterpolationOrder□1];

```
fRap3=Interpolation[PWRank3,InterpolationOrder→1];
fRap4=Interpolation[PWRank4,InterpolationOrder→1];
fRap5=Interpolation[PWRank5,InterpolationOrder→1];
fRap6=Interpolation[PWRank6,InterpolationOrder→1];
fRap7=Interpolation[PWRank7,InterpolationOrder→1];
fRap8=Interpolation[PWRank8,InterpolationOrder→1];
fRap9=Interpolation[PWRank9,InterpolationOrder→1];
fRap10=Interpolation[PWRank10,InterpolationOrder→1];

fLkp1=Interpolation[PWLkne1,InterpolationOrder→1];
fLkp2=Interpolation[PWLkne2,InterpolationOrder→1];
fLkp3=Interpolation[PWLkne3,InterpolationOrder→1];
fLkp4=Interpolation[PWLkne4,InterpolationOrder→1];
fLkp5=Interpolation[PWLkne5,InterpolationOrder→1];
fLkp6=Interpolation[PWLkne6,InterpolationOrder→1];
fLkp7=Interpolation[PWLkne7,InterpolationOrder→1];
fLkp8=Interpolation[PWLkne8,InterpolationOrder→1];
fLkp9=Interpolation[PWLkne9,InterpolationOrder→1];
fLkp10=Interpolation[PWLkne10,InterpolationOrder→1];
fRkp1=Interpolation[PWRkne1,InterpolationOrder→1];
fRkp2=Interpolation[PWRkne2,InterpolationOrder→1];
fRkp3=Interpolation[PWRkne3,InterpolationOrder→1];
fRkp4=Interpolation[PWRkne4,InterpolationOrder→1];
fRkp5=Interpolation[PWRkne5,InterpolationOrder→1];
fRkp6=Interpolation[PWRkne6,InterpolationOrder→1];
fRkp7=Interpolation[PWRkne7,InterpolationOrder→1];
fRkp8=Interpolation[PWRkne8,InterpolationOrder→1];
fRkp9=Interpolation[PWRkne9,InterpolationOrder→1];
fRkp10=Interpolation[PWRkne10,InterpolationOrder→1];

fLhp1=Interpolation[PWLhip1,InterpolationOrder→1];
fLhp2=Interpolation[PWLhip2,InterpolationOrder→1];
fLhp3=Interpolation[PWLhip3,InterpolationOrder→1];
fLhp4=Interpolation[PWLhip4,InterpolationOrder→1];
fLhp5=Interpolation[PWLhip5,InterpolationOrder→1];
fLhp6=Interpolation[PWLhip6,InterpolationOrder→1];
fLhp7=Interpolation[PWLhip7,InterpolationOrder→1];
fLhp8=Interpolation[PWLhip8,InterpolationOrder→1];
fLhp9=Interpolation[PWLhip9,InterpolationOrder→1];
fLhp10=Interpolation[PWLhip10,InterpolationOrder→1];
fRhp1=Interpolation[PWRhip1,InterpolationOrder→1];
fRhp2=Interpolation[PWRhip2,InterpolationOrder→1];
fRhp3=Interpolation[PWRhip3,InterpolationOrder→1];
fRhp4=Interpolation[PWRhip4,InterpolationOrder→1];
fRhp5=Interpolation[PWRhip5,InterpolationOrder→1];
fRhp6=Interpolation[PWRhip6,InterpolationOrder→1];
fRhp7=Interpolation[PWRhip7,InterpolationOrder→1];
fRhp8=Interpolation[PWRhip8,InterpolationOrder→1];
fRhp9=Interpolation[PWRhip9,InterpolationOrder→1];
fRhp10=Interpolation[PWRhip10,InterpolationOrder→1];

(* Average, Subtract, Normalize and Max/Min interpolated data *)
avgDiffA=Table[{2*i,((fLa1[2*i]+fLa2[2*i]+fLa3[2*i]+fLa4[2*i]+fLa5[2*i]+fLa6[2*i]+fLa7[2*i]+fLa8[2*i]+fLa9[2*i]+fLa10[2*i])-
(fRa1[2*i]+fRa2[2*i]+fRa3[2*i]+fRa4[2*i]+fRa5[2*i]+fRa6[2*i]+fRa7[2*i]+fRa8[2*i]+fRa9[2*i]+fRa10[2*i]))/(10*Mass*Height)},{i,0,50}];
```

MaxDiffA=Table[{2*i,Max[fLa1[2*i]-fRa1[2*i],fLa2[2*i]-fRa2[2*i],fLa3[2*i]-fRa3[2*i],fLa4[2*i]-fRa4[2*i],fLa5[2*i]-fRa5[2*i],fLa6[2*i]-fRa6[2*i],fLa7[2*i]-fRa7[2*i],fLa8[2*i]-fRa8[2*i],fLa9[2*i]-fRa9[2*i],fLa10[2*i]-fRa10[2*i]]/(Mass*Height)},{i,0,50}];
MinDiffA=Table[{2*i,Min[fLa1[2*i]-fRa1[2*i],fLa2[2*i]-fRa2[2*i],fLa3[2*i]-fRa3[2*i],fLa4[2*i]-fRa4[2*i],fLa5[2*i]-fRa5[2*i],fLa6[2*i]-fRa6[2*i],fLa7[2*i]-fRa7[2*i],fLa8[2*i]-fRa8[2*i],fLa9[2*i]-fRa9[2*i],fLa10[2*i]-fRa10[2*i]]/(Mass*Height)},{i,0,50}];

avgDiffK=Table[{2*i,((fLk1[2*i]+fLk2[2*i]+fLk3[2*i]+fLk4[2*i]+fLk5[2*i]+fLk6[2*i]+fLk7[2*i]+fLk8[2*i]+fLk9[2*i]+fLk10[2*i])-
(fRk1[2*i]+fRk2[2*i]+fRk3[2*i]+fRk4[2*i]+fRk5[2*i]+fRk6[2*i]+fRk7[2*i]+fRk8[2*i]+fRk9[2*i]+fRk10[2*i]))/(10*Mass*Height)},{i,0,50}];
MaxDiffK=Table[{2*i,Max[fLk1[2*i]-fRk1[2*i],fLk2[2*i]-fRk2[2*i],fLk3[2*i]-fRk3[2*i],fLk4[2*i]-fRk4[2*i],fLk5[2*i]-fRk5[2*i],fLk6[2*i]-fRk6[2*i],fLk7[2*i]-fRk7[2*i],fLk8[2*i]-fRk8[2*i],fLk9[2*i]-fRk9[2*i],fLk10[2*i]-fRk10[2*i]]/(Mass*Height)},{i,0,50}];
MinDiffK=Table[{2*i,Min[fLk1[2*i]-fRk1[2*i],fLk2[2*i]-fRk2[2*i],fLk3[2*i]-fRk3[2*i],fLk4[2*i]-fRk4[2*i],fLk5[2*i]-fRk5[2*i],fLk6[2*i]-fRk6[2*i],fLk7[2*i]-fRk7[2*i],fLk8[2*i]-fRk8[2*i],fLk9[2*i]-fRk9[2*i],fLk10[2*i]-fRk10[2*i]]/(Mass*Height)},{i,0,50}];

avgDiffH=Table[{2*i,((fLh1[2*i]+fLh2[2*i]+fLh3[2*i]+fLh4[2*i]+fLh5[2*i]+fLh6[2*i]+fLh7[2*i]+fLh8[2*i]+fLh9[2*i]+fLh10[2*i])-
(fRh1[2*i]+fRh2[2*i]+fRh3[2*i]+fRh4[2*i]+fRh5[2*i]+fRh6[2*i]+fRh7[2*i]+fRh8[2*i]+fRh9[2*i]+fRh10[2*i]))/(10*Mass*Height)},{i,0,50}];
MaxDiffH=Table[{2*i,Max[fLh1[2*i]-fRh1[2*i],fLh2[2*i]-fRh2[2*i],fLh3[2*i]-fRh3[2*i],fLh4[2*i]-fRh4[2*i],fLh5[2*i]-fRh5[2*i],fLh6[2*i]-fRh6[2*i],fLh7[2*i]-fRh7[2*i],fLh8[2*i]-fRh8[2*i],fLh9[2*i]-fRh9[2*i],fLh10[2*i]-fRh10[2*i]]/(Mass*Height)},{i,0,50}];
MinDiffH=Table[{2*i,Min[fLh1[2*i]-fRh1[2*i],fLh2[2*i]-fRh2[2*i],fLh3[2*i]-fRh3[2*i],fLh4[2*i]-fRh4[2*i],fLh5[2*i]-fRh5[2*i],fLh6[2*i]-fRh6[2*i],fLh7[2*i]-fRh7[2*i],fLh8[2*i]-fRh8[2*i],fLh9[2*i]-fRh9[2*i],fLh10[2*i]-fRh10[2*i]]/(Mass*Height)},{i,0,50}];

avgPDiffA=Table[{2*i,((fLap1[2*i]+fLap2[2*i]+fLap3[2*i]+fLap4[2*i]+fLap5[2*i]+fLap6[2*i]+fLap7[2*i]+fLap8[2*i]+fLap9[2*i]+fLap10[2*i])-
(fRap1[2*i]+fRap2[2*i]+fRap3[2*i]+fRap4[2*i]+fRap5[2*i]+fRap6[2*i]+fRap7[2*i]+fRap8[2*i]+fRap9[2*i]+fRap10[2*i]))/(10*Mass*Height)},{i,0,50}];
MaxPDiffA=Table[{2*i,Max[fLap1[2*i]-fRap1[2*i],fLap2[2*i]-fRap2[2*i],fLap3[2*i]-fRap3[2*i],fLap4[2*i]-fRap4[2*i],fLap5[2*i]-fRap5[2*i],fLap6[2*i]-fRap6[2*i],fLap7[2*i]-fRap7[2*i],fLap8[2*i]-fRap8[2*i],fLap9[2*i]-fRap9[2*i],fLap10[2*i]-fRap10[2*i]]/(Mass*Height)},{i,0,50}];
MinPDiffA=Table[{2*i,Min[fLap1[2*i]-fRap1[2*i],fLap2[2*i]-fRap2[2*i],fLap3[2*i]-fRap3[2*i],fLap4[2*i]-fRap4[2*i],fLap5[2*i]-fRap5[2*i],fLap6[2*i]-fRap6[2*i],fLap7[2*i]-fRap7[2*i],fLap8[2*i]-fRap8[2*i],fLap9[2*i]-fRap9[2*i],fLap10[2*i]-fRap10[2*i]]/(Mass*Height)},{i,0,50}];

avgPDiffK=Table[{2*i,((fLkp1[2*i]+fLkp2[2*i]+fLkp3[2*i]+fLkp4[2*i]+fLkp5[2*i]+fLkp6[2*i]+fLkp7[2*i]+fLkp8[2*i]+fLkp9[2*i]+fLkp10[2*i])-
(fRkp1[2*i]+fRkp2[2*i]+fRkp3[2*i]+fRkp4[2*i]+fRkp5[2*i]+fRkp6[2*i]+fRkp7[2*i]+fRkp8[2*i]+fRkp9[2*i]+fRkp10[2*i]))/(10*Mass*Height)},{i,0,50}];
MaxPDiffK=Table[{2*i,Max[fLkp1[2*i]-fRkp1[2*i],fLkp2[2*i]-fRkp2[2*i],fLkp3[2*i]-fRkp3[2*i],fLkp4[2*i]-fRkp4[2*i],fLkp5[2*i]-fRkp5[2*i],fLkp6[2*i]-fRkp6[2*i],fLkp7[2*i]-fRkp7[2*i],fLkp8[2*i]-fRkp8[2*i],fLkp9[2*i]-fRkp9[2*i],fLkp10[2*i]-fRkp10[2*i]]/(Mass*Height)},{i,0,50}];
MinPDiffK=Table[{2*i,Min[fLkp1[2*i]-fRkp1[2*i],fLkp2[2*i]-fRkp2[2*i],fLkp3[2*i]-fRkp3[2*i],fLkp4[2*i]-fRkp4[2*i],fLkp5[2*i]-fRkp5[2*i],fLkp6[2*i]-fRkp6[2*i],fLkp7[2*i]-fRkp7[2*i],fLkp8[2*i]-fRkp8[2*i],fLkp9[2*i]-fRkp9[2*i],fLkp10[2*i]-fRkp10[2*i]]/(Mass*Height)},{i,0,50}];

avgPDiffH=Table[{2*i,((fLhp1[2*i]+fLhp2[2*i]+fLhp3[2*i]+fLhp4[2*i]+fLhp5[2*i]+fLhp6[2*i]+fLhp7[2*i]+fLhp8[2*i]+fLhp9[2*i]+fLhp10[2*i])-
(fRhp1[2*i]+fRhp2[2*i]+fRhp3[2*i]+fRhp4[2*i]+fRhp5[2*i]+fRhp6[2*i]+fRhp7[2*i]+fRhp8[2*i]+fRhp9[2*i]+fRhp10[2*i]))/(10*Mass*Height)},{i,0,50}];

MaxPDiffH=Table[{2*i,Max[fLhp1[2*i]-fRhp1[2*i],fLhp2[2*i]-fRhp2[2*i],fLhp3[2*i]-fRhp3[2*i],fLhp4[2*i]-fRhp4[2*i],fLhp5[2*i]-fRhp5[2*i],fLhp6[2*i]-fRhp6[2*i],fLhp7[2*i]-fRhp7[2*i],fLhp8[2*i]-fRhp8[2*i],fLhp9[2*i]-fRhp9[2*i],fLhp10[2*i]-fRhp10[2*i]]/(Mass*Height)},{i,0,50}];
MinPDiffH=Table[{2*i,Min[fLhp1[2*i]-fRhp1[2*i],fLhp2[2*i]-fRhp2[2*i],fLhp3[2*i]-fRhp3[2*i],fLhp4[2*i]-fRhp4[2*i],fLhp5[2*i]-fRhp5[2*i],fLhp6[2*i]-fRhp6[2*i],fLhp7[2*i]-fRhp7[2*i],fLhp8[2*i]-fRhp8[2*i],fLhp9[2*i]-fRhp9[2*i],fLhp10[2*i]-fRhp10[2*i]]/(Mass*Height)},{i,0,50}];

(* Plot Interpolated Data *)

(* Change Par # in Plot labels *)
ListPlot[{avgDiffA,MaxDiffA, MinDiffA}, Joined□True, PlotStyle□ {Black,{Black,Dashed},{Black,Dashed}}, AxesLabel□{"% STS Cycle", "JM (Nm/BMxBH)"} ,PlotLabel□ "Par 1 Average Ankle Difference"]
ListPlot[{avgDiffK,MaxDiffK, MinDiffK}, Joined□True, PlotStyle□ {Black,{Black,Dashed},{Black,Dashed}}, AxesLabel□{"% STS Cycle", "JM (Nm/BMxBH)"} ,PlotLabel□ "Par 1 Average Knee Difference"]
ListPlot[{avgDiffH,MaxDiffH, MinDiffH}, Joined□True, PlotStyle□ {Black,{Black,Dashed},{Black,Dashed}}, AxesLabel□{"% STS Cycle", "JM (Nm/BMxBH)"} ,PlotLabel□ "Par 1 Average Hip Difference"]
ListPlot[{avgPDiffA,MaxPDiffA, MinPDiffA}, Joined□True, PlotStyle□ {Black,{Black,Dashed},{Black,Dashed}}, AxesLabel□{"% STS Cycle", "Power (W/BMxBH)"} ,PlotLabel□ "Par 1 Average Ankle Difference"]
ListPlot[{avgPDiffK,MaxPDiffK, MinPDiffK}, Joined□True, PlotStyle□ {Black,{Black,Dashed},{Black,Dashed}}, AxesLabel□{"% STS Cycle", "Power (W/BMxBH)"} ,PlotLabel□ "Par 1 Average Knee Difference"]
ListPlot[{avgPDiffH,MaxPDiffH, MinPDiffH}, Joined□True, PlotStyle□ {Black,{Black,Dashed},{Black,Dashed}}, AxesLabel□{"% STS Cycle", "Power (W/BMxBH)"} ,PlotLabel□ "Par 1 Average Hip Difference"]

(* Calculate Correltaions *)
AvgLa=Table[{2*i,(fLa1[2*i]+fLa2[2*i]+fLa3[2*i]+fLa4[2*i]+fLa5[2*i]+fLa6[2*i]+fLa7[2*i]+fLa8[2*i]+fLa9[2*i]+fLa10[2*i])/(10*Mass*Height)},{i,0,50}];
AvgRa=Table[{2*i,(fRa1[2*i]+fRa2[2*i]+fRa3[2*i]+fRa4[2*i]+fRa5[2*i]+fRa6[2*i]+fRa7[2*i]+fRa8[2*i]+fRa9[2*i]+fRa10[2*i])/(10*Mass*Height)},{i,0,50}];
AvgLk=Table[{2*i,(fLk1[2*i]+fLk2[2*i]+fLk3[2*i]+fLk4[2*i]+fLk5[2*i]+fLk6[2*i]+fLk7[2*i]+fLk8[2*i]+fLk9[2*i]+fLk10[2*i])/(10*Mass*Height)},{i,0,50}];
AvgRk=Table[{2*i,(fRk1[2*i]+fRk2[2*i]+fRk3[2*i]+fRk4[2*i]+fRk5[2*i]+fRk6[2*i]+fRk7[2*i]+fRk8[2*i]+fRk9[2*i]+fRk10[2*i])/(10*Mass*Height)},{i,0,50}];
AvgLh=Table[{2*i,(fLh1[2*i]+fLh2[2*i]+fLh3[2*i]+fLh4[2*i]+fLh5[2*i]+fLh6[2*i]+fLh7[2*i]+fLh8[2*i]+fLh9[2*i]+fLh10[2*i])/(10*Mass*Height)},{i,0,50}];
AvgRh=Table[{2*i,(fRh1[2*i]+fRh2[2*i]+fRh3[2*i]+fRh4[2*i]+fRh5[2*i]+fRh6[2*i]+fRh7[2*i]+fRh8[2*i]+fRh9[2*i]+fRh10[2*i])/(10*Mass*Height)},{i,0,50}];
AvgLap=Table[{2*i,(fLap1[2*i]+fLap2[2*i]+fLap3[2*i]+fLap4[2*i]+fLap5[2*i]+fLap6[2*i]+fLap7[2*i]+fLap8[2*i]+fLap9[2*i]+fLap10[2*i])/(10*Mass*Height)},{i,0,50}];
AvgRap=Table[{2*i,(fRap1[2*i]+fRap2[2*i]+fRap3[2*i]+fRap4[2*i]+fRap5[2*i]+fRap6[2*i]+fRap7[2*i]+fRap8[2*i]+fRap9[2*i]+fRap10[2*i])/(10*Mass*Height)},{i,0,50}];
AvgLkp=Table[{2*i,(fLkp1[2*i]+fLkp2[2*i]+fLkp3[2*i]+fLkp4[2*i]+fLkp5[2*i]+fLkp6[2*i]+fLkp7[2*i]+fLkp8[2*i]+fLkp9[2*i]+fLkp10[2*i])/(10*Mass*Height)},{i,0,50}];
AvgRkp=Table[{2*i,(fRkp1[2*i]+fRkp2[2*i]+fRkp3[2*i]+fRkp4[2*i]+fRkp5[2*i]+fRkp6[2*i]+fRkp7[2*i]+fRkp8[2*i]+fRkp9[2*i]+fRkp10[2*i])/(10*Mass*Height)},{i,0,50}];
AvgLhp=Table[{2*i,(fLhp1[2*i]+fLhp2[2*i]+fLhp3[2*i]+fLhp4[2*i]+fLhp5[2*i]+fLhp6[2*i]+fLhp7[2*i]+fLhp8[2*i]+fLhp9[2*i]+fLhp10[2*i])/(10*Mass*Height)},{i,0,50}];
AvgRhp=Table[{2*i,(fRhp1[2*i]+fRhp2[2*i]+fRhp3[2*i]+fRhp4[2*i]+fRhp5[2*i]+fRhp6[2*i]+fRhp7[2*i]+fRhp8[2*i]+fRhp9[2*i]+fRhp10[2*i])/(10*Mass*Height)},{i,0,50}];
Print["Ankle JM Correlation :"]
Correlation[AvgLa[[1;;50,2]],AvgRa[[1;;50,2]]]
Print["Knee JM Correlation :"]

```
Correlation[AvgLk[[1;;50,2]],AvgRk[[1;;50,2]]]
Print["Hip JM Correlation :"]
Correlation[AvgLh[[1;;50,2]],AvgRh[[1;;50,2]]]
Print["Ankle Power Correlation :"]
Correlation[AvgLap[[1;;50,2]],AvgRap[[1;;50,2]]]
Print["Knee Power Correlation :"]
Correlation[AvgLkp[[1;;50,2]],AvgRkp[[1;;50,2]]]
Print["Hip Power Correlation :"]
Correlation[AvgLhp[[1;;50,2]],AvgRhp[[1;;50,2]]]

(* Plot Symmetry Indexes *)

(* Change Participant Name *)
Per=Table[2*(i-1),{i,1,51}];
SIa=Abs[AvgLa[[1;;51,2]]-AvgRa[[1;;51,2]]]/ (Abs[AvgLa[[1;;51,2]]+AvgRa[[1;;51,2]]]/2)*100;
SIk=Abs[AvgLk[[1;;50,2]]-AvgRk[[1;;50,2]]]/ (Abs[AvgLk[[1;;50,2]]+AvgRk[[1;;50,2]]]/2)*100;
SIh=Abs[AvgLh[[1;;50,2]]-AvgRh[[1;;50,2]]]/ (Abs[AvgLh[[1;;50,2]]+AvgRh[[1;;50,2]]]/2)*100;
SIap=Abs[AvgLap[[1;;50,2]]-AvgRap[[1;;50,2]]]/ (Abs[AvgLap[[1;;50,2]]+AvgRap[[1;;50,2]]]/2)*100;
SIkp=Abs[AvgLkp[[1;;50,2]]-AvgRkp[[1;;50,2]]]/ (Abs[AvgLkp[[1;;50,2]]+AvgRkp[[1;;50,2]]]/2)*100;
SIhp=Abs[AvgLhp[[1;;50,2]]-AvgRhp[[1;;50,2]]]/ (Abs[AvgLhp[[1;;50,2]]+AvgRhp[[1;;50,2]]]/2)*100;
SIank=Table[{Per[[i]],SIa[[i]]},{i,1,51}];
SIkne=Table[{Per[[i]],SIk[[i]]},{i,1,51}];
SIhip=Table[{Per[[i]],SIh[[i]]},{i,1,51}];
SIankp=Table[{Per[[i]],SIap[[i]]},{i,1,51}];
SIknep=Table[{Per[[i]],SIkp[[i]]},{i,1,51}];
SIhipp=Table[{Per[[i]],SIhp[[i]]},{i,1,51}];

ListPlot[SIank, Joined□True, AxesLabel□{"% STS Cycle","SI %"} ,PlotLabel□ "Par 1 Ankle JM SI"]
ListPlot[SIkne, Joined□True, AxesLabel□{"% STS Cycle","SI %"} ,PlotLabel□ "Par 1 Knee JM SI"]
ListPlot[SIhip, Joined□True, AxesLabel□{"% STS Cycle","SI %"} ,PlotLabel□ "Par 1 Hip JM SI"]
ListPlot[SIankp, Joined□True, AxesLabel□{"% STS Cycle","SI %"} ,PlotLabel□ "Par 1 Ankle Power SI"]
ListPlot[SIknep, Joined□True, AxesLabel□{"% STS Cycle","SI %"} ,PlotLabel□ "Par 1 Knee Power SI"]
ListPlot[SIhipp, Joined□True, AxesLabel□{"% STS Cycle","SI %"} ,PlotLabel□ "Par 1 Hip Power SI"]

(* Determine Peak Timing *)
Print["Left Ankle JM Max:"]
Cases[AvgLa,{_,Max@AvgLa[[All,2]]}]
Print["RightAnkle JM Max:"]
Cases[AvgRa,{_,Max@AvgRa[[All,2]]}]
Print["Left Knee JM Max:"]
Cases[AvgLk,{_,Max@AvgLk[[All,2]]}]
Print["Right Knee JM Max:"]
Cases[AvgRk,{_,Max@AvgRk[[All,2]]}]
Print["Left hip JM Max:"]
Cases[AvgLh,{_,Max@AvgLh[[All,2]]}]
Print["Right hip JM Max:"]
Cases[AvgRh,{_,Max@AvgRh[[All,2]]}]
Print["Left Ankle Power Max:"]
Cases[AvgLap,{_,Max@AvgLap[[All,2]]}]
Print["Right Ankle Power Max:"]
Cases[AvgRap,{_,Max@AvgRap[[All,2]]}]
Print["Left Knee Power Max:"]
Cases[AvgLkp,{_,Max@AvgLkp[[All,2]]}]
Print["Right Knee Power Max:"]
Cases[AvgRkp,{_,Max@AvgRkp[[All,2]]}]
Print["Left hip Power Max:"]
```

```
Cases[AvgLhp,{_,Max@AvgLhp[[All,2]]}]
Print["Right hip Power Max:"]
Cases[AvgRhp,{_,Max@AvgRhp[[All,2]]}]

(* Export Difference Values *)
Export["ankleJMdiff.xls",avgDiffA];
Export["KneeJMdiff.xls",avgDiffK];
Export["HipJMdiff.xls",avgDiffH];
Export["anklePWdiff.xls",avgPDiffA];
Export["KneePWdiff.xls",avgPDiffK];
Export["HipPWdiff.xls",avgPDiffH];
```

Appendix C

Summary table of JM peak offsets arranged by participant and lower extremity joint. % STS represents a measure of pseudo-time with 0% representing initiation of STS and 100% representing completion.
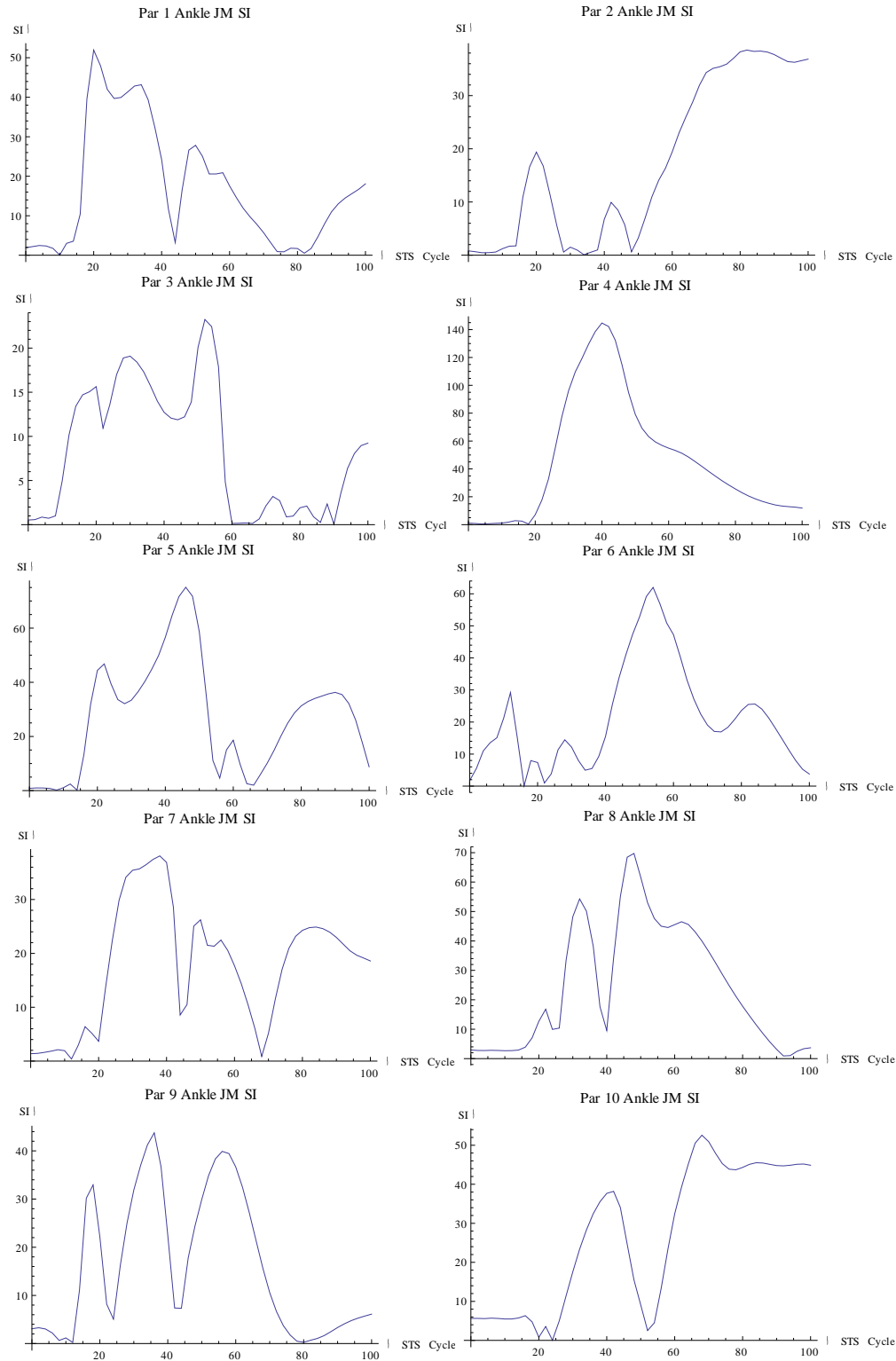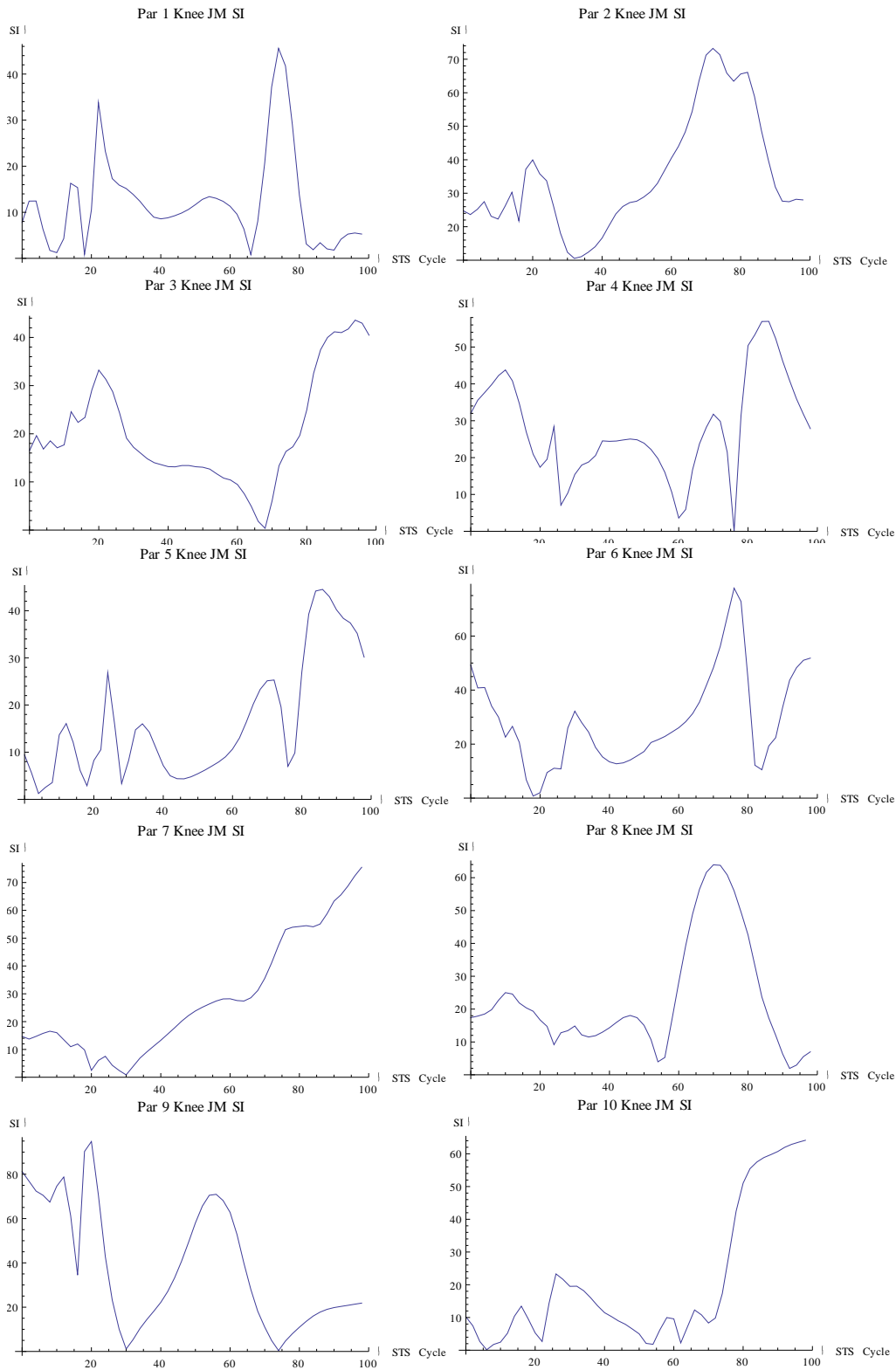
Joint	Participant	Left Peak Time (% STS)	Right Peak Time (% STS)	Offset (% STS)	First to Peak
Ankle	1	100	94	6	Right
Knee		40	40	0	N/A
Hip		36	34	2	Right
Ankle	2	100	100	0	N/A
Knee		36	38	2	Left
Hip		34	34	0	N/A
Ankle	3	100	100	0	N/A
Knee		42	42	0	N/A
Hip		44	44	0	N/A
Ankle	4	100	100	0	N/A
Knee		44	44	0	N/A
Hip		44	44	0	N/A
Ankle	5	88	90	2	Left
Knee		46	46	0	N/A
Hip		46	46	0	N/A
Ankle	6	92	100	8	Left
Knee		46	46	0	N/A
Hip		42	42	0	N/A
Ankle	7	98	96	2	Right
Knee		42	44	2	Left
Hip		38	40	2	Left
Ankle	8	84	100	16	Left
Knee		42	42	0	N/A
Hip		40	24	16	Right
Ankle	9	90	92	2	Left
Knee		34	36	2	Left
Hip		36	36	0	N/A
Ankle	10	100	100	0	N/A
Knee		40	42	2	Left
Hip		40	40	0	N/A

Summary table of JP peak offsets arranged by participant and lower extremity joint. % STS represents a measure of pseudo-time with 0% representing initiation of STS and 100% representing completion.

Joint	Participant	Left Peak Time (% STS)	Right Peak Time (% STS)	Offset (% STS)	First to Peak
Ankle	1	68	70	2	Left
Knee		52	52	0	N/A
Hip		50	54	4	Left
Ankle	2	64	72	8	Left
Knee		52	52	0	N/A
Hip		40	40	0	N/A
Ankle	3	68	76	8	Left
Knee		48	48	0	N/A
Hip		64	62	2	Right
Ankle	4	64	86	22	Left
Knee		48	48	0	N/A
Hip		52	52	0	N/A
Ankle	5	76	82	6	Left
Knee		56	54	2	Right
Hip		52	60	8	Left
Ankle	6	74	74	0	N/A
Knee		60	62	2	Left
Hip		58	60	2	Left
Ankle	7	72	72	0	N/A
Knee		48	50	2	Left
Hip		50	48	2	Right
Ankle	8	64	62	2	Right
Knee		50	48	2	Right
Hip		50	24	26	Right
Ankle	9	62	30	32	Right
Knee		30	40	2	Left
Hip		2	0	0	N/A
Ankle	10	76	36	40	Right
Knee		50	50	0	N/A
Hip		50	50	0	N/A

Appendix D

JM Symmetry Index Plots for each participant's ankle data

Par 1 Ankle JM SI

Par 2 Ankle JM SI

Par 3 Ankle JM SI

Par 4 Ankle JM SI

Par 5 Ankle JM SI

Par 6 Ankle JM SI

Par 7 Ankle JM SI

Par 8 Ankle JM SI

Par 9 Ankle JM SI

Par 10 Ankle JM SI

JM Symmetry Index Plots for each participant's knee data

Par 1 Knee JM SI

Par 2 Knee JM SI

Par 3 Knee JM SI

Par 4 Knee JM SI

Par 5 Knee JM SI

Par 6 Knee JM SI

Par 7 Knee JM SI

Par 8 Knee JM SI

Par 9 Knee JM SI

Par 10 Knee JM SI

JM Symmetry Index Plots for each participant's hip data

Par 1 Hip JM SI

Par 2 Hip JM SI

Par 3 Hip JM SI

Par 4 Hip JM SI

Par 5 Hip JM SI

Par 6 Hip JM SI

Par 7 Hip JM SI

Par 8 Hip JM SI

Par 9 Hip JM SI

Par 10 Hip JM SI

JP Symmetry Index Plots for each participant's ankle data

Par 1 Ankle Power SI

Par 2 Ankle Power SI

Par 3 Ankle Power SI

Par 4 Ankle Power SI

Par 5 Ankle Power SI

Par 6 Ankle Power SI

Par 7 Ankle Power SI

Par 8 Ankle Power SI

Par 9 Ankle Power SI

Par 10 Ankle Power SI

JP Symmetry Index Plots for each participant's knee data

Par 1 Knee Power SI

Par 2 Knee Power SI

Par 3 Knee Power SI

Par 4 Knee Power SI

Par 5 Knee Power SI

Par 6 Knee Power SI

Par 7 Knee Power SI

Par 8 Knee Power SI

Par 9 Knee Power SI

Par 10 Knee Power SI

JP Symmetry Index Plots for each participant's hip data

Par 1 Hip Power SI

Par 2 Hip Power SI

Par 3 Hip Power SI

Par 4 Hip Power SI

Par 5 Hip Power SI

Par 6 Hip Power SI

Par 7 Hip Power SI

Par 8 Hip Power SI

Par 9 Hip Power SI

Par 10 Hip Power SI

Appendix E

Discussions around advantages and disadvantage of each conceptual design

Four unique conceptual designs were purposed. Each design is capable of mechanically achieving sufficient torque to complete a STS movement in a patient suffering from significant muscular weakness. Each concept utilizes a different mechanical means to achieve a torsional moment at the knee. The following represents a brief description of each system and a list of their benefits as well as their draw backs identified by the clinicians and engineers.

Linear Actuators:

A single or a set of linear actuators would be positioned posterior to the knee. The actuator would span between the tibial and femoral portions of the KAFO brace. In sitting position, the actuator would be fully compressed. When initiated, the actuator would extend, forcing knee extension. The actuator would be sized such that at the end of its stroke, the KAFO would be in its fully extended position.

The actuator considered was a gas compression spring. These springs are available in an array of diameters, stroke lengths, and force outputs. They are self-powered and typically use a compressed inert gas to actuate. This style of design would allow for a small and relatively light weight design due to the mechanical forces that can be generated through gas compression. No fluid reservoir would be required as the spring utilizes internal gas pressure to drive extension. Furthermore, gas compression springs are readily available through numerous suppliers. However some draw backs do exist, being a compressed gas driven system, a degree of temperature sensitivity is inherent. Furthermore, consideration must be given to the design as to not interfere with the user's ability to sit in a chair. If the device were positioned posterior to the knee, it would be necessary to design the device such that it does not contact the chair while the user is seated.

Torsion Springs:

A set or single torsional spring would be positioned concentrically with the KAFO knee joint. The springs would be attached such that they resist knee flexion. When in the seated position, the springs would be loaded. A locking mechanism therefore would be required to prevent the loaded torsional spring from unwinding unless initiated by the user. When the knee joint is unlocked the torsional springs would force rotation in the KAFO knee joint. This is a simple design that arguably would require little maintenance. Torsional springs do not require any source of external power, and are readily available through numerous suppliers. One drawback is the potential heavy weight of the steel spring necessary to achieve sufficient torque. Finally, if positioned concentric to the knee consideration must be given to the size of the medial-lateral profile.

Electric Motors:

In this design the torque of an electric motor would be utilized to rotate the knee joint. The motor would have to be mounted in a convenient location on the brace. A mechanism similar to a gear box or sheave and belt system would be required to slow the rotational speed of the motor as well as limit the range of motion in the knee joint. This design would allow for the largest degree of torque control. Variable speeds, and torque could be implemented to meet user-specific requirements. However, incorporating a motor increases the complexity of the design. An external battery pack would be required, and charging issues may lead to reduced reliability. Furthermore the associated hardware may lead to increased cost relative to the other designs.

Tension Cables:

This concept allows for the greatest amount of design flexibility. Fundamentally a set of cables or a belt would be anchored toward the anterior, proximal portion of the upper brace. These cables would be guided over a mechanism functioning as a patella, and anchored along the shank portion of the brace. A mechanism would be designed to put this system into tension much like a quadricep. The force in the cable system would create the necessary moment about the knee joint. This design has the potential to be light weight and small in size. In order to create the required tension force in the cables, a compression spring (or gas compression spring), could be the only mechanical component used. Furthermore, this design has the potential to be simple and

correspondingly affordable as cables and springs can all be easily purchased. However, a drawback presents itself in the mechanics of the design. A sufficiently large tension must be created to develop the necessary torque at the knee to assist STS movements.

Appendix F

Hand calculations performed to verify prototype component safety.

SCREW SHEARING AND ALUMINUM BEARING

USED #8 SCREWS → Ø 0.164" = 4.17mm

SCREWS ASSUMED 301 STAINLESS σ_y = 276 MPa

3003 ALUMINUM FRAME σ_y = 110 MPa
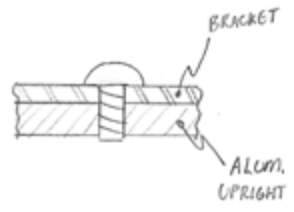
SCREW SHEARING :

$$\tau = F/A \quad \Rightarrow \quad 276 \, MPa = F_{max} / \frac{\pi (4.17)^2}{2} \qquad F_{max} = 3770 \, N.$$

ASSUME ACTUAL WORST LOAD TO EQUAL 900N (MAX SPRING OUTPUT)

SAFETY FACTOR (SF) = $3770N / 900N$ = $\boxed{4.19}$

ALUMINUM BEARING :

h = 6 mm
w = 15 mm

ALUM. UPRIGHTS

BEARING AREA = 4.17mm (6mm) = 25.02 mm²

$$\sigma = F/A = 110 \, MPa = F_{max} / 25.02 \, mm^2$$

$$F_{max} = 2752 \, N$$

ASSUME WORST LOADING EQUALS 900N

SF = $2752N / 900N$ = $\boxed{3.06}$

BEARING STRESS IN GUIDE TRACK.
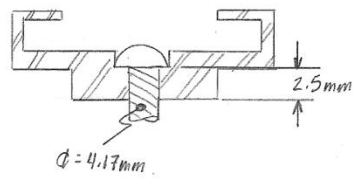
TRACK IS 3003 ALUMINUM $\sigma_y = 110$ MPa.

$$\sigma = F/A$$

$$110 \text{ MPa} = F_{max}/(2.5mm)(4.17mm)$$

$$F_{max} = 1147 N.$$

CALCULATE LOADING ON TRACK
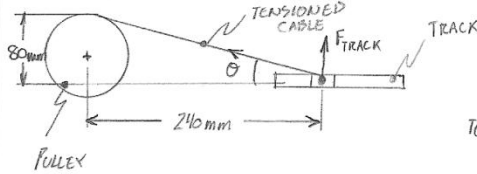
$$\therefore \theta = 18.4°$$

TENSION IN CABLE $= 900N \cos(18.4) = 854N$

$$F_{TRACK} = 854N \sin(18.4) = 270N.$$

$$\therefore SF = 1147N/270N = \boxed{4.2}$$

BENDING IN DISTAL CABLE ANCHOR.
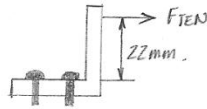
$b = 19mm$ $I = bh^3/12 = 197.92 \text{ mm}^4$

$h = 5mm$

STAINLESS STEEL $\sigma_y = 290$ MPa.

$$\sigma = \frac{mc}{I} = 290 \text{ MPa} = \frac{M_{max}(2.5)}{197.92}$$

$$M_{max} = 22\,959 \text{ Nmm}. \Rightarrow F_{max} = 22959/22 = 1044N.$$

$F_{TEN} = 854N$ (FROM ABOVE)

$$SF = 1044/854 = \boxed{1.2}$$

BEARING STRESS IN SPRING MOUNT BRACKET

MOUNTING PIN DIAMETER = 9.525 mm   STAINLESS BRACKET σ_y = 290 MPa.
BRACKET THICKNESS = 5mm

BEARING AREA = (9.525mm) 5mm = 47.625 mm²

F_{MAX} = (290 MPa) (47.625 mm²) = 13811 N

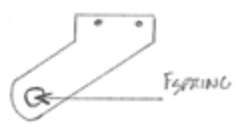MAX POSSIBLE LOADING = 900N. FROM THE SPRING

SF = 13811/900 = 15.3

Appendix G

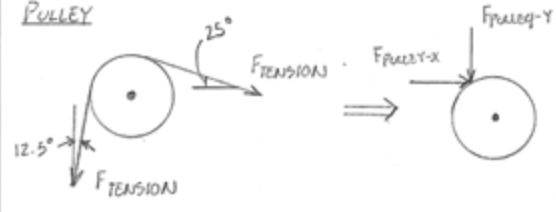Geometry and free body diagrams to describe the finite element model loading conditions

SLIDER:
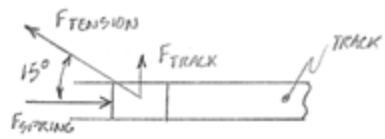
F_{SPRING} = 900 N.

$F_{TENSION}$ = 854 N

F_{TRACK} = 270 N.

SPING MOUNT BRACKET.

F_{SPRING} = 900 N.

PULLEY

$F_{PULLEY-Y}$ = 1194 N
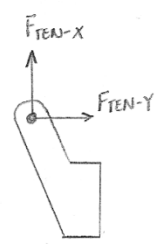
$F_{PULLEY-X}$ = 958 N.

FRONT VEIW CF PULLEY:
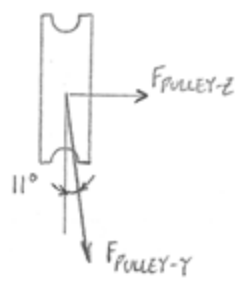
$F_{PULLEY-Y}$ = 1194 N

$F_{PULLEY-Z}$ = 221 N

G-1

CABLE ANCHOR
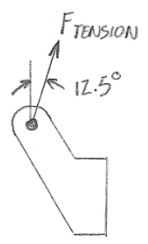
$F_{TENSION}$ = 854N

F_{TEN-X} = 185N

F_{TEN-Y} = 834N.

G-2